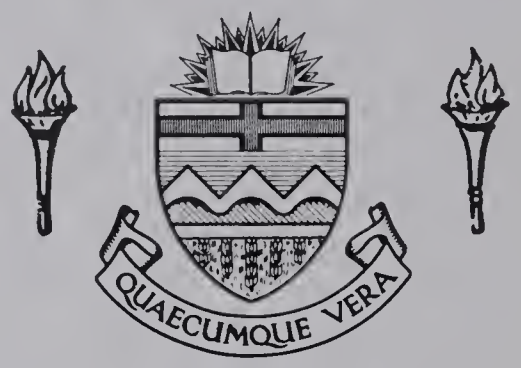
For Reference

NOT TO BE TAKEN FROM THIS ROOM

Ex libris
universitatis
albertaensis



THE UNIVERSITY OF ALBERTA

RELEASE FORM

NAME OF AUTHOR: Jawaid Saeedi

TITLE OF THESIS: A COMPARISON OF THEORETICAL AND EXPERIMENTAL SATURATION PROFILES IN POROUS MEDIA

DEGREE FOR WHICH THESIS WAS PRESENTED: MASTER OF SCIENCE, PETROLEUM ENGINEERING

YEAR THIS DEGREE GRANTED: 1979

Permission is hereby granted to THE UNIVERSITY OF ALBERTA LIBRARY to reproduce single copies of this thesis and to lend or sell such copies for private, scholarly or scientific research purposes only.

The author reserves other publication rights, and neither the thesis nor extensive extracts from it may be printed or otherwise reproduced without the author's written permission.

THE UNIVERSITY OF ALBERTA

A COMPARISON OF THEORETICAL AND EXPERIMENTAL SATURATION PROFILES IN POROUS MEDIA

by

© Jawaid Saeedi

A THESIS

SUBMITTED TO THE FACULTY OF GRADUATE STUDIES AND RESEARCH

IN PARTIAL FULFILMENT OF THE REQUIREMENTS FOR THE DEGREE

OF MASTER OF SCIENCE

IN

PETROLEUM ENGINEERING

DEPARTMENT OF MINERAL ENGINEERING

EDMONTON, ALBERTA

SPRING, 1979

79-100

THE UNIVERSITY OF ALBERTA

FACULTY OF GRADUATE STUDIES AND RESEARCH

The undersigned certify that they have read, and recommend to the Faculty of Graduate Studies and Research, for acceptance, a thesis entitled "A Comparison of Theoretical and Experimental Saturation Profiles in Porous Media", submitted by Jawaid Saeedi in partial fulfilment of the requirements for the degree of Master of Science in Petroleum Engineering.

ABSTRACT

An improved understanding of how one fluid displaces another in a porous medium can be gained by measuring saturation as a function of time and distance, a procedure rarely undertaken. To this end, a series of immiscible displacements were conducted, at various viscosity ratios, in which in situ saturations were measured using a relatively new technique based on micro-wave attenuation. The experimental saturation profiles obtained in this manner were compared with those obtained by numerically solving a recently derived Lagrangian formulation of the immiscible displacement equation. Finally, the results obtained were analyzed in the light of published scaling groups, and a recently proposed stability criterion. The results of this analysis suggest that one-dimensional, immiscible displacement theory unconditionally represents displacements carried out at favourable mobility ratios. For adverse mobility ratio displacements, in horizontal systems, a stability criterion must be satisfied before the theory can be said to represent the displacement process.

ACKNOWLEDGEMENTS

The author gratefully acknowledges the guidance and close supervision provided by Dr. R. G. Bentsen throughout the course of this study.

Acknowledgements are also made to Dr. W. R. Tinga, for his help in arranging the loan of the microwave equipment and guidance on the microwave aspects of the study; to Mr. G. T. Walsh, who did the mechanical design of the chain drive, mobile core-holder mounts and the core holders; and to the Petroleum Aid to Education Fund (Plan B) for their financial support.

TABLE OF CONTENTS

CHAPTER		PAGE
I.	INTRODUCTION	1
	I.1 Background	1
	I.2 Purpose of the Study	2
	I.3 Methodology	3
II.	THEORY AND LITERATURE REVIEW	5
	II.1 Immiscible Displacement	5
	II.1.1 Equations	5
	II.1.2 Normalization of Capillary Pressure and Effective Permeabilities	7
	II.1.3 Review of Theory and Numerical Solutions	9
	II.2 Role of Saturation Profiles	15
	II.3 Saturation Measurement Techniques	16
	II.4 Choice of a Saturation Measurement Technique	18
III.	MICROWAVE THEORY, EXPERIMENTAL EQUIPMENT AND PROCEDURE	19
	III.1 Microwave Theory	19
	III.1.1 Electro-magnetic Approach	20
	III.1.2 Optical Approach	22
	III.1.3 Relationship between Electro-magnetic and Optical Approaches	24
	III.1.4 Quantitative Evaluation of the Extinction Coefficient	25
	III.2 Microwave Instrumentation	26
	III.2.1 Antennas	26
	III.2.2 Instrumentation	27

PAGE

III.2.3 Bench Experiment 27

III.3 Fluid Injection System, Core Holder and Allied Equipment 30

III.4 A Typical Run 33

III.4.1 Preparation of the Core 33

III.4.2 The Oilflood 35

III.4.3 Power Meter Settings and Scale Factors 36

III.4.4 The Waterflood 39

III.5 Analysis of Errors 40

IV. CONVERSION AND PREPARATION OF DATA FOR ANALYSIS 47

IV.1 Introduction 47

IV.2 Conversion of Microwave Response to a Saturation Profile 47

IV.3 Error Analysis on Saturation Profiles 53

IV.4 Pore Volumes Injected, Pore Volumes of Oil Produced and Effective Viscosities 53

IV.5 Pressure Differential and Pore Volumes Injected 57

V. NUMERICAL SOLUTIONS AND COMPARISON WITH EXPERIMENTAL SATURATION PROFILES 58

V.1 Introduction 58

V.2 Numerical Solutions 58

V.2.1 Lagrangian 59

V.2.2 Eulerian 60

V.3 Data Bases for Numerical Simulators 61

V.3.1 Data Obtained by Direct Measurement 62

V.3.2 Estimates of Residual Oil Saturation and Effective Permeability for Adverse Viscosity Ratios. 62

PAGE

V.4 Estimation of Parameters in Relative Permeability Models 64

V.5 Estimation of Capillary Pressure Normalizing Parameter 72

V.5.1 Estimate Based on Capillary Pressure Curve Published by Hagoort 72

V.5.2 Estimate Based on Capillary Pressure Curve Published by Leverett 73

V.5.3 Numerical Experimentation in the Estimation of Capillary Pressure Normalizing Parameter 75

V.6 Comparison of Eulerian and Lagrangian Solution of the Immiscible Displacement Equation 77

V.7 Comparison of Experimental Saturation Profiles with Lagrangian Solution 81

VI. DISCUSSION OF RESULTS 89

VI.1 Introduction 89

VI.2 Attainment of the Stabilized Zone 89

VI.3 Analysis with the Help of Dimensionless Groups 91

VI.4 Experimental Saturation Profiles 99

VI.5 Comments on External Drive Techniques for the Determination of Relative Permeabilities . . 100

VI.6 Analysis of Runs at Favourable Mobility Ratios 102

VII. CONCLUSIONS AND RECOMMENDATIONS 104

VII.1 Summary and Conclusions 104

VII.2 Recommendations 106

* * * * * *

PAGE

REFERENCES 109

BIBLIOGRAPHY 113

APPENDIX A. EXPERIMENTALLY MEASURED SATURATION PROFILES . . . 117

APPENDIX B. TABLES SHOWING PHYSICAL PROPERTIES AND OTHER PARAMETERS FOR THE EXPERIMENTAL RUNS 133

APPENDIX C. MICROWAVE LENS ANTENNA DESIGN

MICROWAVE SIGNAL-WATER SATURATION CALCULATION . . 139

APPENDIX D. PLOTS OF TOTAL PRESSURE DROP, PORE VOLUMES PRODUCED AND EFFECTIVE VISCOSITIES VERSUS PORE VOLUMES INJECTED

DATA IN TABULAR FORM FOR THESE PLOTS 145

APPENDIX E. EULERIAN SOLUTION PROCEDURE FOR IMMISCIBLE DISPLACEMENT EQUATION 173

LIST OF TABLES

TABLE		PAGE
III-1	Dimensions of Core Holders	30
IV-1	Summary of Runs Conducted	48
IV-2	Microwave Calibration Data	52
IV-3	Values of Constant C to Determine Effective Viscosities	56
V-1	Breakthrough Recoveries of Some Runs for Different Parameters Used in the Relative Permeability Models	69
V-2	Values from Leverett Capillary Pressure Curve	73
V-3	Estimates of Capillary Pressure Normalizing Parameter	75
VI-1	Values of Dimensionless Groups and Recoveries for the Runs Conducted	97
B-1	Data for Runs 8, 10 and 11	134
B-2	Data for Runs 12, 13, 14 and 15	135
B-3	Data for Runs 16, 18, 19, 20 and 21	136
B-4	Data for Run 9	137
B-5	Data for Runs 23 and 24	138
C-1	Water Saturations and Theoretical Microwave Power Received	144
D-1	Oil Production and Pressure History - Run 8	158
D-2	Oil Production and Pressure History - Run 10	159
D-3	Oil Production and Pressure History - Run 11	160
D-4	Oil Production and Pressure History - Run 12	161
D-5	Oil Production and Pressure History - Run 13	162
D-6	Oil Production and Pressure History - Run 14	163
D-7	Oil Production and Pressure History - Run 15	164
D-8	Oil Production and Pressure History - Run 16	165

PAGE

D-9 Oil Production and Pressure History - Run 18 166

D-10 Oil Production and Pressure History - Run 19 167

D-11 Oil Production and Pressure History - Run 20 168

D-12 Oil Production and Pressure History - Run 21 169

D-13 Oil Production and Pressure History - Run 9 170

D-14 Oil Production and Pressure History - Run 23 171

D-15 Oil Production and Pressure History - Run 24 172

LIST OF FIGURES

FIGURE		PAGE
II-1	Capillary Pressure-Saturation Relationships	8
II-2	Steps in Normalizing Effective Permeability	10
II-3	Buckley-Leverett Solution and Welge's Tangent Construction	11
II-4	Behaviour of $f_w(S^*, \tau^*)$	14
III-1	Dielectric Constant and Loss Factor Versus Logarithm of Frequency	21
III-2	Loss Factor Versus Frequency for Different Substances	21
III-3	Complete Experimental Set Up Showing Microwave and Fluid Injection Systems	28
III-4	Closer View of Microwave Instrumentation	29
III-5	Horns and Lens Antennas in Position	29
III-6	Schematic Layout (top view) of the Experimental Set Up	31
III-7	Bench Experiment with Horns 3" Apart in Air	32
III-8	Microwave Response Facsimile of the Oilflood - Run 18	37
III-9	Microwave Response Facsimile of the Waterflood at t = 40 min - Run 18	41
III-10	Microwave Response Facsimile of the Calibration Scans - Run 23	42
III-11	Power Meter - Input/Output	43
III-12	X-Y Recorder - Input/Output	43
IV-1	Microwave Response - S_w Correlation	51
IV-2	Error Analysis on Material Balance	54
V-1	Extrapolation to Infinite Pore Volumes Injected	63
V-2	Relative Permeabilities - Run 11	65
V-3	Relative Permeabilities - Run 18	66

PAGE

V-4 Effect of Different Sets of Parameters on Relative Permeability Curves 70

V-5 Effect of Different Sets of Parameters in the Relative Permeability Models on the Saturation Profiles 71

V-6 Estimate for Capillary Pressure Normalizing Parameter 74

V-7 Effect of Capillary Pressure Normalizing Parameter on Saturation Profiles 76

V-8 Comparison of Eulerian and Lagrangian Solutions - Data from Run 24 78

V-9 Comparison of Eulerian and Lagrangian Solutions - Data from Run 11 79

V-10 Comparison of Eulerian and Lagrangian Solutions - Data from Run 18 80

V-11 Comparison of Experimental Saturation Profiles with Lagrangian Solutions - Run 9 83

V-12 Comparison of Experimental Saturation Profiles with Lagrangian Solutions - Run 23 84

V-13 Comparison of Experimental Saturation Profiles with Lagrangian Solutions - Run 24 85

V-14 Comparison of Experimental Saturation Profiles with Lagrangian Solutions - Run 11 87

V-15 Comparison of Experimental Saturation Profiles with Lagrangian Solutions - Run 18 88

VI-1 Reciprocal Capillary Number Versus Breakthrough Recoveries. Data Sets of Runs 11 and 18 95

A-1 Experimental Saturation Profiles - Run 8 118

A-2 Experimental Saturation Profiles - Run 10 119

A-3 Experimental Saturation Profiles - Run 11 120

A-4 Experimental Saturation Profiles - Run 12 121

A-5 Experimental Saturation Profiles - Run 13 122

A-6 Experimental Saturation Profiles - Run 14 123

		PAGE
A-7	Experimental Saturation Profiles - Run 15	124
A-8	Experimental Saturation Profiles - Run 16	125
A-9	Experimental Saturation Profiles - Run 18	126
A-10	Experimental Saturation Profiles - Run 19	127
A-11	Experimental Saturation Profiles - Run 20	128
A-12	Experimental Saturation Profiles - Run 21	129
A-13	Experimental Saturation Profiles - Run 9	130
A-14	Experimental Saturation Profiles - Run 23	131
A-15	Experimental Saturation Profiles - Run 24	132
C-1	Pyramidal Horn	141
C-2	Plano-Convex Lens	141
D-1	Total Pressure Drop History - Runs 8, 10 & 11	146
D-2	Total Pressure Drop History - Runs 12, 13, 14 & 15 . .	147
D-3	Total Pressure Drop History - Runs 16, 18, 19, 20 & 21	148
D-4	Total Pressure Drop History - Runs 9, 23 & 24	149
D-5	Effective Viscosity History - Runs 8, 10 & 11	150
D-6	Effective Viscosity History - Runs 12, 13, 14 & 15 . .	151
D-7	Effective Viscosity History - Runs 16, 18, 19, 20 & 21	152
D-8	Effective Viscosity History - Runs 9, 23 & 24	153
D-9	Oil Production History - Runs 8, 10 & 11	154
D-10	Oil Production History - Runs 12, 13, 14 & 15	155
D-11	Oil Production History - Runs 16, 18, 19, 20 & 21 . . .	156
D-12	Oil Production History - Runs 9, 23 & 24	157

NOMENCLATURE

A = Cross-sectional area

a_o, b_o, a_w, b_w = Parameters in relative permeability models

$\bar{c}$ = Concentration

c = Velocity of light

C = A constant used to determine effective viscosities

C^* = Capillary constant

$C(S^*) = -\frac{1}{M_r} F_w K_{ro} \frac{d\pi_c}{dS^*}$

$E_p = \frac{(M_r - 1)V\mu_w L_x^2 L_y^2}{C^*\gamma K_{wr}(L_x^2 + L_y^2)}$

where L_x, L_y are in cm

γ is in dynes/cm

K_{wr} is in cm^2

μ_w is in poise

f = frequency

f_w = fractional flow of water

$F_w(S^*) = \frac{M_r K_{rw}}{M_r K_{rw} + K_{ro}}$

$G(S^*)$ = $F_w(S^*)$, for horizontal systems

h = Thickness of core

I_o = Incident microwave power

I_x = Attenuated microwave power

i = $\sqrt{-1}$

IOIP = Initial oil in place

$J(S_w)$ = Leverett J-function

k = Extinction coefficient per unit of concentration

$\overline{K}$ = Extinction coefficient

K = Absolute permeability

K_{eo} = Effective permeability to oil

K_{ew} = Effective permeability to water

K_{or} = Effective permeability to oil at initial water saturation

K_{ro} = Normalized permeability to oil

K_{rw} = Normalized permeability to water

K_{wr} = Effective permeability to water at residual oil saturation

L = Length of the core

L_x = Thickness of the core

L_y = Width of the core

m = mass

M_r = $\dfrac{\mu_o K_{wr}}{\mu_w K_{or}}$

n = Refractive index

n^* = Complex refractive index

N_c = $\dfrac{\sigma A K_{wr}}{qL\mu_w}$

where σ is in atm
A is in cm^2
K_{wr} is in darcy
q is in cc/sec
L is in cm
μ_w is in cp

NK	=	Exponent in oil relative permeability model
P	=	Pressure
P_c	=	Capillary pressure
P_o	=	Pressure in oil phase
P_w	=	Pressure in water phase
PV	=	Pore volume
q	=	Volumetric flow rate
q_o	=	Volumetric flow rate for oil
q_w	=	Volumetric flow rate for water
R_s	=	Power meter setting
R	=	Attenuated microwave power
RDRY	=	Logarithm of the average value of R corresponding to 0% S_w
RSAT	=	Average value of $Log_{10}R$ corresponding to 100% S_w
RSWI	=	Average value of $Log_{10}R$ corresponding to $\bar{S}_{wi}$
RSOR	=	Average value of $Log_{10}R$ corresponding to $\bar{S}_{or}$
S_w	=	Water saturation
S_o	=	Oil saturation
S*	=	Normalized saturation
S_{or}	=	Residual oil saturation
S_{wi}	=	Initial water saturation
S^*_f	=	Normalized flood front saturation
$\bar{S}_{wi}$	=	Average initial water saturation
$\bar{S}_{or}$	=	Average residual oil saturation
S_{w2}	=	Water saturation at the outlet end
S^*_{abt}	=	Normalized average saturation at breakthrough

S_c	=	X-Y recorder scale factor
t	=	Time
v_w	=	Superficial velocity of water phase
v_x, V	=	Superficial velocity
v_ϕ	=	Phase velocity
$\left.\begin{matrix}\alpha(S^*)\\ \beta(S^*)\end{matrix}\right\}$	=	Influence functions in relative permeability models
γ	=	Oil-water interfacial tension
ΔP	=	Total pressure drop across the core
$\Delta\tau^*$	=	Time step size
$\Delta\xi$	=	Step size
ε'	=	Dielectric constant
ε''	=	Loss factor
ε^*	=	Complex dielectric constant
$\bar{\lambda}^{-1}$	=	Effective viscosity
λ_2^{-1}	=	Effective viscosity at the outlet end
μ	=	Viscosity
μ_o	=	Viscosity of oil
μ_w	=	Viscosity of water
ξ	=	Normalized distance
π	=	3.13159
π_c	=	Dimensionless capillary pressure
ρ_g	=	Grain density
ρ_o	=	Density of oil
ρ_w	=	Density of water
σ	=	Capillary pressure normalizing parameter

τ^*	=	Recoverable pore volumes injected/produced
τ	=	Pore volumes produced
τ_i	=	Pore volumes injected
τ_{corr}	=	Corrected value of pore volumes produced
τ^*_{bt}	=	Dimensionless pore volumes produced at breakthrough
ϕ	=	Porosity

CHAPTER I

INTRODUCTION

I.1 BACKGROUND

The macroscopic law governing flow of a liquid in porous media was developed by Darcy in 1856. In horizontal, one-dimensional systems, Darcy's law can be written as:

$$v_x = -\frac{K}{\mu}\frac{dP}{dx} \qquad (I\text{-}1)$$

The macroscopic measure of resistance to flow for a particular porous medium is the absolute permeability, K, which must be determined experimentally. Absolute permeability of a porous medium is invariant with the physical properties of the liquid used to evaluate it.

In all hydrocarbon bearing porous media, it is well known that water co-exists with hydrocarbons which are either in the liquid or vapour phase. When water flows with, or displaces, these hydrocarbons, Darcy's law, as formulated for the flow of a single fluid, is not applicable. The concept of absolute permeability is still valid because it is a property of the porous medium. To study the flow of hydrocarbons with water through porous media, Wyckoff and Botset[55] [1936] used gas-water and oil-water mixtures to flow through an unconsolidated sand pack. Their results indicated that the flow of either fluid can still be predicted by a Darcy-type law, provided the absolute permeability is replaced with an effective permeability to that fluid. Effective permeability is a property of a particular

rock and is also a function of the relative amount of the fluid present in an elemental volume of the porous medium. This relative amount is the fraction of pore volume occupied by a fluid in an element of the porous medium and is known as the saturation of that fluid. Darcy's law for water flowing together with hydrocarbons is

$$v_w = - \frac{K_{ew}(S_w)}{\mu_w} \frac{\partial P_w}{\partial x} \qquad \text{(I-2)}$$

Effective permeabilities, although unique functions of saturation for a fluid and a porous medium, do have implicit in them effects of interfacial tensions between the fluids and the wettability characteristics of the porous medium for those fluids. They also depend on saturation history.

The current immiscible displacement theory is based on Darcy's law {Eq.(I-2)} written for both the fluids, an equation to link the two flow relationships and conservation of volume in the porous medium. The linkage between the two flow relationships is the defining equation for capillary pressure [Leverett[35], 1941]. This formulation has inherent uncertainities as it requires experimentally determined effective permeability-saturation and capillary pressure-saturation curves. More often than not mathematical models are used, rather than experimentally derived relationships.

I.2 PURPOSE OF THE STUDY

The conventional immiscible displacement theory gives rise to a second order, non-linear, partial differential equation [Rapoport and Leas[47], 1953] which has no known analytical solution. Despite uncertainities in the relative permeability and capillary pressure

curves, the immiscible displacement equation is solved numerically, resulting in one-dimensional saturation profiles. It was the purpose of this study to experimentally measure these saturation profiles and then analyse them, quantitatively, together with the numerical solutions. These numerical solutions were generated using published relative permeability and capillary pressure models.

Rose[48] [1974, p.233] recognized the dearth of this type of analysis in the literature, and mentions that

> "in the last decade, much progress has been made in the development of stable and rapidly convergent numerical solution techniques for the second order non-linear partial differential equation. This work has yielded at least qualitatively plausible forecasts of the characteristics of immiscible displacement processes. Still no definitive laboratory work has been reported in the literature by which the quantitative significance of the theory can be judged".

Moreover, he also suggested that, to ascertain the consistency of the theory, saturations should be measured as a function of time and distance as this approach was generally considered superior to the analysis of the total pressure drop versus time curve, which has been carried out by Warren and Calhoun[53] [1954].

I.3 METHODOLOGY

The following methodology was devised and executed.

Saturations were measured as a function of time and distance employing a suitable technique, selected on its merits, as enumerated in the literature. Displacement tests were conducted at different viscosity ratios in an unconsolidated sand pack. Rate was also a parameter. A suitable published numerical procedure was chosen to generate calculated saturation profiles. A numerical procedure was also developed in this study. The procedure which gave

a closer match to the experimentally measured saturation profiles was used for comparison purposes. For support of numerical procedures, capillary pressure and relative permeability models were taken from the literature.

Finally an overall analysis of the experimental and numerical results was envisaged in the light of established scaling groups and stability criteria.

CHAPTER II

THEORY AND LITERATURE REVIEW

II.1 IMMISCIBLE DISPLACEMENT

II.1.1 Equations

Immiscible displacement theory is used to predict the saturation behaviour during displacement of oil by water. This theory is based on the solution of the following equations:

Darcy's law as written for both oil and water [55], [Wyckof and Botset, 1936]

$$q_w = \frac{-KK_{rw}(S_w)A}{\mu_w} \frac{\partial P_w}{\partial X} \qquad \text{(II-1)}$$

$$q_o = \frac{-KK_{ro}(S_w)A}{\mu_o} \frac{\partial P_o}{\partial X} , \qquad \text{(II-2)}$$

the capillary pressure definition[35], [Leverett, 1941]

$$P_c(S_w) = P_o(S_w) - P_w(S_w) \qquad \text{(II-3)}$$

and the continuity or material balance equation for incompressible fluids[10], [Buckley and Leverett, 1942]

$$\left(\frac{\partial q_w}{\partial X}\right)_t = -\phi A\left(\frac{\partial S_w}{\partial t}\right)_x \qquad \text{(II-4)}$$

Rapoport and Leas[47] [1953] combined these four equations to illustrate that, according to this theory, the physics of immiscible displacement in porous media can be described by the following second order, non-linear, parabolic, partial differential equation

$$\frac{\partial}{\partial X}\left[\frac{1}{1+\frac{\mu_o K_{rw}(S_w)}{\mu_w K_{ro}(S_w)}}\left\{\frac{\mu_o K_{rw}(S_w)}{\mu_w K_{ro}(S_w)} + \frac{K K_{rw}(S_w) A}{\mu_w}\frac{dP_c}{dS_w}\frac{\partial S_w}{\partial X}\right\}\right] + \phi A \frac{\partial S_w}{\partial t} = 0 \qquad \text{(II-5)}$$

Bentsen[3] [1976] nondimensionalized these equations [(II-1) to (II-4)] utilizing the procedure of Hellums and Churchill[27] [1961]. The normalized equations when written for horizontal systems are,

$$\frac{\partial f_w}{\partial \xi} = -\frac{\partial S^*}{\partial \tau^*} \qquad \text{(II-6)}$$

and

$$f_w = G(S^*) - N_c C(S^*)\frac{\partial S^*}{\partial \xi} \qquad \text{(II-7)}$$

where

$$G(S^*) = F_w(S^*) \quad \text{(for horizontal systems)} \qquad \text{(II-8)}$$

$$C(S^*) = -\frac{1}{M_r} F_w K_{ro}\frac{d\pi_c}{dS^*} \qquad \text{(II-9)}$$

$$F_w(S^*) = \frac{M_r K_{rw}}{M_r K_{rw} + K_{ro}} \qquad \text{(II-10)}$$

$$N_c = \frac{\sigma A K_{wr}}{qL\mu_w} \qquad \text{(II-11)}$$

$$M_r = \frac{K_{wr}\mu_o}{\mu_w K_{or}} \qquad \text{(II-12)}$$

$$\xi = \frac{x}{L} \qquad \text{(II-13)}$$

$$\tau^* = \frac{qt}{A\phi L(1 - S_{or} - S_{wi})} \qquad \text{(II-14)}$$

$$S^* = \frac{S_w - S_{wi}}{1 - S_{or} - S_{wi}} \qquad \text{(II-15)}$$

Normalization of capillary pressure, P_c, and effective permeabilities, K_{eo} and K_{ew}, required special treatment.

II.1.2 Normalization of Capillary Pressure and Effective Permeabilities

Bentsen and Anli[4,5] [1976, 1977] proposed a capillary pressure model and used data obtained from a centrifuge to validate it, as well as to estimate the parameters postulated in the model. This model is for a drainage capillary pressure versus saturation curve but for the purpose of this study it is also considered to represent an imbibition capillary pressure versus saturation curve. The model is,

$$\pi_c = -\ell n S^* \qquad \text{(II-16)}$$

or

$$\frac{d\pi_c}{dS^*} = -\frac{1}{S^*} \qquad \text{(II-17)}$$

where

$$\pi_c = \frac{P_c}{\sigma} \qquad \text{(II-18)}$$

and the capillary normalizing parameter, σ, has the units of pressure. Mathematically, σ is the area under the π_c versus S* curve and physically it is influenced by interfacial tension, pore-size distribution and wettability. Figure II-1 shows the P_c versus S_w and π_c versus S* curves.

Bentsen[3] [1976] normalized the effective permeabilities after the manner of Perkins and Collins[44] [1960]. That is,

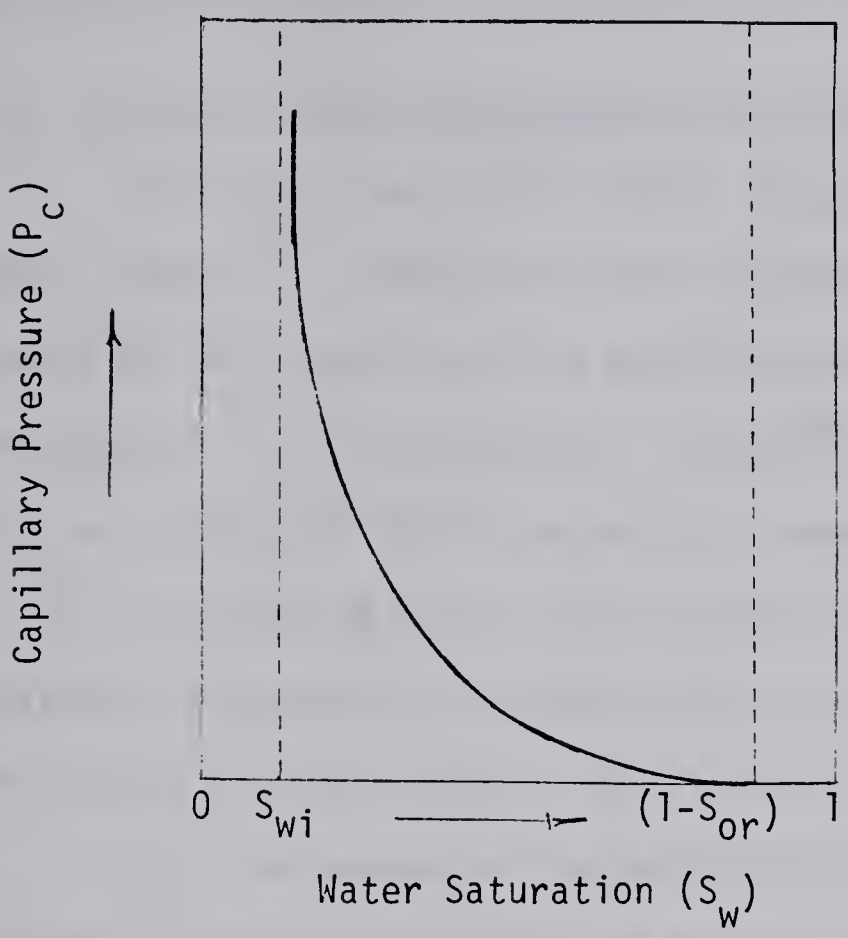
$$K_{rw}(S^*) = \frac{K_{ew}(S^*)}{K_{wr}} \qquad \text{(II-19)}$$

and

$$K_{ro}(S^*) = \frac{K_{eo}(S^*)}{K_{or}} \qquad \text{(II-20)}$$

CAPILLARY PRESSURE-SATURATION RELATIONSHIPS

(Bentsen, 1976)



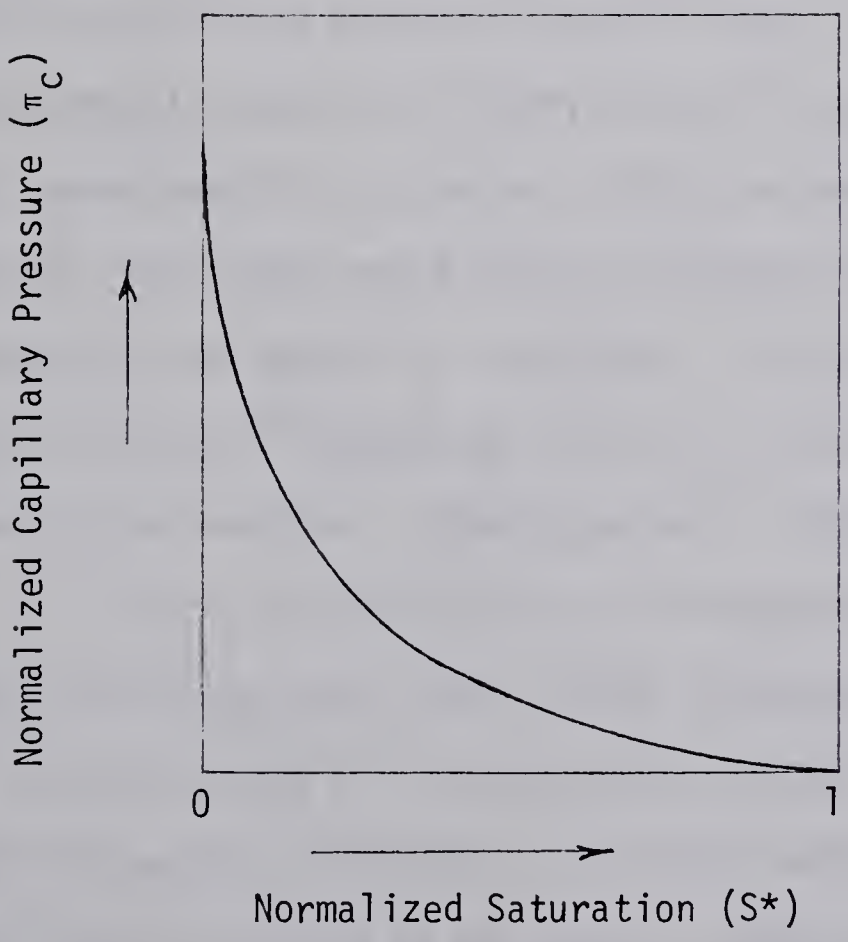


FIGURE II-1

where K_{wr} and K_{or} are effective permeabilities to water at $(1 - S_{or})$ and to oil at S_{wi}, respectively. Figure II-2 shows how the normalization of effective permeabilities is carried out.

II.1.3 Review of Theory and Numerical Solutions

Terwilliger et al.[51] [1951], Welge[54] [1952] and Rapoport and Leas[47] [1953], with their experimental and analytical treatment of the immiscible flow equations, enhanced the physical understanding of such displacement. Welge[54], essentially using the Buckley and Leverett[10] [1942] equations, demonstrated that balancing areas on a S* versus ξ plot, to get around the absurdity of multiple saturations at one point, is equivalent to drawing a tangent to the $F_w(S^*)$ versus S* curve from S* = 0. [Figure II-3].

As a consequence of the philosophical argument put forward by Cardwell[11] [1959], regarding the multi-valued solutions obtained using non-capillary Buckley-Leverett theory, doubts were cast on the experimentally determined $F_w(S^*)$ versus S* curve. Because $F_w(S^*)$ needs experimentally determined effective permeabilities, Cardwell inferred that either the effective permeabilities are erroneously measured or the theory is incomplete. During all this time Buckley-Leverett[10] theory was being put to use in solving field waterflooding problems. [Dardaganian[14], (1958); Kufus[33], (1959)].

With the advent of digital computers, Douglas[16] et al. [1958] solved the non-linear partial differential equation [Eq.(II-5)] by a transformation of the dependent variable, S_w, and by employing a set of boundary and initial conditions which allowed for a mobile water saturation ahead of the front. Outlet end effects were accounted for by allowing the outlet end saturation to build up to

STEPS IN NORMALIZING EFFECTIVE PERMEABILITY

(Perkins, et. al., 1960; Bentsen, 1976)

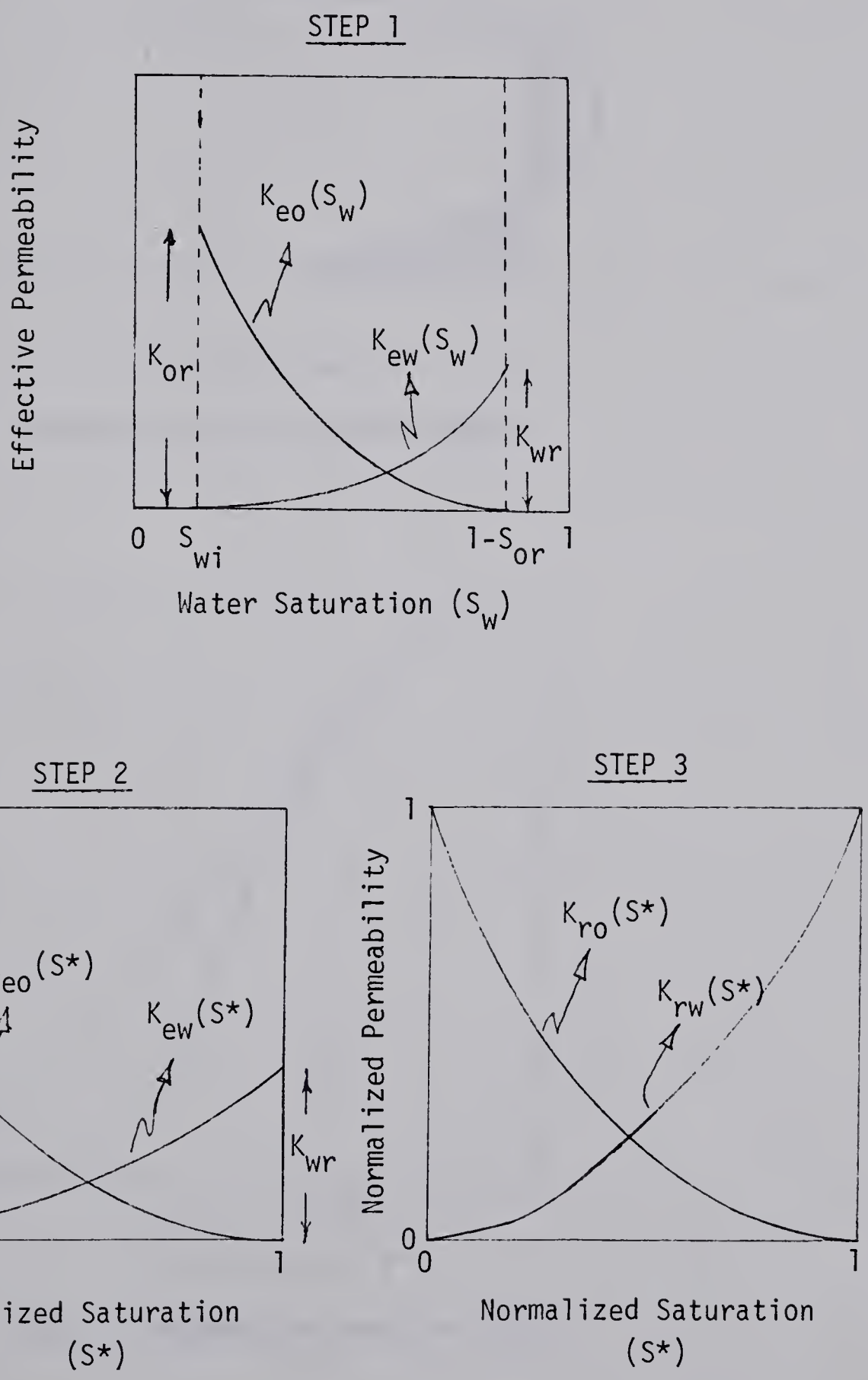
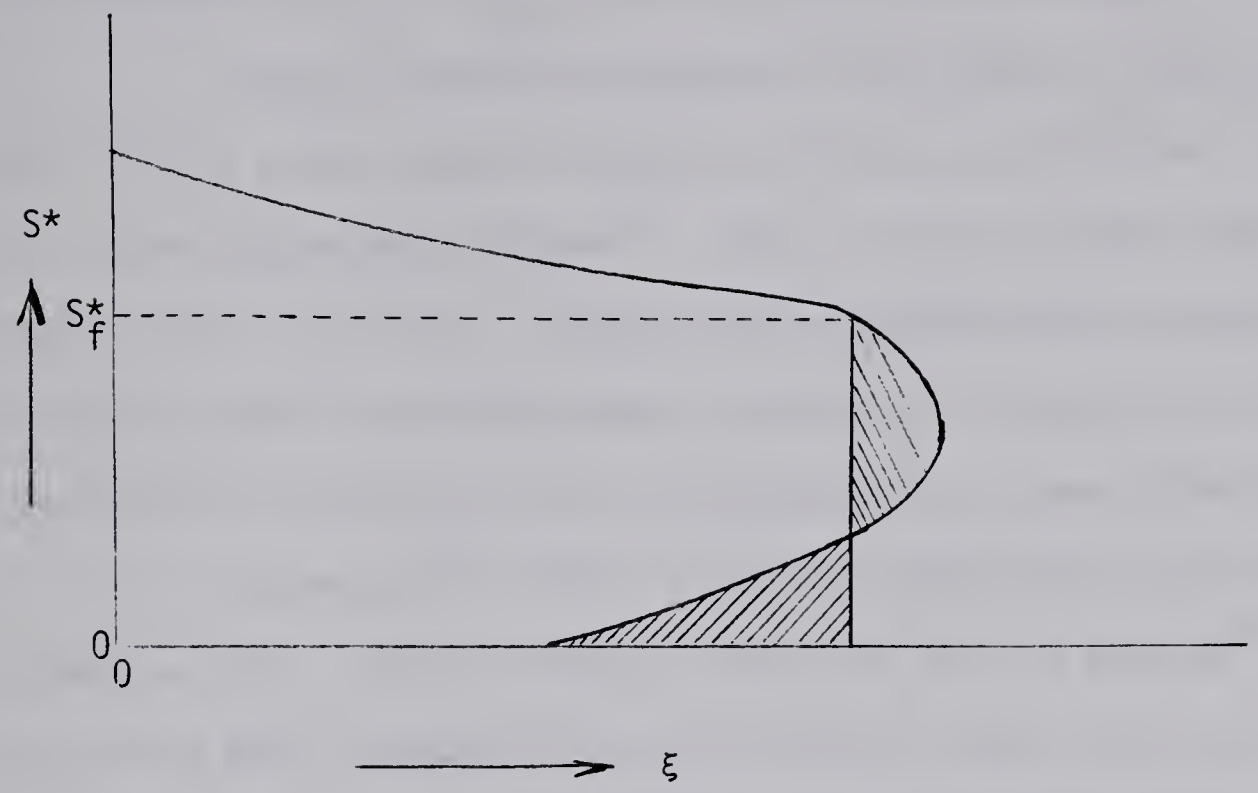
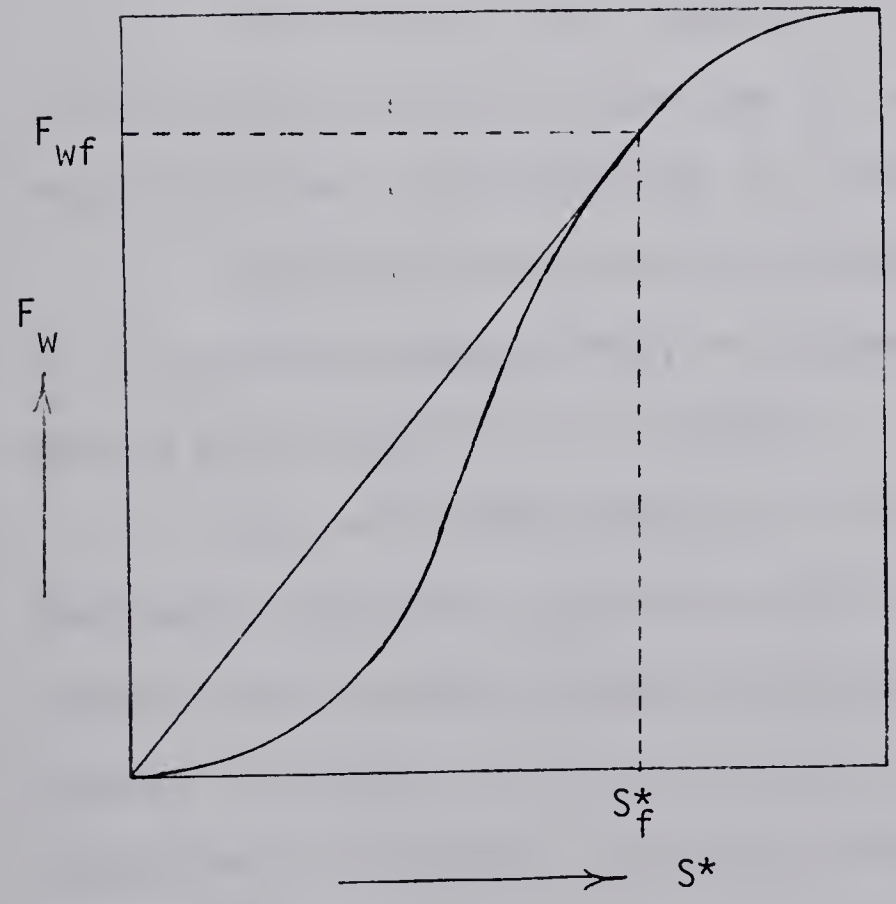


FIGURE II-2



Buckley-Leverett Solution (1942)



Welge's Tangent Construction (1952)

FIGURE II-3

its maximum value, $1 - S_{or}$, prior to water breakthrough.

Interest was also focussed on solving Eq. (II-6) and Eq. (II-7), either combined together, [Fayers and Sheldon[17], 1959] or solved seperately, [McEwen[38], 1959] in the fractional flow domain, viz. $f_w(S^*, \tau^*)$. These studies demonstrated that when the complete immiscible displacement equation is solved (i.e. including the capillary term) the multi-valued saturations were eliminated.

Hovanessian[28] [1961] solved the immiscible displacement equation using a transformation similar to that of Douglas[16] et al. and found that the magnitude of the initial water saturation distribution, essential in getting the numerical procedure started, did not effect the shape of the profiles later on in the life of the flood.

After these initial numerical solutions, stress was placed on optimizing the various algorithms for accuracy and computer processing time. [Gottfried[22] et al. (1966); Blair[8] et al. (1969)].

Numerical solution of the immiscible displacement equation in the saturation domain, $S^*(\xi, \tau^*)$, without any transformation, was carried out by Flock[19] et al. [1977].

Bentsen[6] [1977] solved Eq. (II-6) and Eq. (II-7) in the fractional flow domain, $f_w(S^*, \tau^*)$, with a more appropriate inlet boundary condition which allows the saturation to build-up to a maximum, in contrast to all the previous solutions which fixed the saturation at the maximum. This was physically realistic. [Perkins[43], 1957]. It was also demonstrated that the Buckley-Leverett[10] solution is, in fact, the steady state solution to the immiscible displacement equation. Eq.(II-6) and Eq.(II-7), when combined and

the variable ξ eliminated, results in, [Bentsen[6], p.26],

$$[f_w(S^*, \tau^*) - G(S^*)]^2 \frac{\partial^2 f_w(S^*, \tau^*)}{\partial S^{*2}} = N_c C(S^*) \frac{\partial f_w(S^*, \tau^*)}{\partial \tau^*} \qquad \text{(II-21)}$$

As a consequence of Eq.(II-21), Bentsen[6] postulated that the $f_w(S^*, \tau^*)$ function approaches the $G(S^*)$ function in the fractional flow domain. [Fig.II-4]. The $G(S^*)$ function is the non-capillary fractional flow curve. At that instant when $f_w(S^*, \tau^*)$ becomes invariant with time (steady state), Eq.(II-21) can be written as,

$$[f_w(S^*) - G(S^*)]^2 \frac{\partial^2 f_w}{\partial S^{*2}} = 0 \qquad \text{(II-22)}$$

For Eq.(II-22) to hold, either of the terms on the left hand side can be equated to zero resulting in either

$$f_w(S^*) = G(S^*) \qquad S_f^* \leq S^* \leq 1 \qquad \text{(II-23)}$$

or

$$f_w(S^*) = f_{wf} \frac{S^*}{S_f^*} \qquad 0 \leq S^* \leq S_f^* \qquad \text{(II-24)}$$

Eq.(II-23) and Eq.(II-24) are also evident from Fig.II-4.

As a consequence, the analysis undertaken by Bentsen[6] in the $f_w(S^*, \tau^*)$ domain resulted in an interesting observation in the $S^*(\xi, \tau^*)$ domain. As the $f_w(S^*, \tau^*)$ function approaches $G(S^*)$, the saturation profiles tend toward a fixed configuration for saturations less than S_f^*, which is the "stabilized zone" postulated by Terwilliger[51] et al. [1951] and further analysed by Jones-Parra and Calhoun[31] [1953].

BEHAVIOUR OF $f_w(S^*, \tau^*)$

(after Bentsen, 1977)

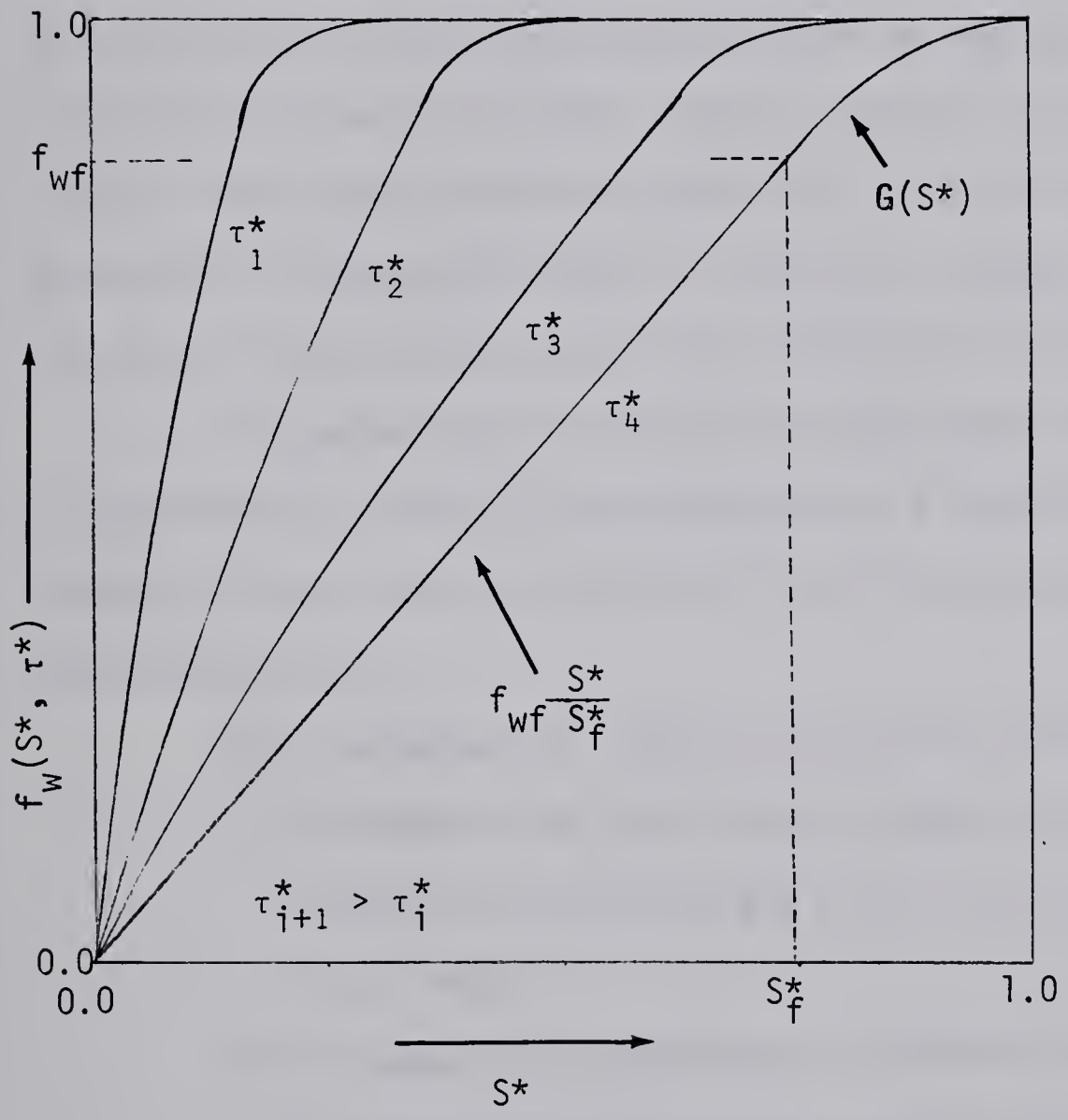


FIGURE II-4

II.2 ROLE OF SATURATION PROFILES

It is well established that the solutions to Eq.(II-6) and Eq.(II-7) or Eq.(II-5) are saturation profiles which in turn dictate the oil recovery from porous media. To solve these equations, independently determined or modelled relative permeability and capillary pressure functions are required. The numerical solution of the immiscible displacement equation can be analysed for different displacement rates or viscosity ratios. Parallel to the numerical studies, displacement experiments can also be conducted. Various oils can be used to study the effect of interfacial tension. By changing the type of porous medium the role of wettability can also be analyzed.

A rigorous test of immiscible displacement theory would be to experimentally measure the saturations as a function of time and distance. These saturation profiles could then be studied for different displacement tests.

Two approaches for analyzing saturation profiles are:

i) To compare the experimental saturation profiles amongst themselves by varying any one of the parameters. (viz. rate).

ii) To compare the experimental saturation profiles with the numerically generated ones based on the current immiscible displacement theory.

The second approach requires a judicious selection of relative permeability and capillary pressure models.

II.3 SATURATION MEASUREMENT TECHNIQUES

Saturations have been measured over a gross elemental volume, using the principle of discrimination between resistivities of brine and hydrocarbons. Wyckoff and Botset[55] [1936] and Leverett[34] [1939] used this technique to determine relative permeability curves. Levine[36] [1954] published one set of saturation prifiles using the same technique. This particular displacement test was an oil-flood at a favourable viscosity ratio (μ_w/μ_o = 0.52). Steber and Marsden[50] [1956] suggested one based on matched refractive indices. This was a step towards optical techniques.

Again using the resistivity technique, Perkins[43] [1957] reported two sets of saturation profiles, one at a low rate and another at a high rate. These two runs were waterfloods in the presence of connate water. The viscosity ratio was slightly adverse (μ_o/μ_w = 2.0).

Bail and Marsden[7] [1957], using a resitivity-brine saturation correlation, reported six runs with rates ranging from 0.00145 cc/sec (5.2 cc/hr) to 0.0098 cc/sec (35.28 cc/hr) giving a superficial velocity for their core from 7.727 (10^{-5}) cm/sec to 52.2 (10^{-5}) cm/sec. In their water-floods they maintained a constant viscosity ratio (μ_o/μ_w) of 2.44 at 30°C.

Scrutinising the saturation profiles published upto this time it was evident that much more experimentation needed to be done both qualitatively and quantitatively. Efforts were being made in this direction and different techniques were proposed.

X-rays can be used in the determination of liquid saturations as their intensity loss exhibits a linear relationship with saturation

on a semi-log plot. [Geffen and Gladfelter[20], 1952]. For X-rays to be effective, the water has to be doped with sodium iodide or iodo-benzene has to be added to the liquid hydrocarbons.

In his paper on displacement stability, Hagoort[23] [1974] presented one profile from an experiment conducted at a low rate and compared it with the non-capillary Buckley-Leverett[10] solution. The technique he used was based on selective absorption of light. He used a transparent model and added 1% (wt.) cobalt-chloride to the water to colour it blue. The viscosity ratio in his experiments was 21.58. He did not present any profiles for those experiments in which displacements were termed "unstable".

Parsons[40] [1975], taking advantage of selective absorption of electro-magnetic radiation at certain frequencies for some substances, chose microwaves at 21.2 GHz which exhibit a strong absorption preference to water. He presented saturation profiles which were superior in quality to any published before. He presented two sets of profiles, an oil-flood with a viscosity ratio (μ_w/μ_o) of (1/8.5) [Parsons[42], 1978] and a subsequent water-flood on the same system after connate water was established. Using this technique to generate saturation profiles during a micellar flood, Parson and Jones[41] [1977] developed the concept of linear scaling. Baker[2] [1975] reported his results on the use of microwaves during a steam-flood. He reported difficulty in identifying water vapour in this kind of flood but suggested that quantitative calibration was possible for air-water, oil-water and oil-alcohol systems. Gladfelter[21] [1978] also used a set up, similar to that of Parsons[40], for saturation measurements.

II.4 CHOICE OF A SATURATION MEASUREMENT TECHNIQUE

To generate saturation profiles for this study, a technique based on microwave attenuation was chosen. Reasons for the selection of this technique were:

i) Resistivity techniques are cumbersome and measurements are made at discrete points with electrodes in contact with the core holder.

ii) X-rays and optical techniques need doping of one of the liquids with a foreign substance.

iii) Dissection or post-mortem of the porous medium essentially gives a qualitative view at one point in time.

iv) The microwave technique does not require physical contact with the core-holder and allows continuous monitoring of saturations[40].

v) Among the published saturation profiles, those measured using microwave techniques were of high quality.

CHAPTER III

MICROWAVE THEORY, EXPERIMENTAL EQUIPMENT AND PROCEDURE

III.1 MICROWAVE THEORY

The broad spectrum of electro-magnetic radiation encompasses frequencies ranging from X-rays having frequencies of more than $3(10^{17})$ Hz to very low frequencies. The electro-magnetic radiation termed microwaves has frequencies ranging from $3(10^{8})$ Hz to $3(10^{11})$ Hz. Visible light has a frequency range of $0.43(10^{16})$ Hz to $1.33(10^{16})$ Hz, greater than microwaves but less than X-rays. Vankoughnett[39] [1973, p.21] contends that

> "the fact that visible light and microwaves are both electro-magnetic waves suggests that they share common properties."

The laws governing microwave-material interaction, specifically microwave-water interaction, are important in understanding the experiments conducted to generate saturation profiles. Microwaves interact differently with different types of substances. Basically there are three classes of material: [Tinga[52], 1970] conductors, insulators and dielectrics. Conductors reflect microwaves so they are used to contain and guide them. Insulators reflect and transmit microwaves without any appreciable loss of power. They are almost "transparent" to microwaves.

Dielectrics, like water, are substances which absorb microwaves. This absorption of microwaves can be quantitatively predicted by two different approaches.

III.1.1 Electro-magnetic Approach

In a non-magnetic material, the absorption of microwaves depends on the dielectric constant for that material. A high dielectric constant indicates a greater absorption of microwaves.

A water molecule has a dipole moment associated with it. When an oscillating field is applied to water molecules they try to align themselves with the continuously changing field. This phenomenon is known as polarization. As a consequence the potential of the electric field is reduced. This reduction is dictated by the dielectric constant, ε', for the material. The dielectric constant is determined experimentally. [Hasted[26], et al., 1953].

In addition to the decrease in potential, there is a loss of power or irreversible degradation of energy manifested as heat. This loss of power or "attenuation" depends on the magnitude of another experimentally determined[26] quantity, ε'', known as the "loss factor".

A complex dielectric constant then can be defined as,

$$\varepsilon^* = \varepsilon' - i\varepsilon'' \qquad \text{(III-1)}$$

where variation of ε' and ε'' with frequency is shown in Fig.III-1. The loss factor, ε'', shows a definite peak at a specific frequency {Fig. III-2}. For water molecules this peak occurs at about 20 GHz[52].

DIELECTRIC CONSTANT AND LOSS FACTOR
VERSUS LOGARITHM OF FREQUENCY

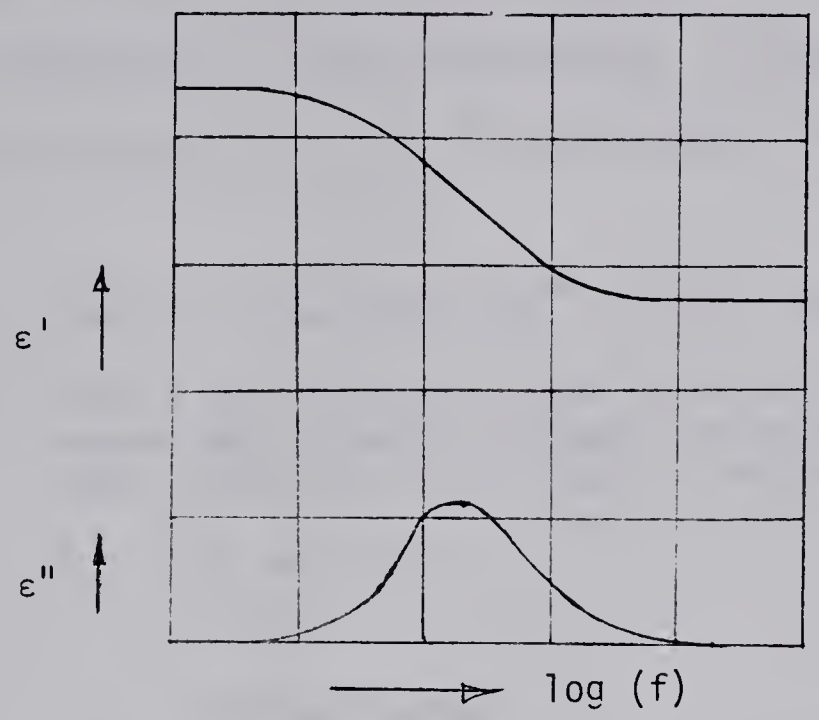


FIGURE III-1 (ref: Harvey, p.233)

LOSS FACTOR VERSUS FREQUENCY FOR DIFFERENT SUBSTANCES

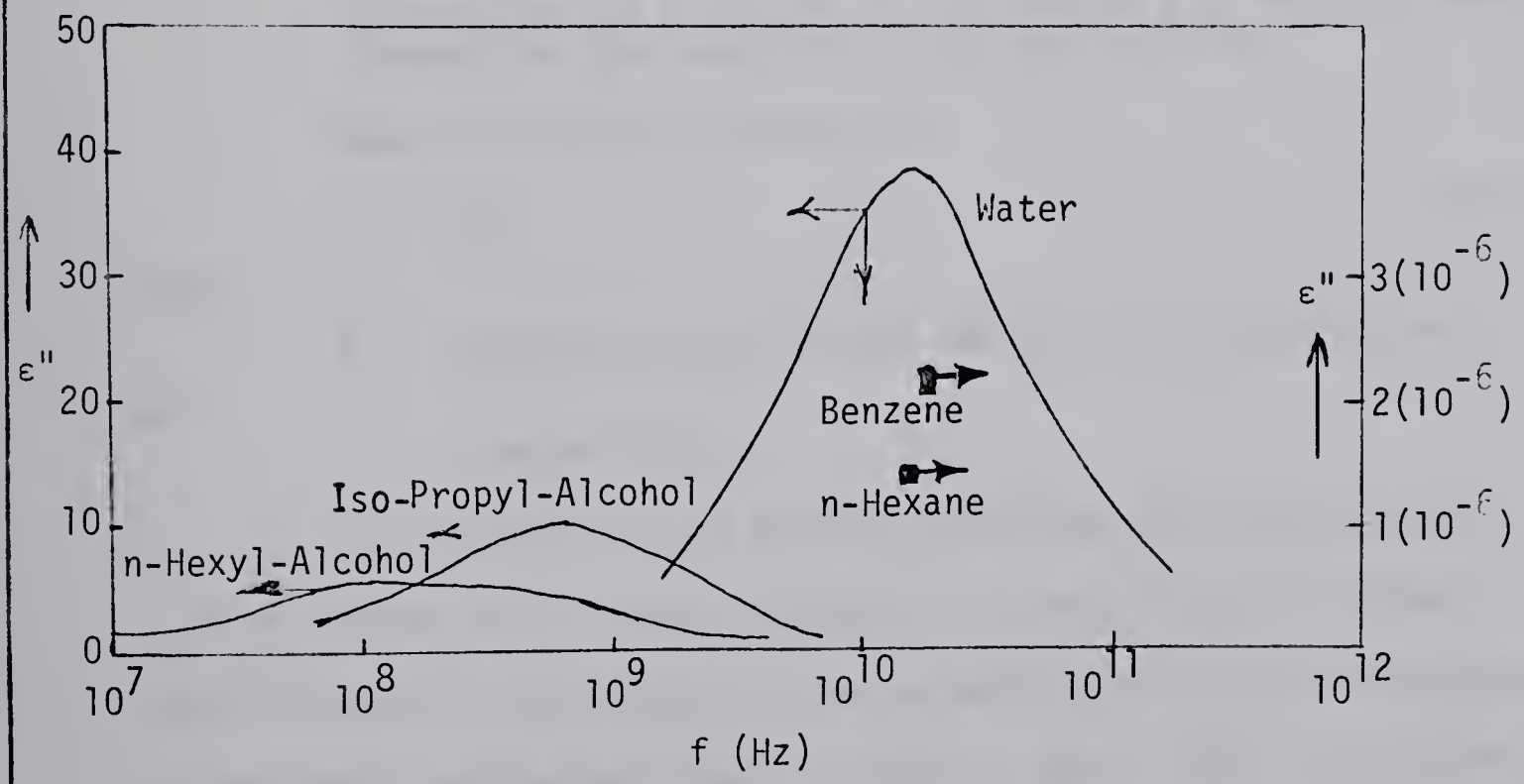


FIGURE III-2 (ref: Parsons, p.304)

III.1.2 Optical Approach

Both the electro-magnetic and the optical treatment of microwave-dielectric interaction is necessary to the understanding of the measurement of water saturations. Two laws of radiation absorption, extensively used in spectroscopy, are quoted here,

Lambert's Law [Harrison[24], p.363, 1948] which states that

> When a parallel beam (plane wave) of monochromatic radiation passes rectilinearly through a homogeneous medium, the power intensity of the beam is reduced as follows,

$$I_x = I_o \exp\{-Kx\} \qquad \text{(III-2)}$$

where

I_o = incident power

I_x = power after the beam has traversed a distance, x,

and

$\bar{K}$ = extinction coefficient.

Beer's Law [Harrison[24], p.364, 1948] which states that

> "If the absorbing medium is a substance in solution, the attenuation of radiation on traversing a given path length depends on the concentration of the solution".

Beer's Law can be written as,

$$\bar{K} = k\bar{c} \qquad \text{(III-3)}$$

where

k = extinction coefficient per unit of concentration,

and

$\bar{c}$ = concentration.

It is worthwhile to mention here that the concentration, $\bar{c}$, is analogous to the water saturation in that elemental volume which is being traversed by a plane, monochromatic beam of radiation. The remaining substances, like oils used in this study, Ottawa sand (silica) and PVC (material of core-holder), are almost transparent

to microwave radiation at 27 GHz. Figure III-2, taken from Parsons[40] [p.304], indicates the relative magnitudes of loss factors, ε'', for water and some organic compounds.

Equations (III-2) and (III-3) result in the relationship known as Beer-Lambert's Law,

$$I_x = I_o \exp\{-k\bar{c}x\} \qquad \text{(III-4)}$$

Several variations of this equation are employed, depending on the context of its usage. For use in the discussion of absorption, as derived from classical electro-magnetic theory [Harrison[24], p.369], the following equation is commonly used.

$$I_x = I_o \exp\{-(4\pi fxK)/c\} \qquad \text{(III-5)}$$

where

f = frequency, Hz,

x = distance traversed, cm,

and

c = velocity of light, cm/sec.

The extinction coefficient, $\bar{K}$, is related to the unit extinction coefficient and concentration as indicated by Eq.(III-3). In the context of the experiments conducted in this study, the concentration of the absorptive substance in the path of the microwave beam is

$$\bar{c} = \phi S_w \qquad \text{(III-6)}$$

Also x is the thickness of the core, h. One may substitute for K in Eq.(III-5) from Eq.(III-3) and for $\bar{c}$ from Eq.(III-6) to obtain

$$I_x = I_o \exp\{-(4\pi fhk\phi S_w)/c\} \qquad \text{(III-7)}$$

or

$$\log_{10} \frac{I_x}{I_o} = -\frac{4\pi fhk\phi S_w}{2.303c} \qquad \text{(III-8)}$$

III.1.3 Relationship Between Electro-magnetic and Optical Approaches

The two approaches can be related and the analysis by Dekker[15] [1957, p.156] is used to illustrate this. When there is absorption, the electrical component of the "light wave" polarized in the y-direction and propagated in the x-direction may be represented as

$$E_y(x, t) = E_i \exp\{-(2\pi fkx/c)\} \exp\{i2\pi f(t - \frac{nx}{c})\} \qquad \text{(III-9)}$$

where

E_i = electric field strength at x = 0,

$E_y(x,t)$ = electric field strength at a distance x, after time t,

and

n = refractive index.

This equation can be written as

$$E_y(x,t) = E_i \exp\{i2\pi f(t - n^*x/c)\} \qquad \text{(III-10)}$$

where the complex index of refraction is

$$n^* = n - ik, \qquad \text{(III-11)}$$

For a non-magnetic insulator, the velocity of propagation is given by

$$v_\phi = c/\sqrt{\varepsilon'}, \qquad \text{(III-12)}$$

while the index of refraction is defined as

$$n = c/v_\phi \qquad \text{(III-13)}$$

Equations (III-12) and (III-13) lead to

$$\varepsilon' = n^2 \qquad \text{(III-14)}$$

which can be written for a dielectric as

$$\varepsilon^* = n^{*2} \qquad \text{(III-15)}$$

Re-writing Eq.(III-1) and Eq.(III-11),

$$\varepsilon^* = \varepsilon' - i\varepsilon'' \qquad \text{(III-1)}$$

and

$$n^* = n - ik \qquad \text{(III-11)}$$

Substituting for ε^* and n^* in Eq.(III-15) yields

$$\varepsilon' - i\varepsilon'' = n^2 - 2ink - k^2. \qquad \text{(III-16)}$$

Equating the real and imaginary parts one obtains

$$\varepsilon' = n^2 - k^2 \qquad \text{(III-17)}$$

and

$$\varepsilon'' = 2nk \qquad \text{(III-18)}$$

These equations relate the extinction coefficient, k, to dielectric constant, ε', and the loss factor, ε''.

III.1.4 Quantitative Evaluation of the Extinction Coefficient

For the analysis of microwave responses obtained in this work, a theoretical guideline is given by Eq.(III-8). This equation indicates that for a constant porosity-thickness product, ϕh, along the length of the core, a plot of log I_x versus S_w will result in a straight line at a fixed frequency, f. In order to do a preliminary analysis so as to get some feel for this correlation, the equation can be solved for varying power inputs, I_o, and water saturations, S_w, to have an estimate of attenuated power outputs, I_x. To this end firstly, a theoretical estimate of the extinction coefficient, k, is needed.

Hasted, et al. have determined the dielectric constant, ε', and the loss factor, ε'', experimentally, for water at 20°C and

a microwave frequency of 23.6 GHz. Using Eq.(III-17) and Eq.(III-18) and the experimentally determined values of

$$\varepsilon' = 30.5$$

and

$$\varepsilon'' = 35.6$$

a value for the extinction coefficient, k, is obtained as 2.86. A simple analysis, using this theoretical value of k, is undertaken in Appendix C.

III.2 MICROWAVE INSTRUMENTATION

III.2.1 Antennas

Special kinds of directional antennas are needed to have a linearly polarized, plane, wave of electro-magnetic radiation. The transmitting and receiving antennas have to be identical by the general theorem of electro-magnetic reciprocity. [Chu and Barrow[12], 1939, p.333].

For the purpose of measuring water saturations a pyramidal horn with a lens antenna to alter the radiation pattern was selected[40]. The pyramidal horn transmits a spherical wave with primary and secondary lobes, but when a lens is placed on the mouth of the horn this spherical wave is transformed to a plane wave, given a suitable choice of refractive index and shapes of lens surfaces. [Fradin[18], 1961, p.13].

Based on the theory of refraction, in optics, [Fradin[18], p.265] a pair of lenses were designed for a pyramidal horn. The details are given in Appendix C. Polystyrene was chosen as the material for the lens because of its low loss factor, ε''. The

refractive index of the polystyrene used was 1.6 [Brown[9], 1953, p.32].

III.2.2 Instrumentation

A schematic plan view of the experimental set-up is shown in Figure III-6. Microwaves, at a constant frequency of 27 GHz, were generated by an oscillator/R.F. unit. (Hewlett Packard, HP8679A). This unit has an automatic level control which senses a feedback from a crystal detector (HP R422A). The crystal detector takes a minute fraction of the radiation with the help of a directional coupler (HP R752D) placed downstream of the oscillator. A filter (HP R362A) and a tuner were also placed in the circuit between the directional coupler and the oscillator. The operating frequency of 27 GHz lies in the R-band of the microwave spectrum, so appropriate waveguides were used for transmission. From the directional coupler the microwaves were transmitted to the sending horn and lens antenna. The sending and receiving horns are shown in position, relative to the core-holder, in Figure III-5.

The microwaves were attenuated in accordance with Eq.(III-8) and were received on the opposite side by the horn and lens antenna. A thermistor mount (HP R486A) was used for detection and conversion to a signal suitable for the power meter (HP 431C). The power meter indicated the power magnitude in milli-watts and this power, converted to a proportional d.c. voltage, was fed to the Y-axis of the X-Y recorder. A close up of the microwave instrumentation is shown in Figure III-4.

III.2.3 Bench Experiment

A semi-log plot of attenuation versus power transmitted and received by the horns is shown in Figure III-7. Power received is

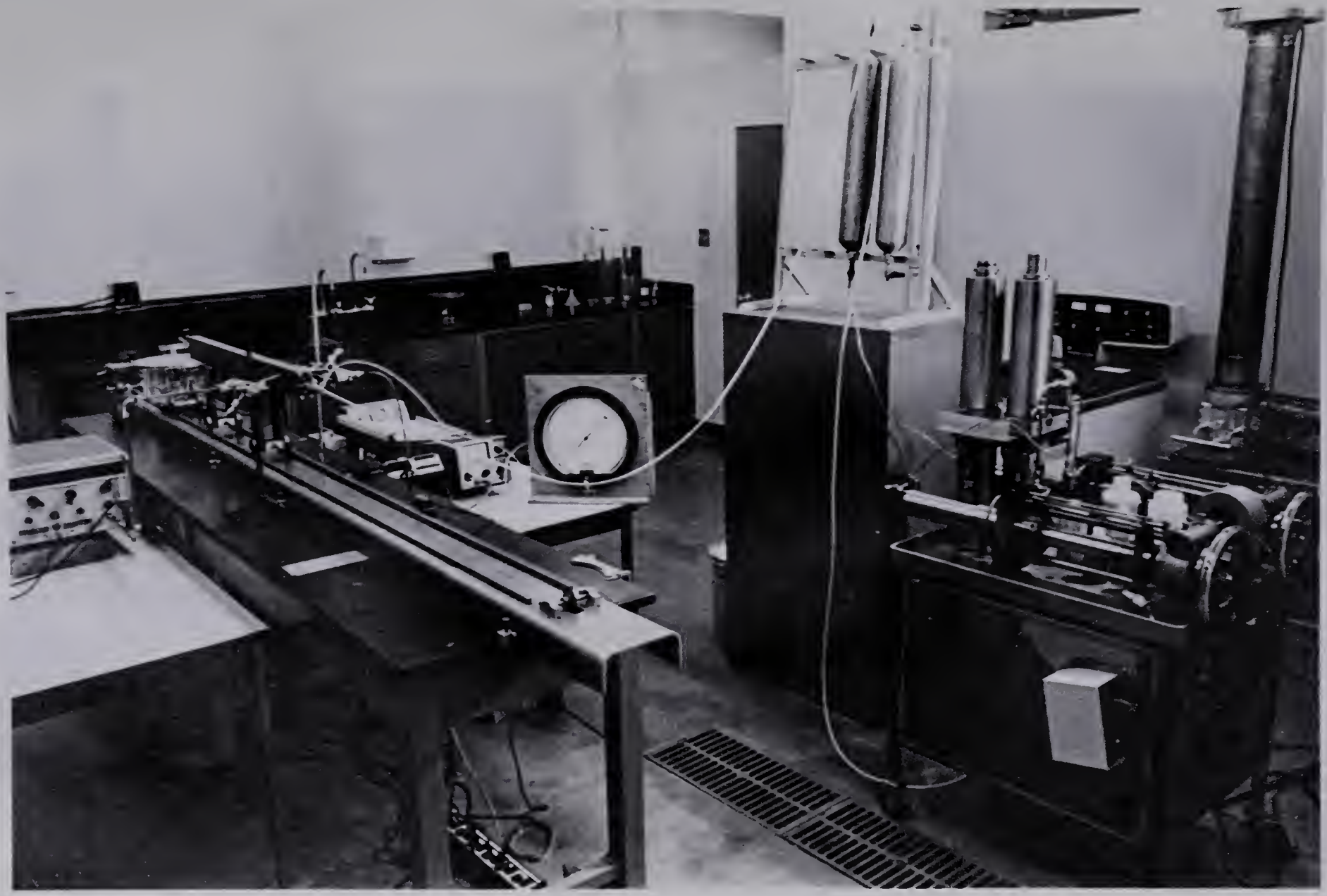


FIGURE III-3

COMPLETE EXPERIMENTAL SET UP SHOWING MICRO-
WAVE AND FLUID INJECTION SYSTEMS



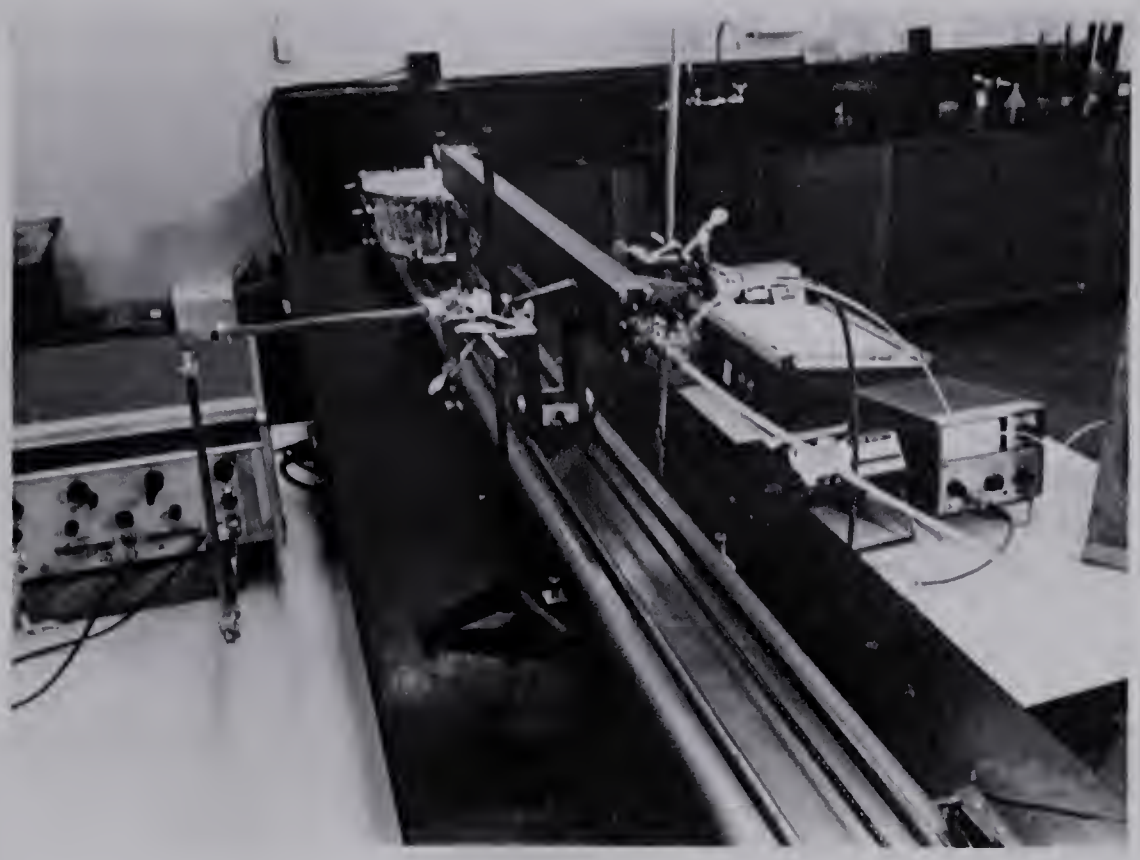


FIGURE III-4

CLOSER VIEW OF MICROWAVE INSTRUMENTATION

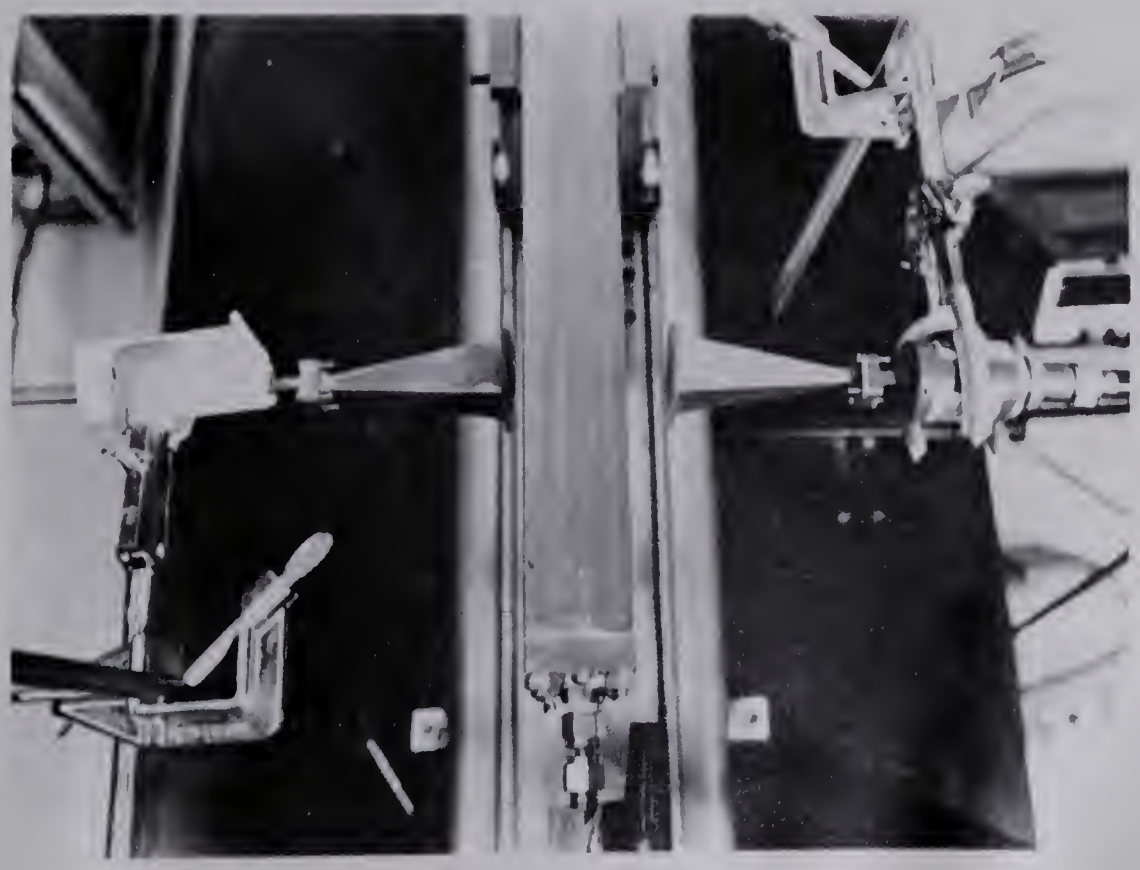


FIGURE III-5

HORN AND LENS ANTENNAS IN POSITION



shown along two straight lines, one with the lenses on, and one without them. This bench experiment, with the antennas three inches apart in the air, clearly demonstrates the advantage of using a lens in conjunction with the horn. An eighteen percent gain in received power is observed because the spherical wave is converted to a plane wave, thus reducing the leakage to atmosphere.

III.3 FLUID INJECTION SYSTEM, CORE HOLDER AND ALLIED EQUIPMENT

A Ruska pump was used to inject mercury into the cylinders (Fig.III-6). This mercury, in turn, displaced either oil or water, whichever the case may be. This liquid was injected into the core holder through flexible Tygon tubing and the usual valves and fittings. Pressure was measured just before the inlet to the core holder with a Heise pressure gauge having a precision of 0.2 psi (1.379 kPa).

The core holder had a rectangular cross-section so that the microwaves would traverse the same thickness along the height of the core. The core holder was fabricated from PVC and no appreciable attenuation of microwave power was observed through it. The PVC sheet was 1.27 cm thick. Two core holders were used in this study. These were approximately of the same dimensions. Details concerning the core holders are available in Table III-1.

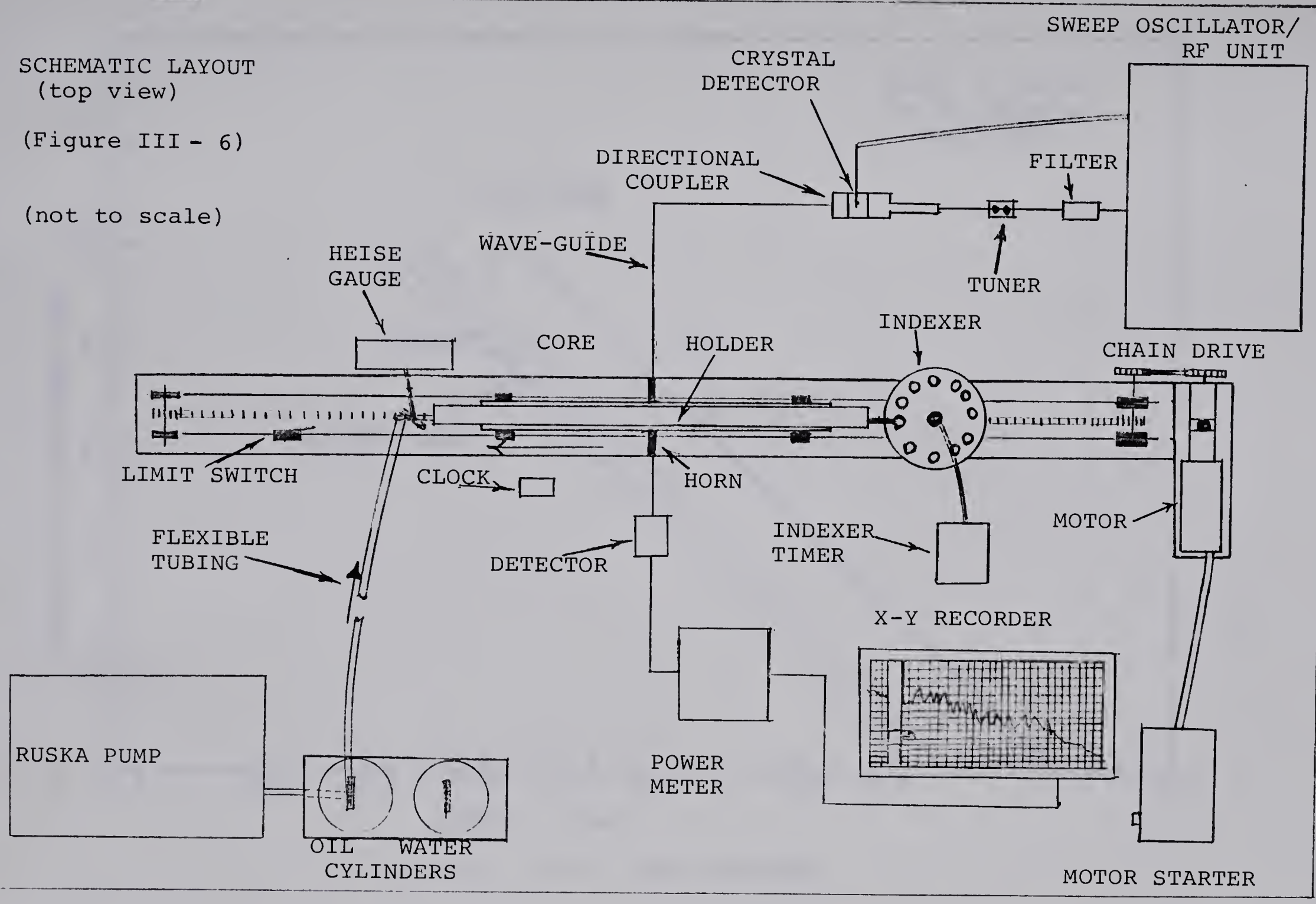
TABLE III-1

Core Holder No.	Thickness (cm)	Cross-sectional Area (cm^2)	Length (cm)	Run Nos.
1	1.350	6.859	91.44	8 to 15
2	1.270	6.477	91.93	16,18-21, 23, 24

SCHEMATIC LAYOUT
(top view)

(Figure III - 6)

(not to scale)



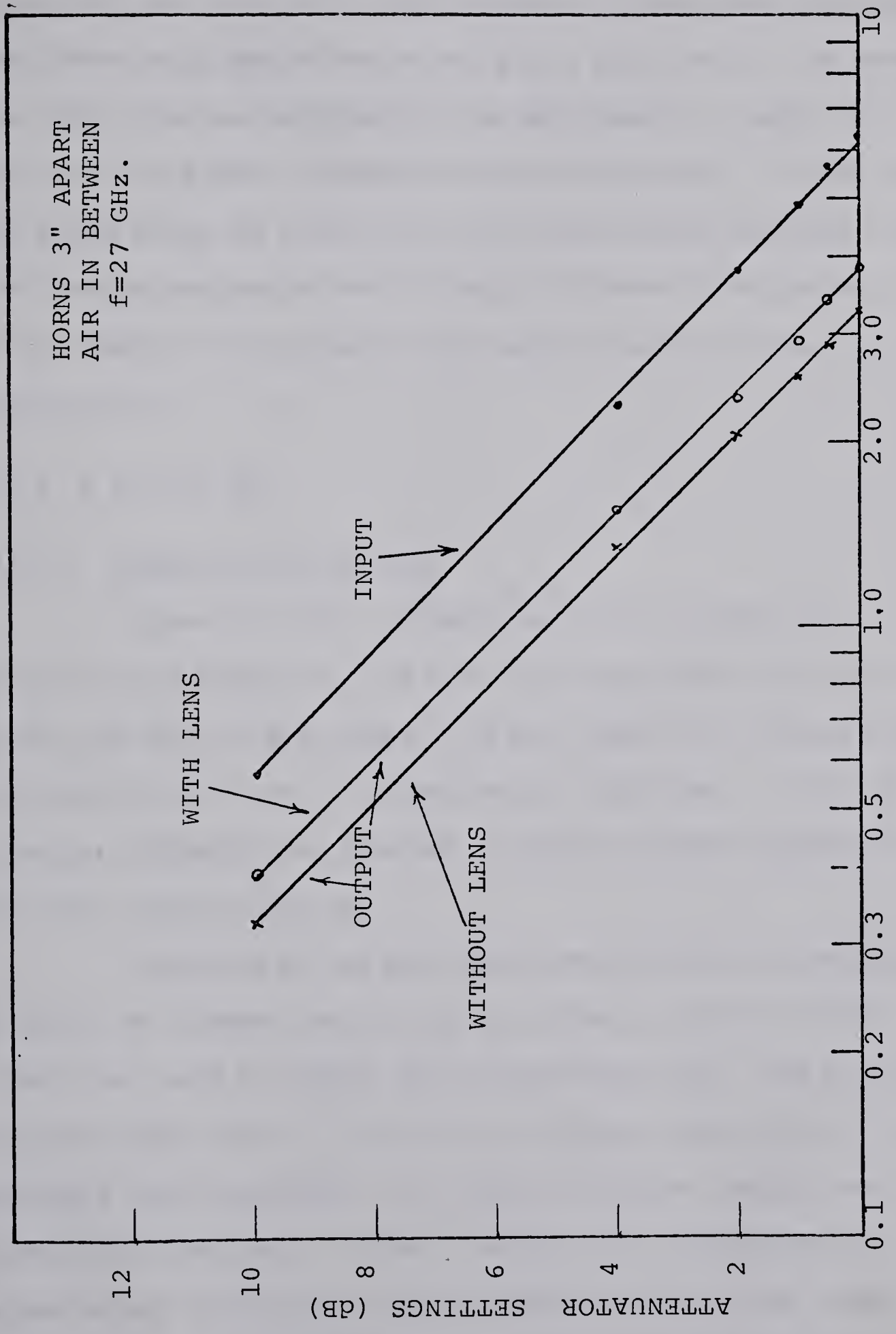


FIGURE III-7 BENCH EXPERIMENT



The liquids were collected in 50 cc tubes which were placed in a fractional collector. The core-holder was mounted on brackets with wheels and, similarly, the fractional collector was also mobile. Both these units were driven on rails by a chain drive. The power to the chain drive was imparted by a variable speed d.c. motor, of one-sixth horse power, through a series of sprockets. A limit switch was placed along the rails and its position could be adjusted. The limit switch was used to shut the motor off when it was pushed by one of the wheels. A photograph of the complete set-up is shown in Figure III-3.

III.4 A TYPICAL RUN

III.4.1 Preparation of the Core

Ottawa sand (80 - 120 mesh) was used to prepare an unconsolidated sand pack. The mass of the core holder was determined before and after it was packed. The core holder was vibrated using low amplitude vibrators for approximately eight hours. During this time some settlement was observed. The sand was then topped-off and the inlet end plate put on.

The design of the core holder was such that the outlet end plate was an integral part of the core holder. Sintered teflon inserts were used to contain the unconsolidated sand, both at the inlet and outlet ends. The thickness of these inserts was 0.3 cm and they were highly permeable. The sand pack and the inserts were changed for every run. The total length of the core-holder was approximately 10 cm longer than the effective length (the length containing sand). These 10 cm were at the inlet end and contained

the inlet end extension (made of PVC) plus the inlet end teflon insert. This measure was taken to keep the stainless steel bolts, used for securing the inlet end plate, away from the microwave beam, so as not to cause interference. The core holder, with the sand in it, was first weighed and then mounted on the brackets.

The position of the limit switch and the speed of the d.c. motor were adjusted so that the travel time of the core-holder was 15 seconds, from the inlet to the outlet end, relative to the position of horn antennas. This was done because the speed of the stylus along the X-axis of the X-Y recorder was kept constant at 1 inch/sec, while the length of the X-axis was 15 inches. This synchronized the movement of the core holder, relative to the microwave beam, with the travel time of the stylus of the X-Y recorder in the x-direction, during a scan.

The microwave equipment was turned on, and the horns properly aligned (Fig.III-5). First, a scan, with only air between the horns, was taken and the power meter setting, R_s, and X-Y recorder scaling factor, S_c, noted. Then a dry scan was carried out (S_w = 0%) along the length of the core holder (Fig.III-8). The scan was conducted by simultaneously starting the motor and the X-Y recorder. A microwave response was obtained. This enabled the calculation of the power, RDRY, coming out of the core at 0% water saturation.

In order to saturate the core with water or a glycerine-water mixture (displacing liquid in the subsequent waterflood), a vacuum was pulled on the core. Water was injected at a rate of 1000 cc/hr and the volume was noted.

A preliminary estimate of the pore volume was calculated using the equation,

$$\text{Pore Volume} = \left\{ V - \frac{m}{\rho_g} \right\} \text{cc} \qquad \text{(III-19)}$$

where

m = mass of the sand in the core-holder, gm,

V = volume of the core-holder, cc,

and

ρ_g = grain density of Ottawa sand = 2.64 gm/cc.

When this calculated pore volume, PV, was approached during saturation of the core, the pressure rose and the outlet valve was opened. The liquid through-put was allowed to stabilize and the total pressure drop across the core, ΔP, was recorded for subsequent computation of the absolute permeability. After a careful material balance on the liquid, the pore volume, PV, was determined.

Because of equipment considerations, described later on, a microwave response was not obtained at 100% S_w when water was the saturating liquid. But for favourable ($\mu_o/\mu_w < 1$) water-floods a mixture of glycerine and water was used as the displacing liquid. The glycerine-water mixture, as can be seen later, has a lower extinction coefficient, k, and consequently, with the equipment used, a response was obtained at 100% S_w. (Figure III-10).

The pack was kept saturated with water (or glycerine-water mixture) for ten to fifteen hours so as to render the sand water-wet.

III.4.2 The Oilflood

In order to establish an initial water saturation, S_{wi}, an oilflood was conducted. The rate during each oilflood was the same

in a particular series of runs (same μ_o/μ_w), irrespective of the rates used in the subsequent waterfloods. This was considered important so as to have similar conditions for every run (in a series) during the establishment of S_{wi}.

Several random microwave scans were conducted during an oilflood (Fig.III-8). This helped to keep a check on the displacement and to follow the flood front during the course of the oilflood. The oilflood was continued till no water was produced. At this time a microwave scan gave the response at S_{wi}.

III.4.3 Power Meter Settings and Scale Factors

Before describing a typical waterflood, it is necessary to briefly discuss power meter settings, X-Y recorder scale factors and the various techniques used in getting complete microwave responses.

Figure III-7 indicates that, with zero attenuation and a lens-horn antenna combination, the power measured at the receiving horn, through air, is approximately 3.85 mW. In Appendix C an analysis using Eq.III-7 is undertaken which shows that the attenuated signal coming out from the core can vary from 3 mW at 0% S_w to $0.6(10^{-6})$ mW at 100% S_w, when water is used as the displacing liquid.

During a single scan the power meter setting, R_s, and the X-Y recorder scale factor, S_c, have to be fixed. The microwave power output, which ranges from 3mW to $0.6(10^{-6})$ mW (say), cannot be recorded with a single combination of R_s and S_c. As water saturations vary from $1 - S_{or}$ to S_{wi} during a waterflood, such a spread in microwave responses is always to be expected.



FIGURE III-8 FACSIMILE OF RAW DATA

Consider a power of R mW coming out of the core. With a power meter setting of R_s the corresponding d.c. voltage at the output of the power meter will be, (Fig.III-11),

$$V(\text{volts}) = \frac{R(\text{mW})}{R_s(\text{mW/V})} \qquad \text{(III- 20)}$$

where

$$0 \leq V \leq 1.0$$

This d.c. voltage is recorded as a proportional length (in inches) on the Y-axis of the X-Y recorder. The scale factor, S_c, is related, to the voltage, V, and the distance travelled, Y, by the stylus of the X-Y recorder along the ordinate, through the equation.

$$Y(\text{inches}) = \frac{10^3 V(\text{volts})}{S_c(\text{mV/inch})} \qquad \text{[Ref. Fig.III-12]} \quad \text{(III-21)}$$

where

$0 \leq Y \leq 10$ (because the length of Y-axis is 10 inches)

Re-writing Eq.(III-21),

$$V = \frac{(S_c)(Y)}{10^3} \qquad \text{(III-22)}$$

Substituting for V in Eq.(III-20) from Eq.(III-22) and solving for R one obtains

$$R = (R_s)(S_c)(Y)10^{-3}\text{mW} \qquad \text{(III-23)}$$

In the experiments conducted for this study, power meter settings, R_s, took the values of 0.01, 0.1, 1.0 and 10 mW/V while scale factors, S_c, of 10, 50 and 100 mV/inch were employed. Considering the extrame case of S_c = 10 mV/inch and R_s = 0.01 mW/V, with Y being read, quite accurately, at a minimum of (say) 0.5 inches, then the value of R measurable using this equipment can be computed

as follows:

Substituting for S_c, R_s and Y in Eq.(III-23), there results,

$$R = (0.01)(10)(0.5)10^{-3}mW$$

or

$$R = 0.5(10^{-4})\ mW$$

or

$$\log_{10}R = -4.3 \qquad \text{(III-24)}$$

A cursory glance at the saturation profiles in Appendix A, for those runs in which water was the displacing liquid, will show that the minimum $\log_{10}R$ response is close to the number computed in Eq.(III-24).

III.4.4 The Waterflood

Before a constant rate waterflood is started, the total pressure drop at the initial water saturation is recorded. This pressure drop is required to compute the effective permeability, K_{or}, at $\bar{S}_{wi}$. The initial water saturation, $\bar{S}_{wi}$, is an average value based on a knowledge of the pore volume, PV, and the material balance on the oil in the preceding oilflood.

The waterflood was now started. A TIME-IT* precision watch was used to record the time from the inception of the flood. This gave the time in minutes with a precision of one-hundredth of a minute.

Usually one pore volume of displacing liquid was injected before the constant rate waterflood was culminated. This also gave

* Precision Scientific Co., Chicago, Ill., U.S.A.

the opportunity to record the oil production after the breakthrough of the displacing liquid.

Saturation scans were undertaken at suitable time intervals. To obtain a complete microwave response, at any instant, the core was scanned thrice. The three scans were conducted using different power meter settings, R_s, but usually the same scale factor, S_c. Figure III-9 is a facsimile of a raw data sheet as observed on the X-Y recorder, at forty minutes since the inception of the waterflood, during Run 18. The figure shows three responses at power meter settings of 0.01, 0.1 and 1 mW/V, the scale factor, S_c, being the same in all the three scans (50 mV/inch). The importance of conducting three scans becomes evident upon inspecting the raw data. For example, the microwave response at an R_s of 1 mW/V is virtually zero for the region, $0.4 \leq \xi \leq 0.6$, but in the same region, at an R_s of 0.1 mW/V, the response indicates a saturation gradient behind the front. This saturation gradient could not have been recorded, if different settings of the power meter were not used.

The total pressure drop across the core and the cumulative oil or oil/water produced were also recorded, whenever saturation scans were undertaken. The breakthrough point was taken as the instant when the first water droplet was seen coming out of the core.

III.5 ANALYSIS OF ERRORS

Errors which could have occurred during the course of experimentation are itemized below. Where possible, an attempt has been made to estimate a quantitative upper bound for them.

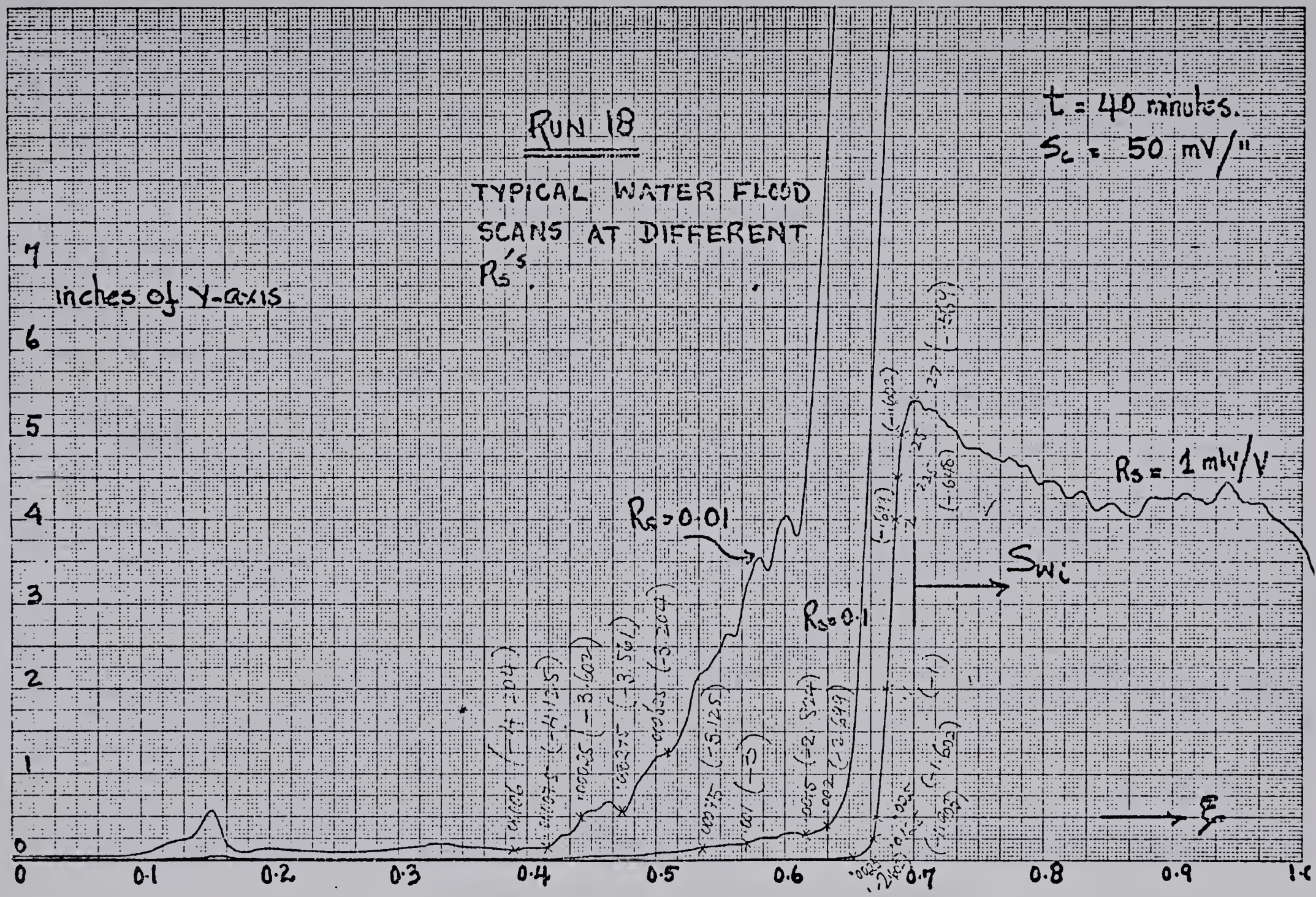


FIGURE III-9 FACSIMILE OF RAW DATA

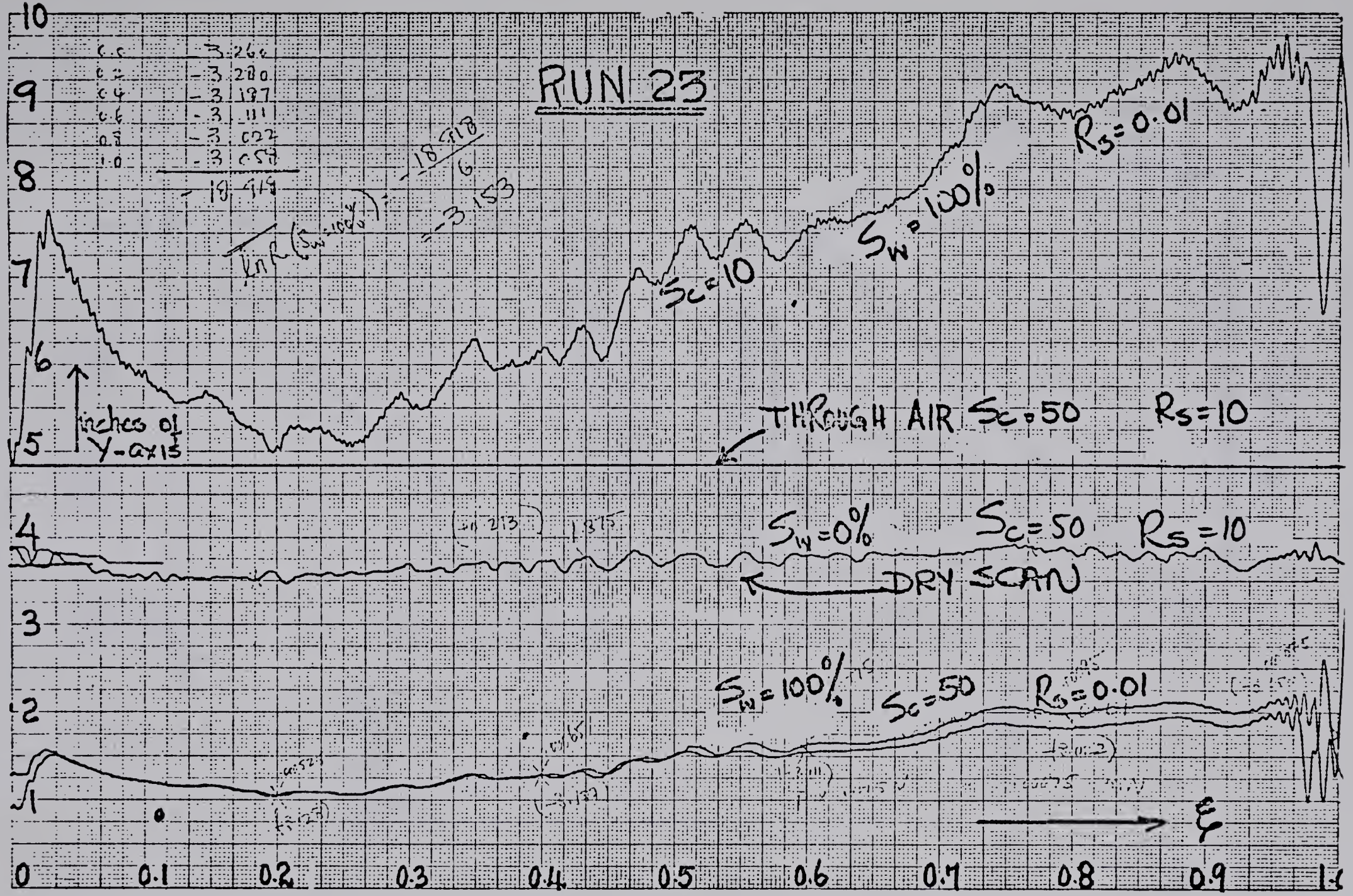


FIGURE III-10 FACSIMILE OF RAW DATA

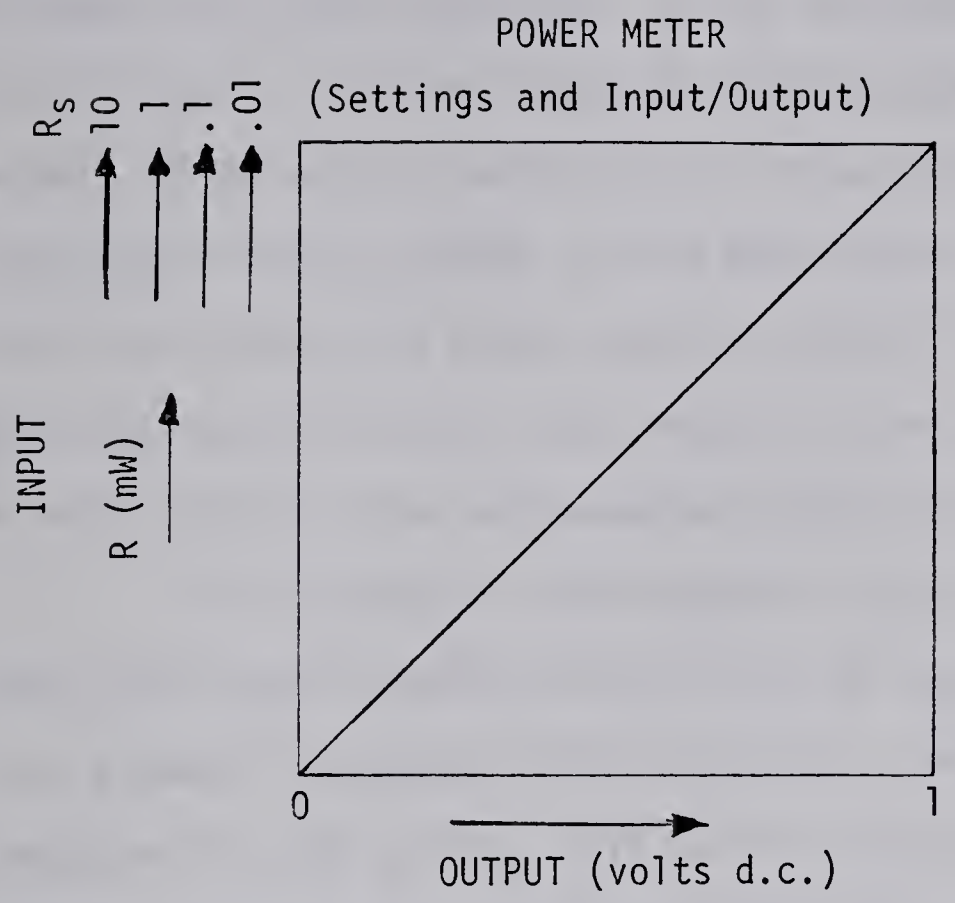


FIGURE III-11

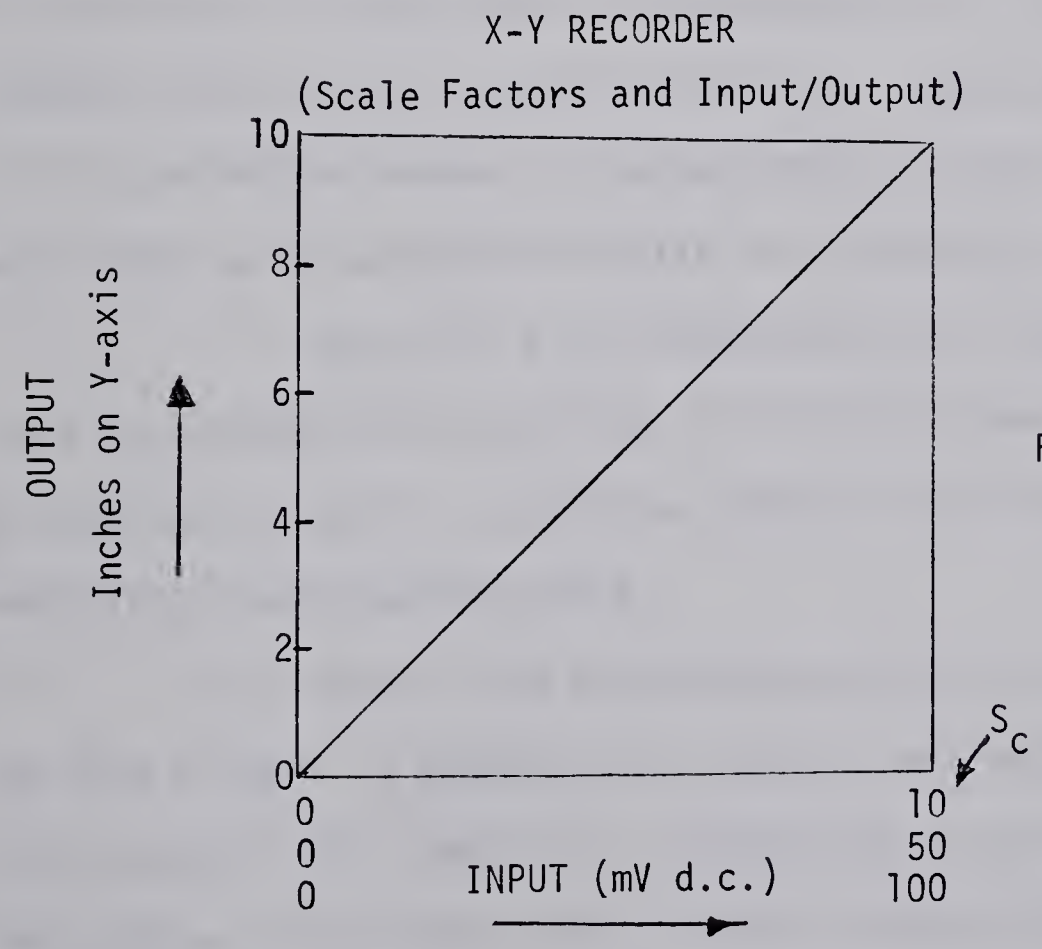


FIGURE III-12

i) During a water flood, for a particular time, three microwave scans were conducted. In the conversion to a saturation profile these scans were assumed to depict saturations at the same instant, which was not exactly true. It was estimated that it takes a maximum of ninety seconds to scan three times. For a 300 cc/hr waterflood, using core holder number 2 (Table III-1), the maximum percentage relative error, with respect to the length of the core, in the location of the last measured saturation, was 1.26 percent.

ii) Saturation scans appear to be continuous but, in actual fact over an infinitesimal period of time, an average saturation in an elemental volume was being recorded. The horn antenna had a dimension of 3.462 cm (Fig. C-1) in the vertical plane. The vertical dimension of the core holder was 5.08 cm. Thus, 68% of the height was penetrated and was taken as representative of the elemental volume computed using the full height of the core. Based on the dimensions of the core holder number 2, the percentage of total volume which was penetrated, at a particular instant, was computed as 2.33%.

Also, for a core holder having a length of 91.93 cm and a beam width of 2.15 cm (Fig. C-1), forty three electrodes would be required to obtain a resolution similar to microwave scans, if the resistivity technique were used.

iii) Energy loss through attenuation was dissipated in the form of heat. A quantitative analysis carried out for the power levels used in this study gave a temperature rise of 0.432°C/min. The exposure to microwaves for the whole length of the core was fifteen seconds in any one scan, so the temperature rise was not an influence of any consequence [Parsons[40], p.305].

iv) Another source of error could have been the disturbance of the horn alignment while the run was being conducted. The horns were aligned, both in the vertical and horizontal planes, to give maximum power at the receiving end through air. This had to be done before the dry core scan and the proper alignment should have remained till the last water flood scan. Utmost care was taken in this regard, and periodic checks of the power received through the air were carried out. Power meter readings could have been in error, due to standing waves, if the load (core) was not matched. A tuner was included in the circuit to match the load.

v) The displacement of oil by the displacing liquid usually commenced in the inlet end fitting and along the PVC inlet insert. These have a cumulative volume of 7 cc. This volume of displacing liquid was injected and, as a consequence, the same volume of oil produced, before the actual displacement in the porous medium commenced at $\xi = 0$. Due to this, microwave scans measured saturation profiles which did not measure the first 7 cc of volume injected, although this volume was included in the material balance on oil. The material balance was corrected when experimental saturation profiles were compared with the numerical results. Corrected material balance values were used in the data bases compiled for the numerical simulators.

vi) At the moment when a waterflood commenced, the whole system from the Ruska pump to the outlet end of the core was at atmospheric pressure. The displacement took place above atmospheric pressure. The liquids in the core, theoretically, were considered incompressible, but the liquid system as a whole including the mercury

and the liquids in the cylinders had to be slightly compressed. The system compressibility shows up in the oil produced versus pore volume injected curve. Consequently, the linear portion of the oil produced, τ, versus pore volume injected, τ_i, curve does not always pass through the origin [Figures D-9 to D-12].

vii) The Heise pressure gauge used to measure the pressure at the inlet end (taken as ΔP, as outlet end was at atmospheric pressure) had a full scale reading of 100 psi. The precision was 0.2 psi. Thus errors may have been introduced at pressures of 1 psi and below.

viii) The water breakthrough point was taken at the instant when the first drop of water was visible at the outlet end. The outlet end fitting had a volume of 5 cc so the breakthrough from the porous medium occurred 5 cc before that. As this error was consistent in all the runs, the comparison between runs was done without regard to it. For absolute comparison with numerical results the breakthrough point has to be corrected accordingly. If due to the capillary discontinuity at the outlet end, the displacing liquid broke through after building up to a maximum, then this delay was also considered when runs were being compared among themselves.

CHAPTER IV

CONVERSION AND PREPARATION OF DATA FOR ANALYSIS

IV.1 INTRODUCTION

Fifteen displacement runs were conducted in this study. These were conducted on nearly identical, unconsolidated sand packs and were grouped according to the viscosity ratios (μ_o/μ_w). The water used as the displacing liquid at adverse viscosity ratios was of 1N salinity. At favourable viscosity ratios a mixture of water and glycerine was used. This mixture served two purposes: firstly it resulted in a high viscosity for the displacing liquid and secondly the extinction coefficient, k, was reduced. This enabled a response at 100% saturation of the displacing liquid to be obtained.

Table IV-1 gives a brief description of the runs conducted. Comprehensive data sets on individual runs are available in Appendix B.

The interfacial tension between the displaced and displacing liquids was determined using a Spinning Drop Tensiometer. The kinematic viscosity was measured using a Cannon Fenske Viscometer. The density was determined using a specific gravity bottle and a precision balance.

IV.2 CONVERSION OF MICROWAVE RESPONSE TO A SATURATION PROFILE

The relationship which governs microwave attenuation and saturation is given by Eq.(III-8). Rearranging this equation, one obtains

$$\log_{10} I_x = \log_{10} I_o - \frac{4\pi f h k \phi S_w}{2.303c} \qquad \text{(IV-1)}$$

TABLE IV-1

SUMMARY OF RUNS CONDUCTED

Run No.	μ_o/μ_w	Displacing Liquid	Displaced Liquid	Rate (cc/hr)
8	9.34	1N Saline Water	Dow-Corning	200
10	9.34	1N Saline Water	Dow-Corning	100
11	9.34	1N Saline Water	Dow-Corning	300
12	73.33	1N Saline Water	Paraffin Oil	25
13	73.33	1N Saline Water	Paraffin Oil	50
14	73.33	1N Saline Water	Paraffin Oil	80
15	73.33	1N Saline Water	Paraffin Oil	100
16	12.25	1N Saline Water	Mineral Oil*	100
18	12.25	1N Saline Water	Mineral Oil	100
19	12.25	1N Saline Water	Mineral Oil	100
20	12.25	1N Saline Water	Mineral Oil	200
21	12.25	1N Saline Water	Mineral Oil	300
9	0.266	Water + Glycerine	Kerosine	100
23	0.184	Water + Glycerine	Kerosine	100
24	0.184	Water + Glycerine	Kerosine	50

* Mineral oil was a blend of paraffin oil and heptane.

A constant power of I_o is being radiated towards the core holder at a fixed frequency, f. It is assumed that the porosity thickness product is essentially uniform along the length of the core. The extinction coefficient, k, is constant because during a run the same dielectric, either water or a glycerine-water mixture, is being injected. Given these assumptions, a linear relationship exists between $\log_{10} I_x$ and S_w.

The raw data facsimile of Figure III-8 is analysed and converted first. An average value for R (or I_x) from the dry scan response was determined. This was an arithmetic average along the length of the core. The power measured, R, was computed using Eq.(III-23). The logarithm of the average value of R gave RDRY. In all the runs conducted, RDRY varied between +1.0 and 0. An axis was laid out on the ordinate between +1.0 and -5.0, decreasing in the upward direction. The abscissa represented the normalized distance, ξ.

For those runs in which a glycerine-water mixture was used as the displacing liquid, the microwave response at 100% S_w was also obtained (Figure III-10). An arithmetic average of log R was taken which was denoted by RSAT.

The initial water saturation scan was converted next. By picking suitable points along the response curve, R was obtained using Eq.(III-23). The logarithms of the measured power were plotted against the normalized distance, ξ. The initial water saturation need not be uniform along the length of the core and, in reality, it varied. The variation was slight when the oilflood viscosity ratio was favourable, but significant (Run 9, Run 23 and Run 24) when it was adverse. An arithmetic average of log R was computed for the S_{wi} just plotted.

The average value of log R was termed RSWI and was taken as being representative of the average S_{wi} obtained by material balance.

The waterflood microwave responses (Figure III-9) were then converted to saturation profiles. Usually three scans were conducted to obtain one profile. Points were picked on these three responses according to the degree of resolution at different normalized distances. Only one response is read to obtain R, at every ξ. Eq.(III-23) enables the conversion of these responses to R. A plot of log R versus ξ gives the saturation profile for that time.

The microwave scan at residual oil saturation, S_{or}, was only obtained for runs conducted at favourable viscosity ratios. Like the initial water saturation, S_{or} also need not be uniform. An average log R for the S_{or} response was determined and this number, RSOR, was taken as being representative of the S_{or} computed from material balance considerations.

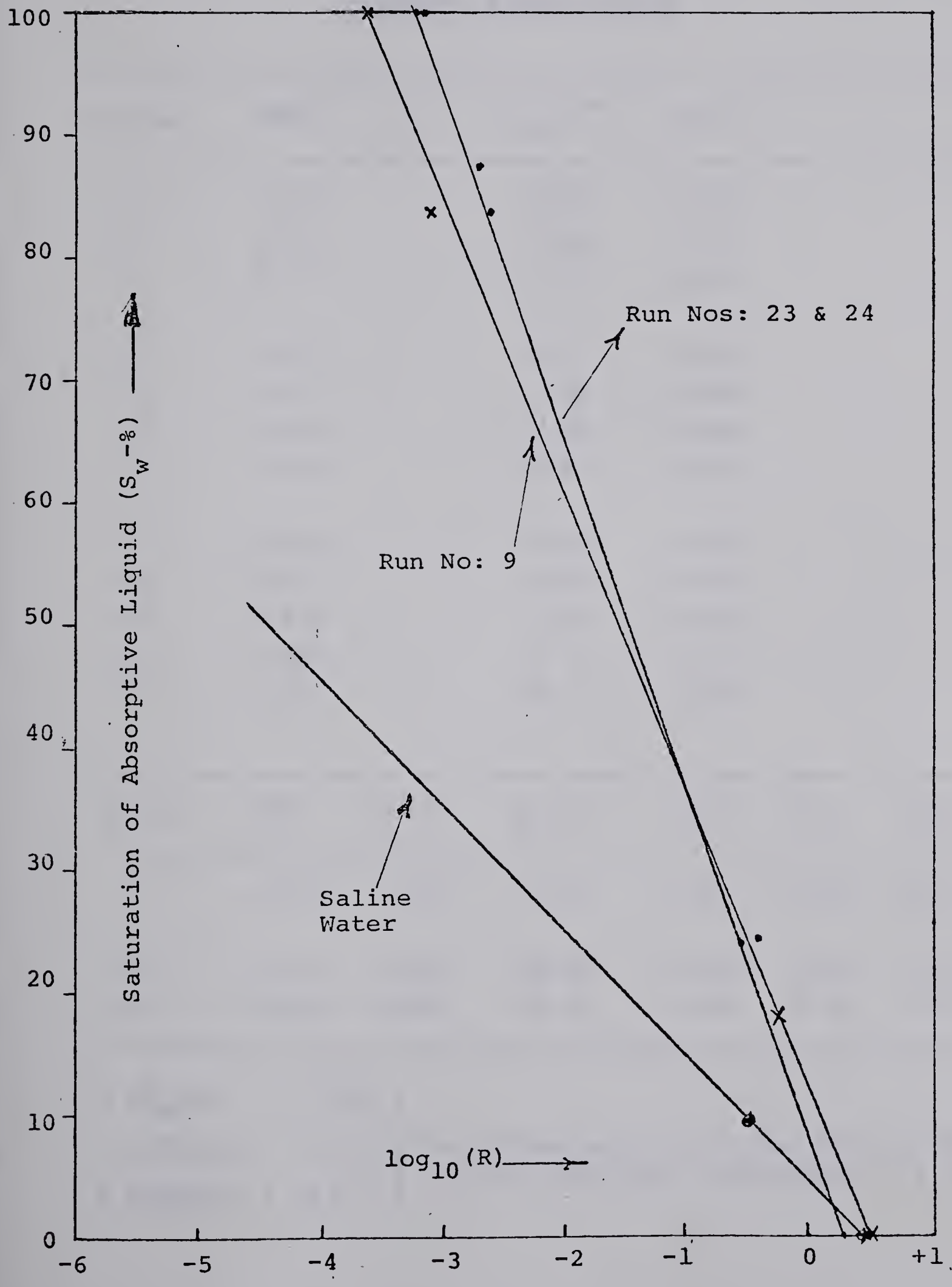
For all the runs, RDRY and RSWI were computed, but RSOR and RSAT could only be measured for the favourable viscosity ratio waterfloods. Figure IV-1 shows the plot of log R versus S_w. Three straight lines are drawn for illustration. The line for saline water represents all the runs conducted at adverse viscosity ratios. The remaining two are for the glycerine-water mixtures used at favourable viscosity ratios. Similar data are found in Table IV-2.

Saturation profiles, for all the runs plotted and calibrated, are available in Appendix A. The number written beside each profile is the cumulative pore volume produced, τ, up to the time the scans were conducted. These are uncorrected values of τ. In the profiles shown for runs 9, 23, 24 and 15 two numbers are

MICROWAVE SIGNAL-S_w CORRELATION: UNCONSOLIDATED OTTAWA SAND

P.V.C. CORE-HOLDER

(FIGURE IV-1)



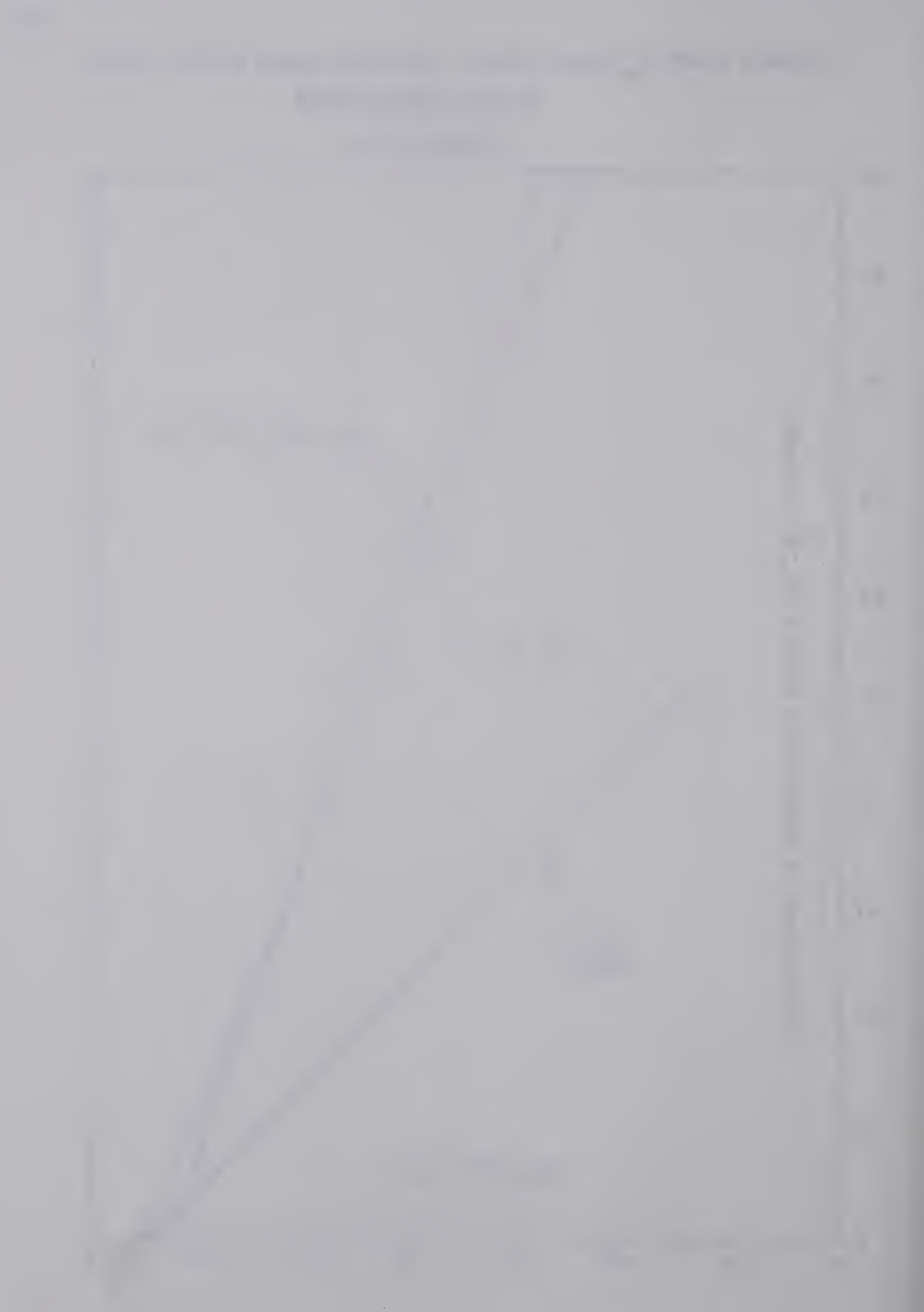


TABLE IV-2

MICROWAVE CALIBRATION DATA

Run No.	RDRY#	$\bar{S}_{wi}$(%)*	RSWI+
8	0.500	10.82	-0.450
10	0.470	12.60	-0.450
11	0.480	9.00	-0.450
12	0.520	9.10	-0.310
13	0.440	7.90	-0.280
14	0.340	7.90	-0.300
15	0.440	8.47	-0.350
16	0.273	10.65	-0.600
18	0.327	8.70	-0.500
19	0.317	6.10	-0.575
20	0.300	11.10	-0.550
21	0.460	10.18	-0.600

Run No.	RDRY	RSAT	$\bar{S}_{wi}$(%)	RSWI	$\bar{S}_{or}$	RSOR
9	0.510	-3.625	17.90	-0.250	16.34	-3.1
23	0.273	-3.153	23.80	-0.550	12.66	-2.7
24	0.474	-3.219	24.35	-0.400	16.30	-2.6

* $(\Sigma\bar{S}_{wi})/n$ = 9.38%

\+ $(\Sigma RSWI)/n$ = -0.451

\# $(\Sigma RDRY)/n$ = 0.41

These values were used to draw the straight line for saline water displacements in Fig.IV-1.

written beside the saturation profiles. The lower value is the planimetered area under the profile. By definition this number should be exactly equal to the oil produced in pore volumes, τ. But due to the experimental errors, mentioned before, the area under the profiles and the pore volume of oil produced are not exactly equal. Moreover τ has also to be corrected for the volume of the inlet end fittings.

IV.3 ERROR ANALYSIS ON SATURATION PROFILES

Relative errors for the material balance were computed for runs 9, 23, 24 and 15 using Eq.(IV-2).

$$\text{Relative Error} = \frac{(\tau_{corr} - \text{Area})100}{\tau_{corr}} \qquad \text{(IV-2)}$$

where

$$\tau_{corr} = \left\{\tau - \frac{7}{PV}\right\} \qquad \text{(IV-3)}$$

The relative errors are plotted against the corrected values of pore volumes of oil produced, τ_{corr}, and are depicted in Figure IV-2.

IV.4 PORE VOLUMES INJECTED, PORE VOLUMES OF OIL PRODUCED AND EFFECTIVE VISCOSITIES

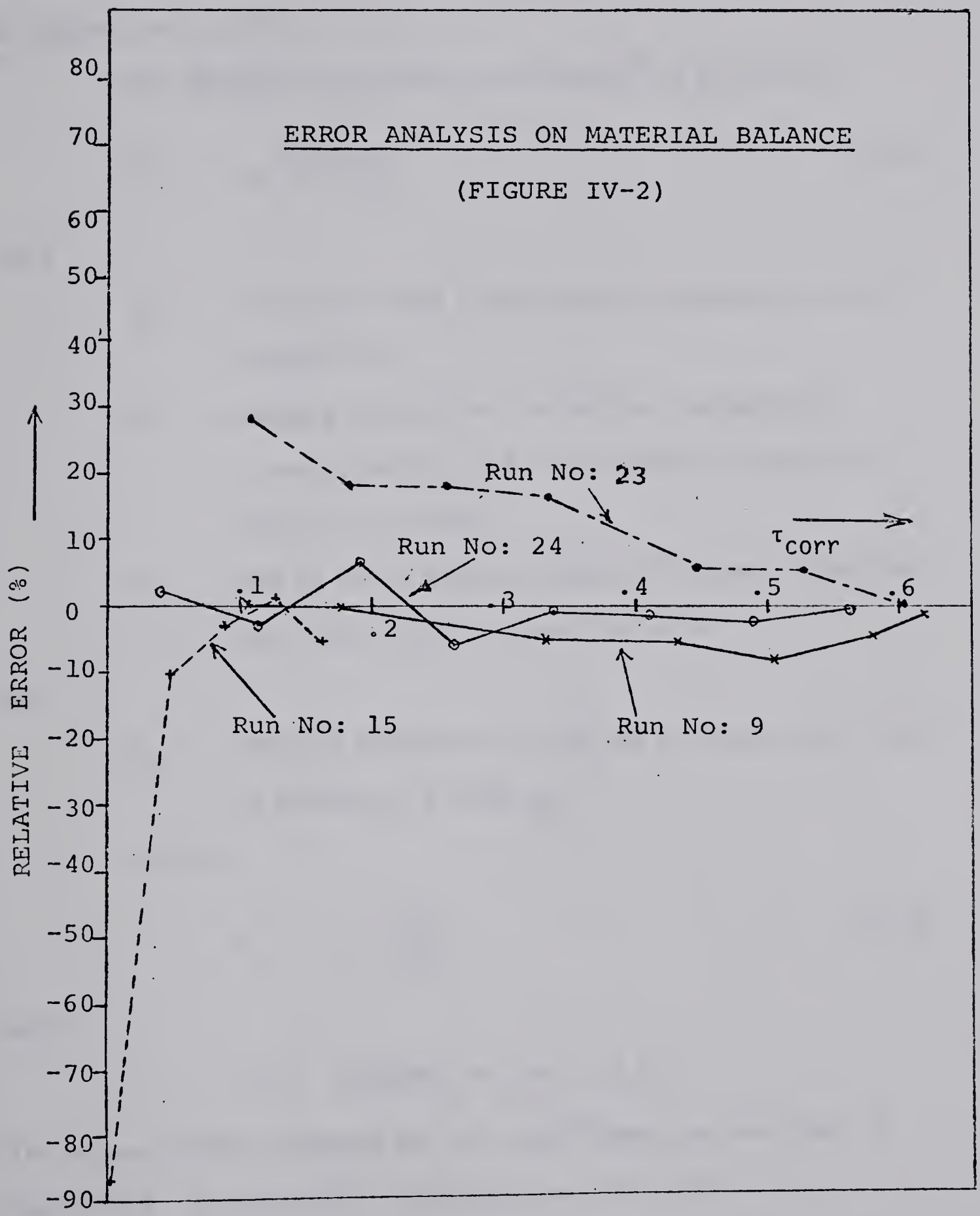
To estimate relative permeabilities from displacement data [Johnson[29] et al., 1959], the following curves have to be generated [Jones and Roszelle[30], 1978].

i) Effective viscosities, $\bar{\lambda}^{-1}$, versus pore volumes injected, τ_i

ii) Pore volumes of oil produced, τ, versus pore volumes injected, τ_i

ERROR ANALYSIS ON MATERIAL BALANCE

(FIGURE IV-2)



Data sets for τ (N_p/PV) versus τ_i are tabulated in Tables D-1 to D-15. Plots have also been generated and are placed in Appendix D, as Figures D-9 to D-12.

The effective viscosities are defined[30] by Eq.(IV-4),

$$\bar{\lambda}^{-1} = \mu_b \left(\frac{\Delta P}{q}\right)\left(\frac{q_b}{\Delta P_b}\right) \qquad \text{(IV-4)}$$

where

μ_b = viscosity of the liquid used to determine relative permeability,

ΔP = pressure across the core during a waterflood: it varies with τ, and is tabulated in Appendix D, Tables D-1 to D-15,

q_b = rate at which absolute permeability was determined,

q = waterflood rate for a particular run,

and

ΔP_b = pressure difference across the core when one liquid is flowing at a rate q_b.

Define

$$C_i = \mu_b \left(\frac{q_b}{q\Delta P_b}\right) \qquad \text{(IV-5)}$$

where

C_i = constant for the i-th run.

The values of this constant for all the fifteen runs are given in Table IV-3. To obtain $\bar{\lambda}^{-1}$, multiply C by ΔP in kPa.

Plots of $\bar{\lambda}^{-1}$ versus τ_i are placed in Appendix D as Figures D-5 to D-8.

TABLE IV-3

VALUES OF CONSTANT C TO DETERMINE
EFFECTIVE VISCOSITIES

Run No.	C(mPa-sec/kPa)
8	0.163
10	0.291
11	0.111
12	1.161
13	0.691
14	0.462
15	0.345
16	0.367
18	0.333
19	0.382
20	0.179
21	0.121
9	0.065
23	0.052
24	0.112

All the plots found in Appendix D, whether $\bar{\lambda}^{-1}$ versus τ_i or τ versus τ_i, are grouped according to the viscosity ratio used during a particular series of waterfloods.

IV.5 PRESSURE DIFFERENTIAL AND PORE VOLUME INJECTED

In order to compare ΔP versus τ_i, behaviour vis a vis experimental saturation profiles, plots of ΔP versus τ_i were generated. They were also grouped according to their viscosity ratios. The plots are shown in Figures D-1 to D-4 in Appendix D.

CHAPTER V

NUMERICAL SOLUTIONS AND COMPARISON WITH EXPERIMENTAL SATURATION PROFILES

V.1 INTRODUCTION

The one-dimensional immiscible displacement equation has been solved numerically by many researchers such as Douglas[16], et al. [1958], McEwen[38] [1959], Hovannessian[28] [1961] and Flock[19], et al. [1977] in the Eulerian domain and by Fayers and Sheldon[17] [1959] and Bentsen[6] [1977] in the Lagrangian domain. As experimentally measured saturation profiles are now available {Appendix A}, it is possible to compare the experimental profiles with solutions of the one-dimensional, immiscible displacement equation. This comparison was undertaken for the following reasons:

i) To gain more confidence in the experimental technique.

ii) To determine which numerical solution, Lagrangian or Eulerian, compares more favourably with the experimental saturation profiles.

iii) To gain further insight into the physics of immiscible displacement in porous media.

V.2 NUMERICAL SOLUTIONS

The one-dimensional immiscible displacement equation as nondimensionalized by Bentsen[3] [1976] may be written and solved in the following two formulations.

V.2.1 Lagrangian [Bentsen[6], 1977]

This formulation is in the fractional flow domain, $\{f_w(S^*, \tau^*)\}$, and the following three equations are solved successively, using their finite difference analogs, to arrive at a saturation profile, $S^*(\xi, \tau^*)$.

Consider the frontal advance formula [Buckley and Leverett[10]]

$$\left(\frac{\partial \xi}{\partial \tau^*}\right)_{S^*} = \left(\frac{\partial f_w}{\partial S^*}\right)_{\tau^*} \qquad \text{(V-1)}$$

Taking derivative of both sides of Eq.(V-1) and integrating between the limits zero and τ^*, the first equation in the solution procedure is obtained,

$$\left(\frac{\partial \xi}{\partial S^*}\right)_{\tau^*} = \left(\frac{\partial \xi}{\partial S^*}\right)_{\tau^*=0} + \int_0^{\tau^*} \frac{\partial^2 f_w}{\partial S^{*2}}\, d\tau^* \qquad \text{(V-2)}$$

This gives an estimate of $(\partial\xi/\partial S^*)_{\tau^*}$ at every node, on the saturation axis, at the end of a particular time step. Of course, an initial estimate of $\partial^2 f_w/\partial S^{*2}$ is required to start the numerical procedure. The second of the equations is the fractional flow equation [Leverett[35]] as adapted by Bentsen[3] in Eq.(II-7), but written as

$$f_w(S^*, \tau^*) = G(S^*) - \frac{N_c C(S^*)}{\left(\frac{\partial \xi}{\partial S^*}\right)_{\tau^*}} \qquad \text{(V-3)}$$

The values of $(\partial\xi/\partial S^*)_{\tau^*}$ Eq.(V-2) at every node are used in Eq.(V-3) to obtain a current value for $f_w(S^*, \tau^*)$ which, in turn, results in the evaluation of an improved value for $\partial^2 f_w/\partial S^{*2}$. Equations (V-2) and (V-3) are iterated upon till convergence is obtained on $\partial^2 f_w/\partial S^{*2}$.

In this formulation S* is a dependent variable so no iterations are required on the G(S*) and C(S*) functions.

Finally to obtain a relationship between ξ and S*, at a particular time, the third equation to be solved successively is

$$\xi(S^*, \tau^*) = \xi(S^*, 0) + \int_0^{\tau^*} \frac{\partial f_w}{\partial S^*} d\tau^* \qquad \text{(V-4)}$$

which is obtained by integrating Eq.(V-1) between zero and τ^*.

The boundary and initial conditions used by Bentsen[6] in the solution of Equations (V-2) and (V-3) were

$$\left.\begin{aligned} f_w(0, \tau^*) &= 0 \qquad \text{(V-5)} \\ f_w(1, \tau^*) &= 1 \qquad \text{(V-6)} \end{aligned}\right\} \quad \tau^* > 0$$

and

$$f_w(S^*, 0) = 1 \qquad 0 < S^* < 1 \qquad \text{(V-7)}$$

In contrast to all other numerical solutions published till that time this particular Lagrangian formulation allowed the inlet saturation to build-up with time to its maximum value. The Lagrangian solution of Fayers and Sheldon[17] did not give the time elapsed for a particular saturation profile. This shortcoming was also overcome in this particular [Bentsen[6]] Lagrangian solution.

V.2.2 Eulerian {see Appendix E for details}

The Eulerian formulation in the saturation domain can be obtained by differentiating Eq.(II-7) with respect to ξ, and then substituting for $\partial f_w/\partial \xi$ in Eq.(II-6) resulting in Eq.(V-8), which is

$$\frac{\partial S^*}{\partial \tau^*} = \frac{\partial}{\partial \xi} \{N_c C(S^*) \frac{\partial S^*}{\partial \xi}\} - \frac{dG(S^*)}{dS^*} \frac{\partial S^*}{\partial \xi} \qquad \text{(V-8)}$$

A form of Eq.(V-8) was solved by Flock[19], et al. using a semi-implicit integration scheme. They assumed an instantaneous jump of the inlet end saturation to its maximum value. It could not be ascertained how the non-linearities, C(S*) and G(S*), in Eq.(V-8), were handled in their solution procedure.

In this study, Eq.(V-8) was solved using its finite difference analog and an implicit scheme in the time derivative. An attempt was also made to let the saturation build up to its maximum value at the inlet end. Appendix E gives details regarding the treatment of the G(S*) and C(S*) functions.

The boundary and initial conditions used to solve Eq.(V-8) were,

$$S^*(\xi, 0+) = F(\xi) \qquad 0 \leq \xi \leq 1 \qquad \text{(V-9)}$$

$$S^*(1, \tau^*) = 0 \qquad 0 \leq \tau^* \leq \tau^*_{bt} \qquad \text{(V-10)}$$

The initial saturation at the inlet end, SI, was determined by numerical trials and then allowed to build-up with the help of Eq.(V-8). The particular finite difference analog of this equation is given as Eq.(E-18) in Appendix E. After S* has built up to one the third boundary condition becomes

$$S^*(0, \tau^*) = 1 \qquad \text{(V-11)}$$

V.3 DATA BASES FOR NUMERICAL SIMULATORS

The numerical simulators based on the Lagrangian and Eulerian formulations both required identical data bases, in so far as the physical and geometrical properties in the runs were concerned. The experimentally generated saturation profiles in Runs 9, 23 and 24 were selected for comparison, because they were representative of

those obtained in runs made at favourable viscosity ratios. For adverse viscosity ratios, Runs 11 and 18 were chosen. This choice was based on an inspection of the saturation profiles generated in all the runs.

V.3.1 Data Obtained by Direct Measurement

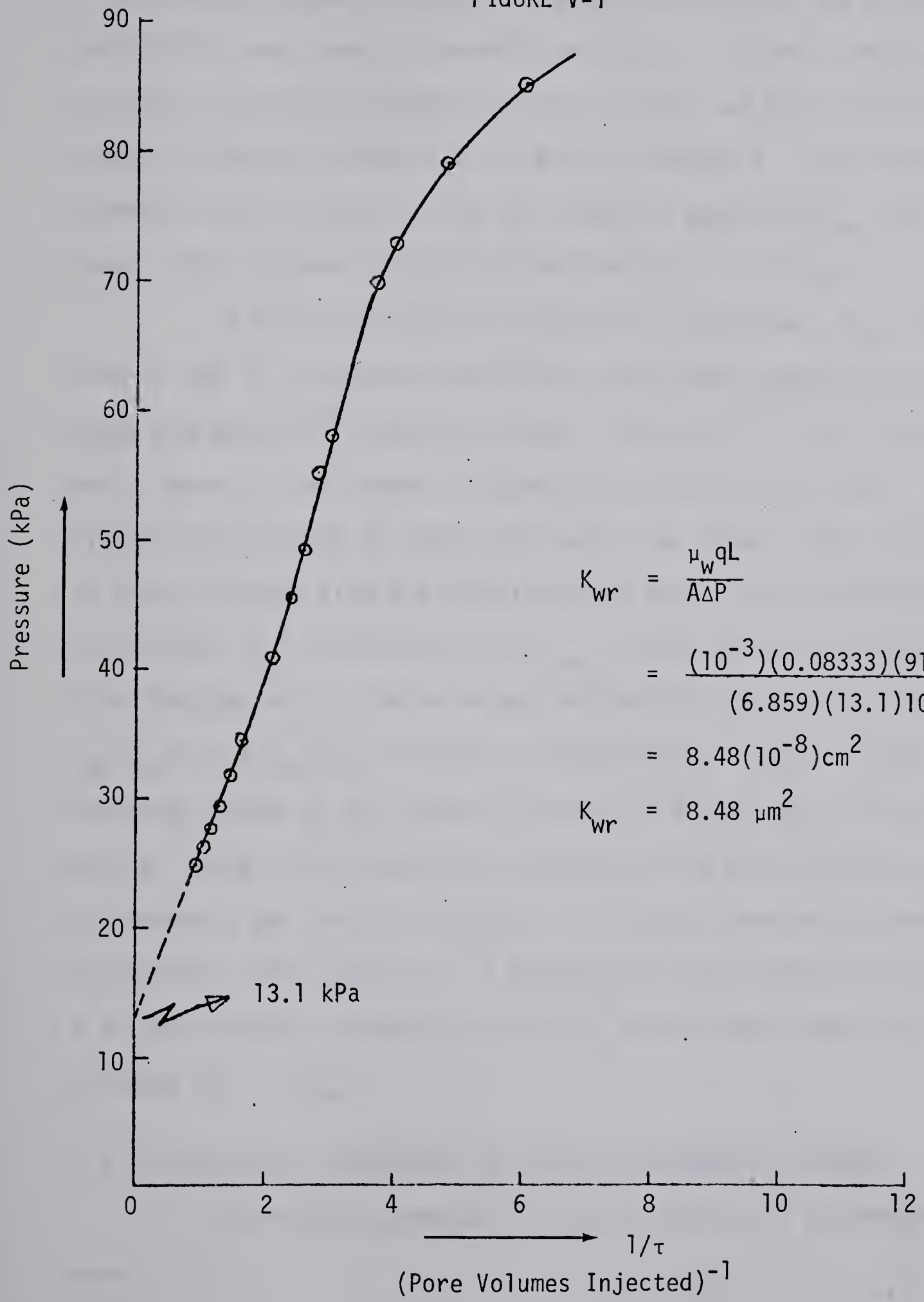
The area and length of the core was taken as the inner dimensions of the core holder. The viscosities of the displaced and displacing liquids were measured in the laboratory at room temperature. At the end of every oilflood, when $\overline{S}_{wi}$ was established, the effective permeability, K_{or}, to oil at $\overline{S}_{wi}$ was evaluated. The material balance derived $\overline{S}_{wi}$, which is an average value, was used as input to the numerical simulators. For Runs 9, 23 and 24 the residual oil saturation, $\overline{S}_{or}$, and the effective permeability to water, K_{wr}, at $\overline{S}_{or}$ was also obtained experimentally. This was facilitated by a quick cessation of oil production after breakthrough of the displacing liquid (glycerine + water). For adverse viscosity ratios the waterflood was continued until about one pore volume of water had been injected. As oil production was still continuing at that time, $\overline{S}_{or}$ and K_{wr} could not be determined experimentally.

V.3.2 Estimates of Residual Oil Saturation and Effective Permeability for Adverse Viscosity Ratio

In Appendix D, tables of data are provided for each run giving values for dimensionless pore volumes injected, τ_i, cumulative volume of oil produced, N_p, and pressure drop across the core, ΔP. Extrapolation of the $1/\tau_i$ versus ΔP curve gave an estimate of ΔP at infinite pore volumes injected, because $1/\tau_i$ tends to zero

EXTRAPOLATION OF ΔP - $1/\tau$ RELATIONSHIP
TO INFINITE PORE VOLUMES INJECTED
(data from Run 11)

FIGURE V-1



$$K_{wr} = \frac{\mu_w qL}{A\Delta P}$$

$$= \frac{(10^{-3})(0.08333)(91.44)}{(6.859)(13.1)10^{3}}$$

$$= 8.48(10^{-8})\,cm^2$$

$$K_{wr} = 8.48\ \mu m^2$$

as τ_i tends to infinity. At infinite pore volumes injected, the residual oil saturation, $\bar{S}_{or}$, was deemed to have been achieved. So the calculated value of effective permeability, using the extrapolated value of ΔP, was taken as an estimate of K_{wr}. This was done for all the runs conducted at adverse viscosity ratios and the resulting K_{wr} values are given in Tables B-1 to B-3 in Appendix B. For conducting numerical runs for Runs 11 and 18, similarly generated K_{wr} values were used. This procedure is illustrated for Run 11 in Figure V-1.

In order to estimate residual oil saturations, S_{or}, for Runs 11 and 18, relative permeability curves were generated using the Jones and Roszelle[30] graphical method. Plots of $\bar{\lambda}^{-1}$ {see Table VI-3} and τ versus τ_i were drawn. Tangents at points on the after-breakthrough portion of these plots were then drawn. The intersection of these tangents with the ordinates gave values for the effective viscosities, λ_2^{-1}, and saturations, S_{w2}, at the outlet end of the core, as a function of τ_i. These values enabled the calculation of the $K_{eo}(S_w)/K$ and $K_{ew}(S_w)/K$ functions respectively. Plots of these functions versus S_w are shown in Figures (V-2) and (V-3) for Runs 11 and 18. Next a line parallel to the saturation axis was drawn, so as to intersect the ordinate at K_{wr}/K. The K_{ew}/K curve was extrapolated to intersect this line at P. A perpendicular was dropped from point P to the abscissa intersecting it at Q. Point Q was taken as an estimate of $(1 - \bar{S}_{or})$.

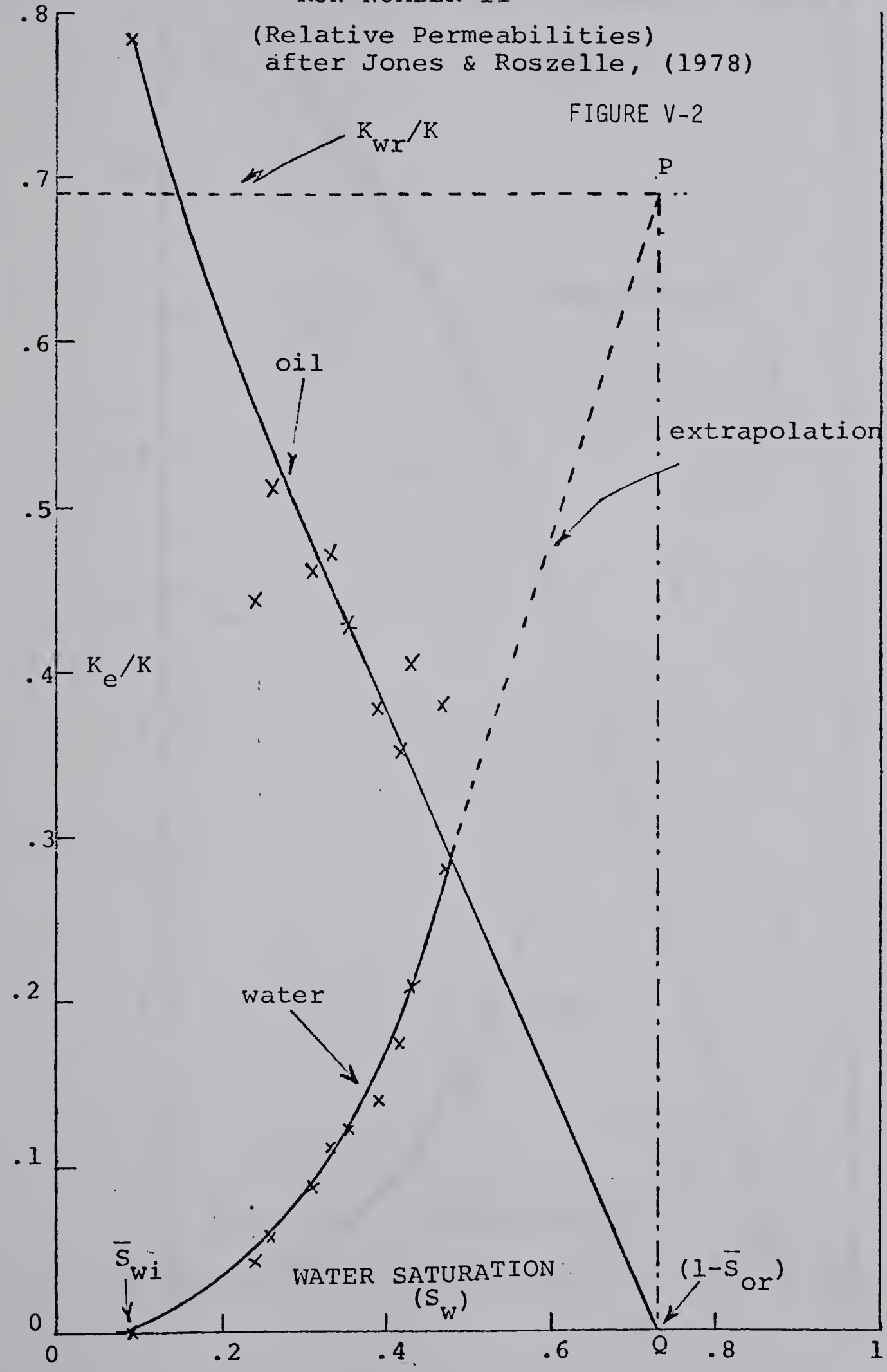
V.4 ESTIMATION OF PARAMETERS IN RELATIVE PERMEABILITY MODELS

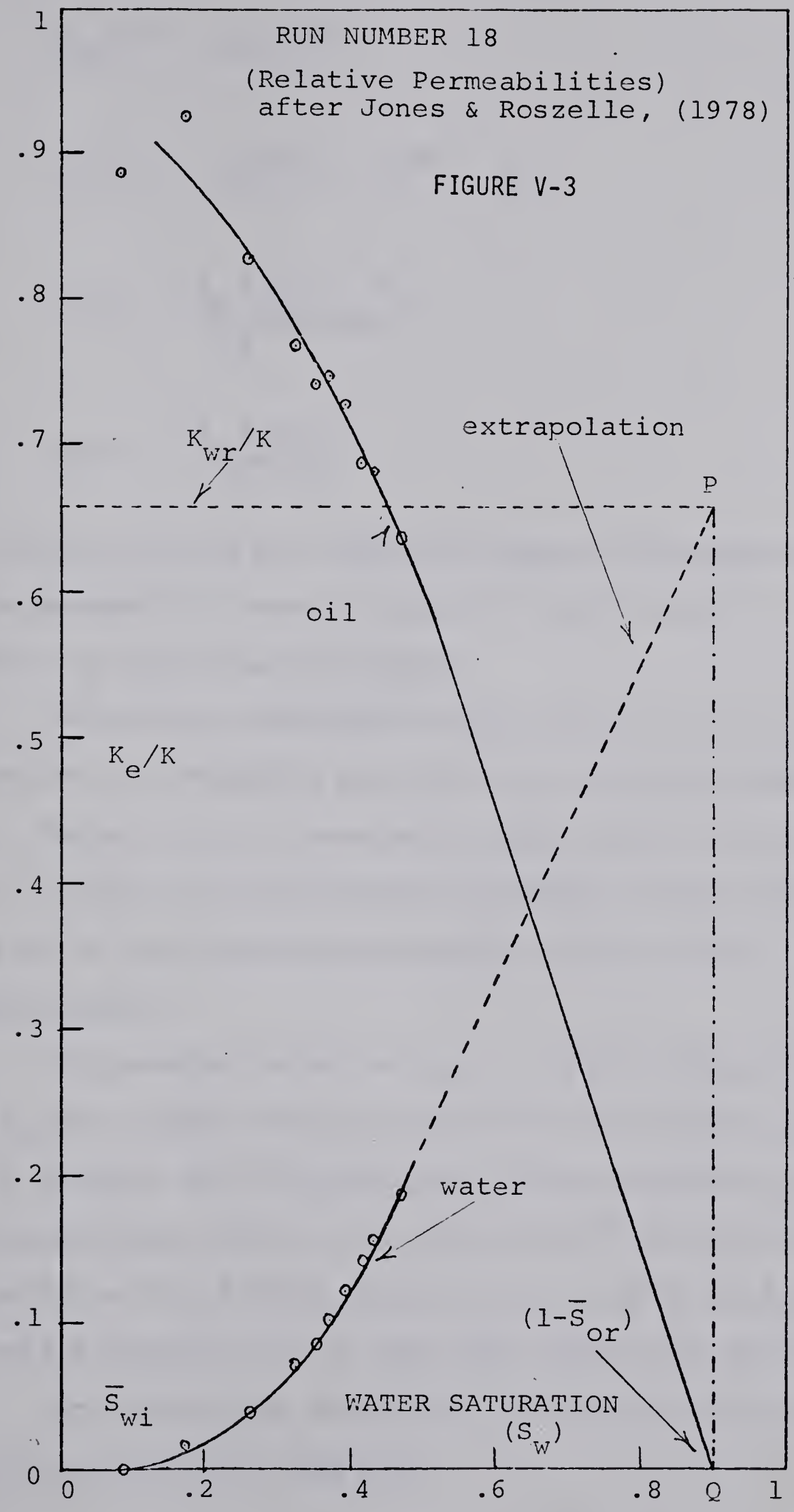
The relative permeability models introduced by Bentsen[3] were

RUN NUMBER 11

(Relative Permeabilities)
after Jones & Roszelle, (1978)

FIGURE V-2




RUN NUMBER 18
(Relative Permeabilities)
after Jones & Roszelle, (1978)
FIGURE V-3
1
.9
.8
.7
.6
.5
.4
.3
.2
.1
0
K_{wr}/K
extrapolation
P
oil
K_e/K
water
$(1-\bar{S}_{or})$
$\bar{S}_{wi}$
WATER SATURATION
(S_w)
0
.2
.4
.6
.8
Q
1

$$K_{rw}(S^*) = \alpha(S^*)S^{*2} \qquad \text{(V-12)}$$

and

$$K_{ro}(S^*) = \beta(S^*)(1 - S^*)^{NK} \; ; \quad NK = 1 \qquad \text{(V-13)}$$

where

$$\alpha(S^*) = \frac{a_w + b_w(1 - S^*)}{a_w + 1 - S^*} \qquad \text{(V-14)}$$

and

$$\beta(S^*) = \frac{a_o + b_o S^*}{a_o + S^*} \qquad \text{(V-15)}$$

The functions $\alpha(S^*)$ and $\beta(S^*)$ modify the shape of the normalized relative permeability curves to account for the influence of wettability and pore size distribution.

To ascertain representative values for a_w, b_w, a_o, b_o and NK, numerical experimentation was carried out on the data base for Run 11. The experimentally measured saturation profile at τ_{corr} of 0.24 $\{\tau^* = 0.375\}$ was chosen to match the numerical profile generated using a set of the aforementioned parameters in the relative permeability model.

The parameters varied were a_o, b_o and NK. The parameters a_w and b_w were assigned the value unity as this value gave a good match of the model {Eq.(V-12)},with the relative permeability curve for water, generated using the Jones and Roszelle[30] method {Fig.V-4}. For a particular set of values chosen for a_o, b_o and NK the $K_{eo}(S_w)/K$ curve and the saturation profile were drawn {Figures V-4 and V-5}.

Two criteria were assigned for the selection of a particular choice of a_o, b_o and NK. These were:

i) The saturation profile generated using the selected values of a_o, b_o and NK should match the experimentally measured saturation profile.

ii) Experimentally measured breakthrough recoveries should agree closely with the numerical results calculated using the chosen values of a_o, b_o and NK.

Both the Lagrangian and Eulerian numerical solution procedures were tested. Table V-1 shows the calculated breakthrough recoveries for different values of parameters used in the relative permeability models. Experimental breakthrough recoveries are also listed in Table V-1.

Eulerian solutions {for NK = 2, a_o = 1 and b_o = 1} gave much lower breakthrough recoveries than the experimental recoveries. Because of numerical dispersion the foot of the saturation profile arrived at the outlet end earlier than dictated by the Lagrangian solution of the immiscible displacement equation (Figures V-8 to V-10).

The saturation profile generated using the Lagrangian procedure {for NK = 1, a_o = 2, b_o = -1} gave the closest match (Fig.V-5) to the experimental profile and for the same set of parameters the breakthrough recovery agreed well with the experimental recovery. These values for the parameters {NK = 1, a_o = 2, b_o = -1} were used to calculate numerical profiles which were in turn compared with the experimentally measured saturation profiles {Figs.(V-11) to (V-15)}. The choice of the Lagrangian procedure was also in agreement with Fayers and Sheldon's[17] conclusion that Lagrangian techniques should be used to calculate accurate front profiles.

TABLE V-1

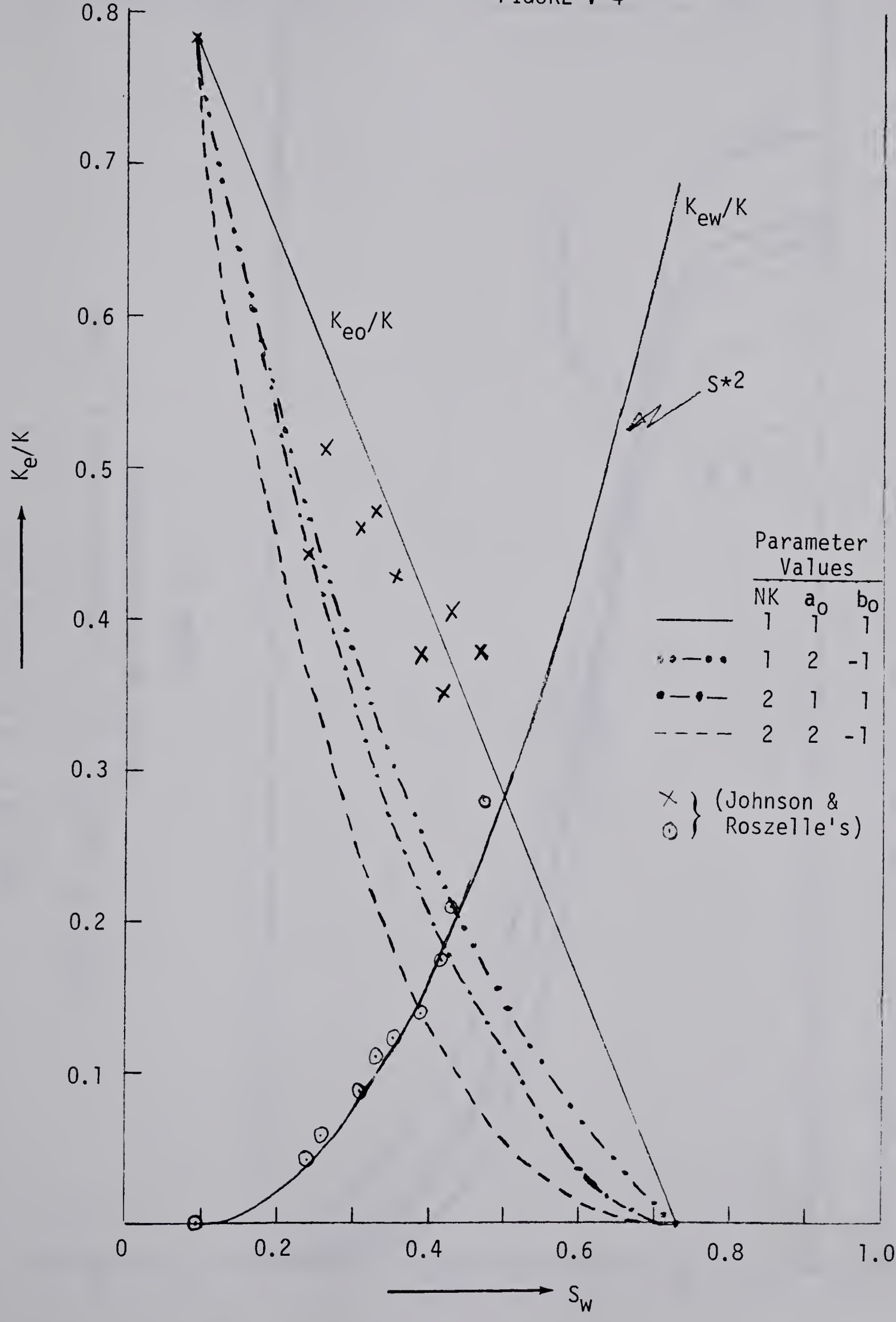
BREAKTHROUGH RECOVERIES OF SOME RUNS FOR DIFFERENT PARAMETERS
USED IN THE RELATIVE PERMEABILITY MODELS
(% of Pore Volume)

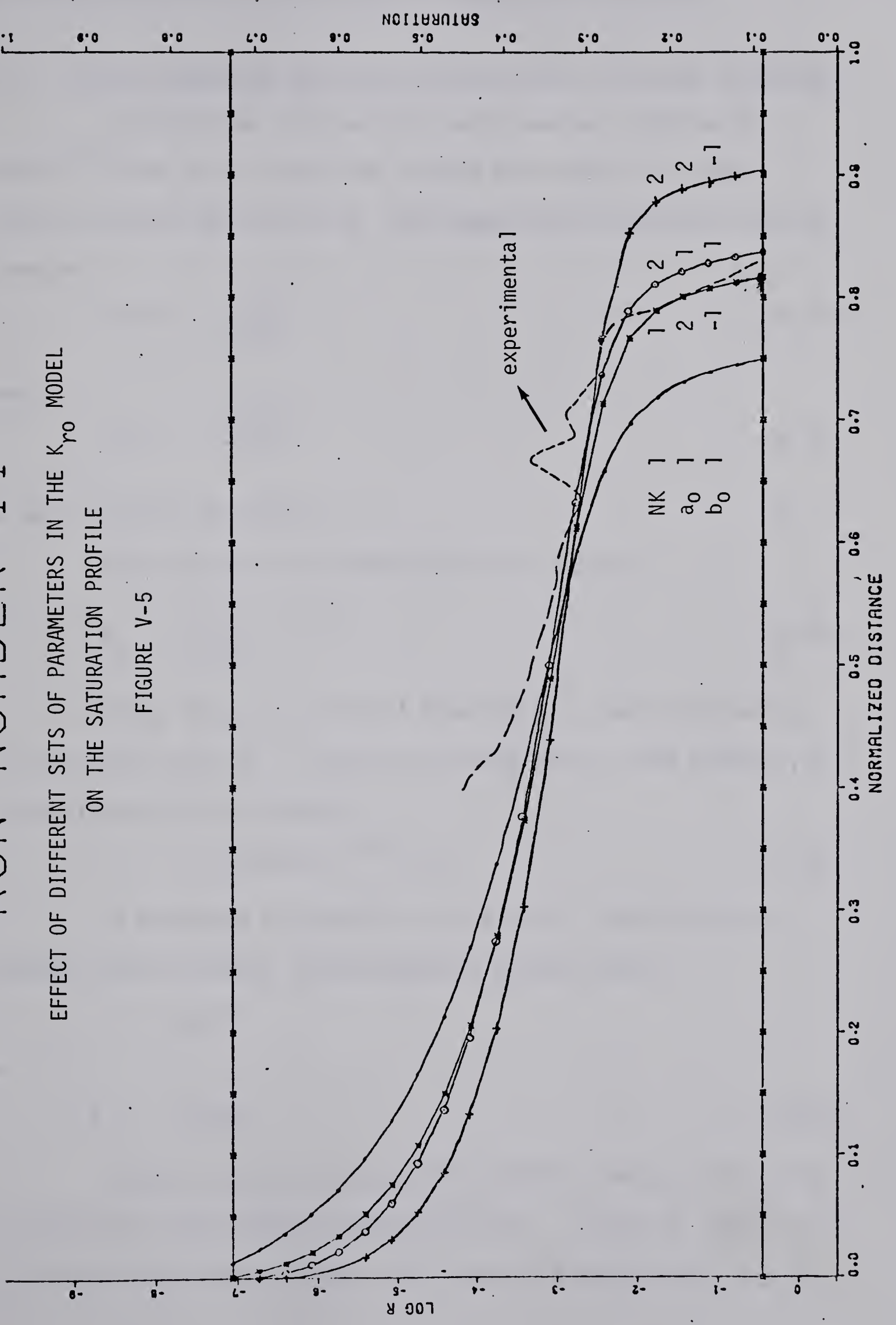
Run No.	Lagrangian Solution				Eulerian Solution	Experimental*
NK:	2	2	1	1	2	
a_o:	2	1	2	1	1	
b_o:	-1	1	-1	1	1	
11	26.8	29.3	29.8	33.0	27.9	32.93
18	33.7	37.0	37.6	41.8	35.2	42.17
24			58.2		52.2	57.18

* corrected for the volume of outlet end fitting

EFFECT OF DIFFERENT SET OF PARAMETERS ON K_{eo}/K CURVE

FIGURE V-4




RUN NUMBER 11
EFFECT OF DIFFERENT SETS OF PARAMETERS IN THE K_{ro} MODEL
ON THE SATURATION PROFILE
FIGURE V-5
SATURATION
NORMALIZED DISTANCE
LOG R
experimental
NK 1
a_o 1
b_o 1
2
2
-1
1
2
1
2
-1
1
-1

V.5 ESTIMATION OF CAPILLARY PRESSURE NORMALIZING PARAMETER

V.5.1 Estimate Based on Capillary Pressure Curve Published by Hagoort

An imbibition capillary pressure curve was reported by Hagoort[23] [1974, p.70, Fig.6] for crushed Pyrex glass of sieve fraction between 450 and 715 μm. The functional relationship for the curve was

$$J(S^*) = \frac{0.14}{S^{*0.4}} \qquad \text{(V-16)}$$

where

$$J(S^*) = \frac{P_c\sqrt{K/\phi}}{\gamma}, \qquad \text{(V-17)}$$

is the Leverett[35] J-function.

Equating Eq.(V-16) and Eq.(V-17) one obtains

$$P_c = \frac{0.14\gamma}{\sqrt{K/\phi}}\, S^{*-0.4} \qquad \text{(V-18)}$$

Using the data for Run 11 from Table B-1 and substituting for interfacial tension, γ, absolute permeability, K, and porosity, ϕ, in consistent units one obtains

$$P_c \cong 0.00482244\ S^{*-0.4}\ \text{atm} \qquad \text{(V-19)}$$

As mentioned in Chapter II Eq.(II-16) , the following capillary pressure model is considered to be applicable:

$$\pi_c = -\ell n S^*$$

or

$$P_c = -\sigma \ell n S^* \qquad \text{(V-20)}$$

Values of P_c were obtained for different values of S* using the functional relationship given by Eq.(V-19). A plot of $\ell n S^*$ versus P_c was drawn using these values. This was the best straight line for

these data {Fig.(V-6), straight line A}. As is evident from Eq.(V-20), the slope of this straight line is the capillary pressure normalizing parameter, σ. For Pyrex glass beads a value of σ was estimated as 0.003125 atm.

V.5.2 Estimate based on Capillary Pressure Curve Published by Leverett

Leverett[35] [p.161, Fig.4] reported a capillary pressure - saturation relationship for clean unconsolidated sands.

Using Eq.(V-17) and the data base for Run 11, as before, the relationship between the Leverett J-function and capillary pressure, P_c, is

$$P_c = 0.03446\ J(S_w)\ \text{atm} \qquad \text{(V-21)}$$

Values for the Leverett J-function were read-off the aforementioned capillary pressure saturation curve and Table V-2 was generated using Eq.(V-21) and the normalized saturation definition, Eq.(II-15)

$$S^* = \frac{S_w - S_{wi}}{1 - \bar{S}_{wi} - \bar{S}_{or}}$$

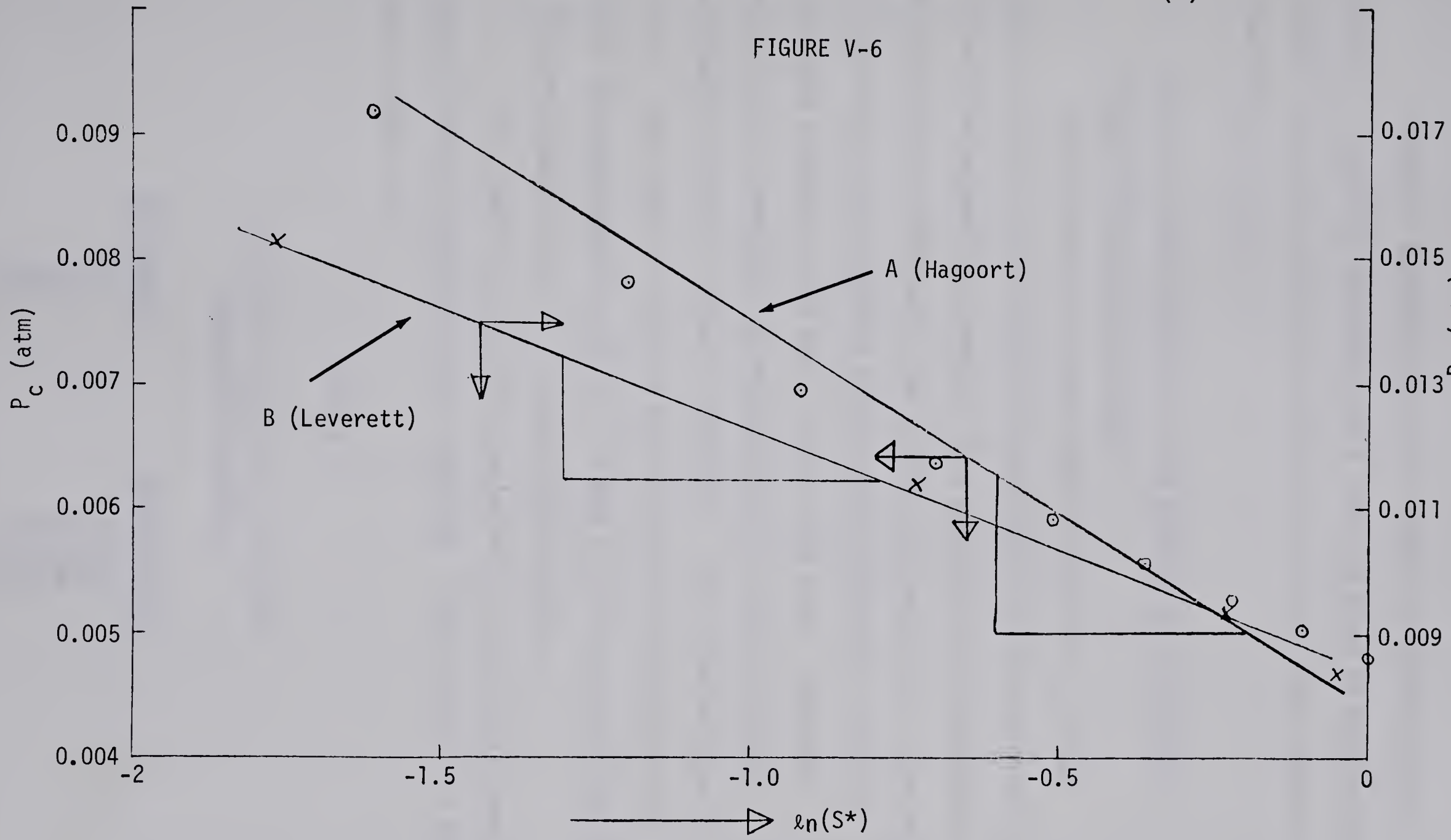
TABLE V-2

VALUES FROM LEVERETT CAPILLARY PRESSURE CURVE

$J(S_w) = \frac{P_c\sqrt{K/\phi}}{\gamma}$ {read-off Leverett's work}	P_c {Eq.V-21} atm	S_w	S^* {Eq.II-15}	ℓnS^*
0.2625	0.0090	0.80		
0.3000	0.0103	0.70	0.953	-0.048
0.3250	0.0112	0.60	0.797	-0.227
0.3875	0.0133	0.40	0.484	-0.726
0.5000	0.0172	0.20	0.172	-1.760

ESTIMATE FOR CAPILLARY PRESSURE NORMALIZING PARAMETER (σ)

FIGURE V-6



Using the tabulated values in Table V-2, ℓnS^* is plotted versus P_c Fig.(V-6), straight line B and the slope of the resulting straight line gave a value of 0.004 atm for the capillary pressure normalizing parameter, σ.

V.5.3 Numerical Experimentation in the Estimation of Capillary Pressure Normalizing Parameter

Having obtained an approximate estimate of σ, it was possible to do a similar analysis as was done with the parameters of the relative permeability models. Once again the same experimental saturation profile for Run 11 was chosen for comparison. Three values of σ were used and saturation profiles were generated, using the Lagrangian procedure, with Run 11 as the data base. Comparison between these numerically generated saturation profiles and the experimental profile is shown in Fig.(V-7). The criterion used for choosing σ was that the slope of the calculated front should match that of the experimental profile. For Run 11 a value of 0.02 atm for σ gave the closest match to the experimental profile.

For other runs requiring a value of σ in their data bases, similar numerical experiments were conducted. These values of σ are given in Table V-3.

TABLE V-3

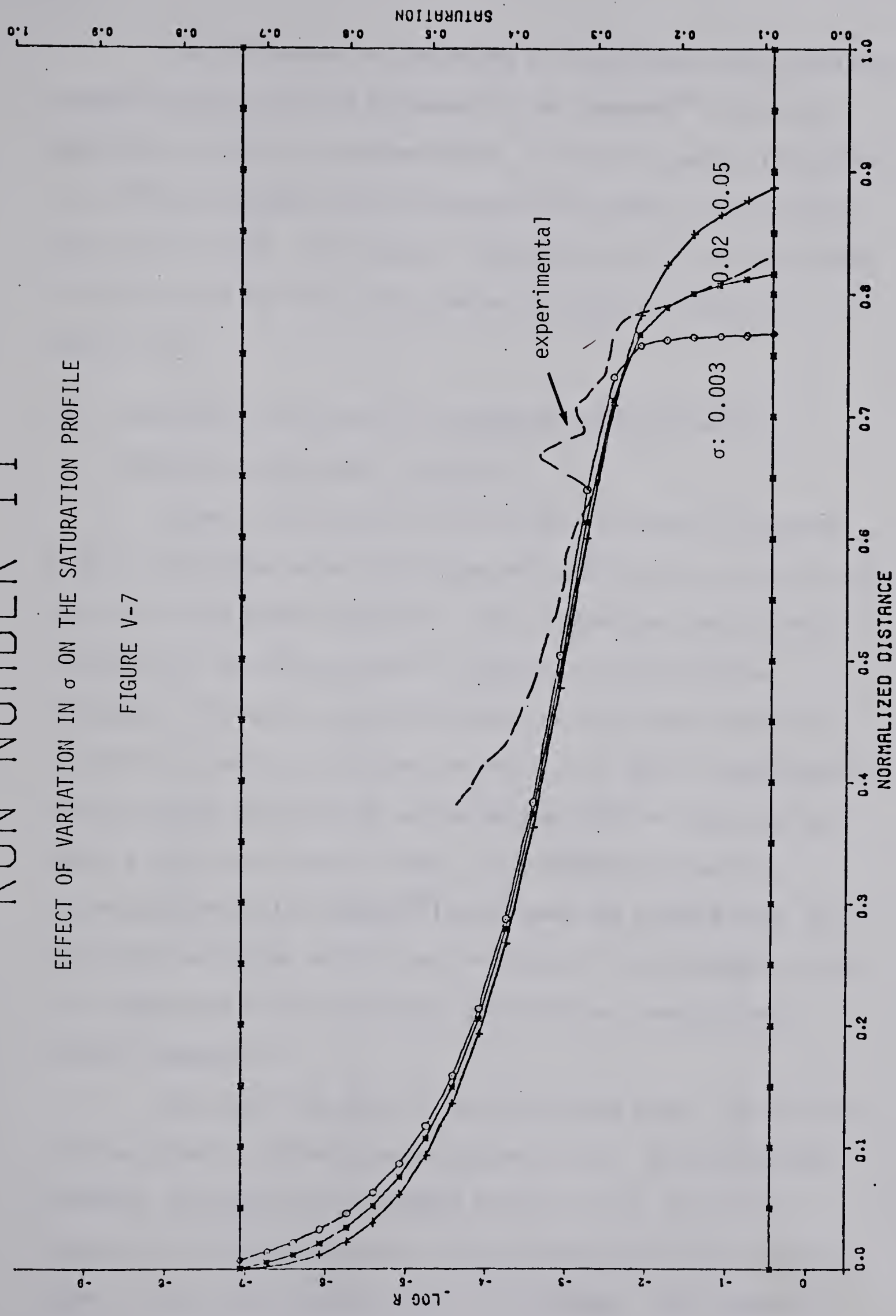
ESTIMATES OF CAPILLARY PRESSURE NORMALIZING PARAMETER

Run Number	σ (atmospheres)
11	0.020
18	0.005
9	0.007
23	0.007
24	0.007

RUN NUMBER 11

EFFECT OF VARIATION IN σ ON THE SATURATION PROFILE

FIGURE V-7



The difference in the values of σ estimated using capillary pressure curves published by Hagoort[23] and Leverett[35] with that obtained by numerical experimentation, for Run 11, may be indicative of a different wettability characteristic for the oil-sand system used in this study. The Leverett J-function, Eq.(V-17), as defined in the analysis for this work, does not include the effect of wettability.

V.6 COMPARISON OF EULERIAN AND LAGRANGIAN SOLUTIONS OF THE IMMISCIBLE DISPLACEMENT EQUATION

Fayers and Sheldon[17] [p.153, Fig.17] compared saturation profiles calculated using Lagrangian and Eulerian formulations of the immiscible displacement equation. Their comparison qualitatively indicated the relative position of saturations using the two approaches. As their Lagrangian scheme could not give the time elapsed for a particular saturation profile, it was not quantitatively evident whether the Eulerian and Lagrangian profiles have the same relative positions at equal times. As a procedure based on a Lagrangian formulation [Bentsen[6]] which gave the elapsed time, for a particular saturation profile, was available it was decided to carry out a comparison of this sort with the solutions based on the Eulerian formulation.

Data sets from Runs 11, 18 and 24 were used. The results from the Eulerian procedure were obtained first. As the Eulerian procedure, developed and programmed for this study, calculated saturation profiles at multiples of $\Delta\tau^*$ (time step size), a specific number of them were generated until breakthrough. For a material

FIGURE V-8

COMPARISON OF EULERIAN AND LAGRANGIAN SOLUTIONS

(DATA FROM RUN 24)

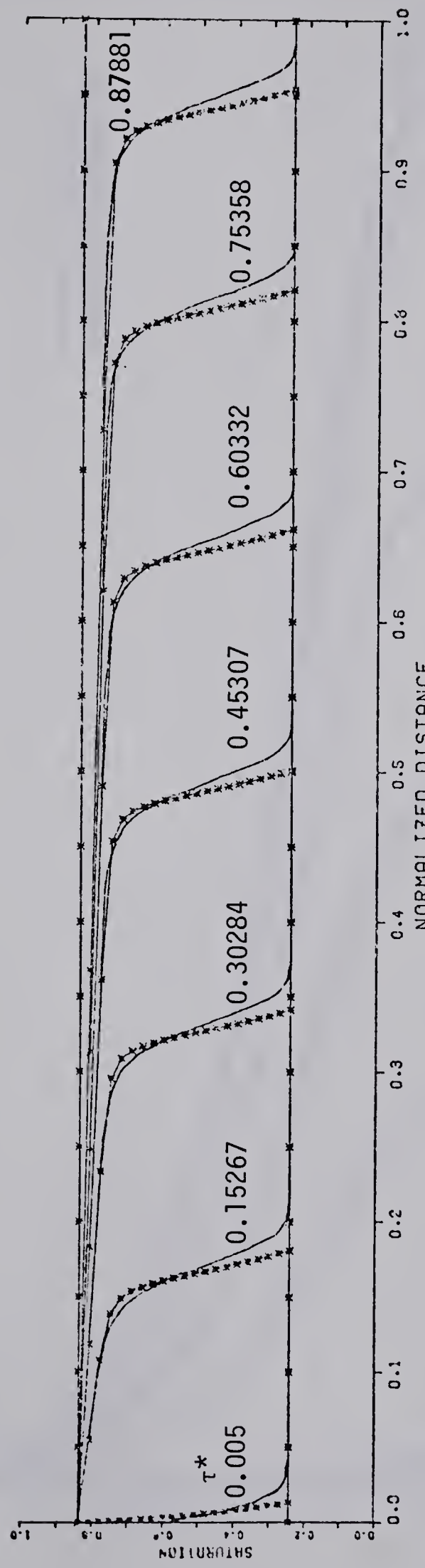


FIGURE V-9

COMPARISON OF EULERIAN AND LAGRANGIAN SOLUTIONS
(DATA FROM RUN 11)

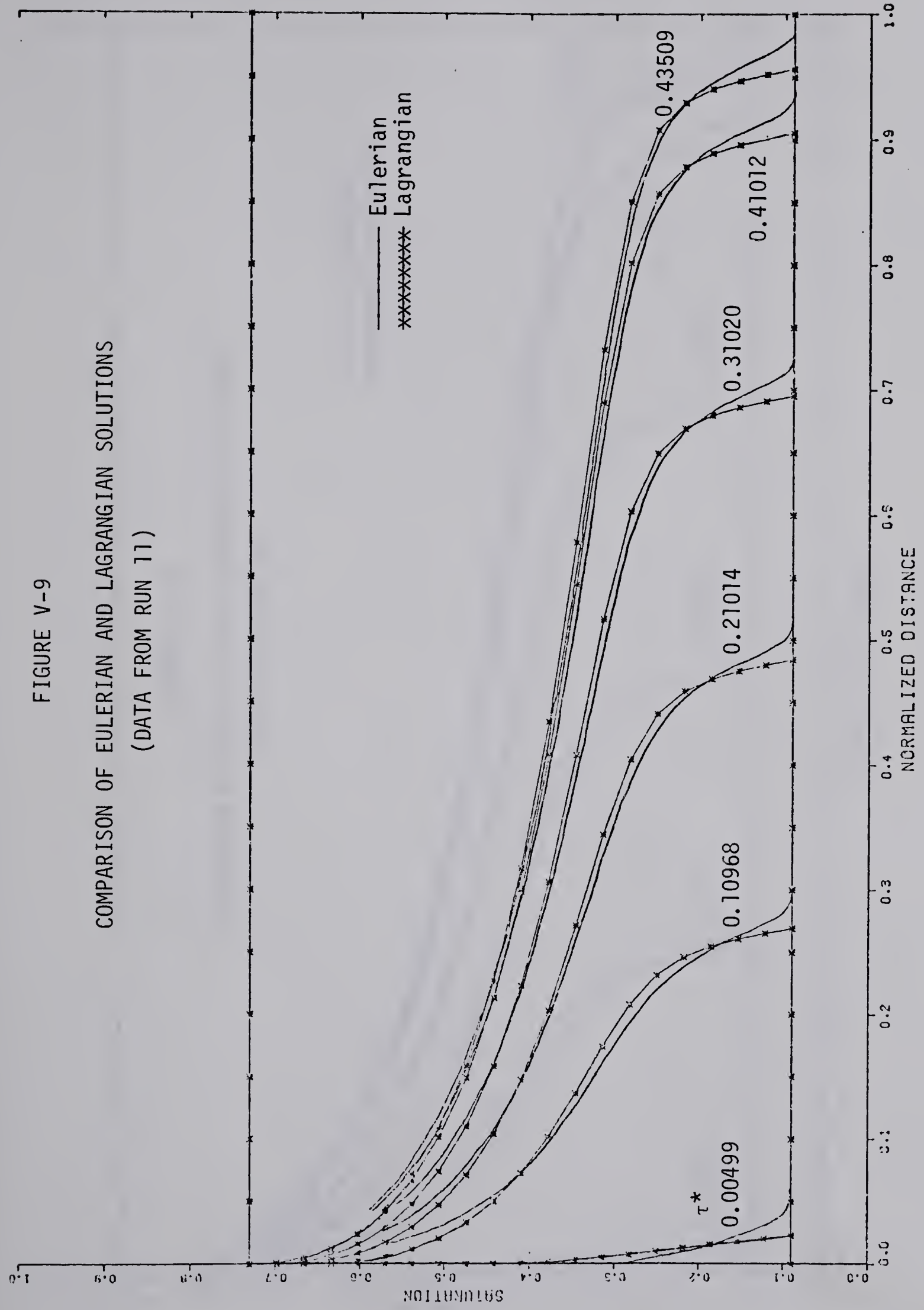
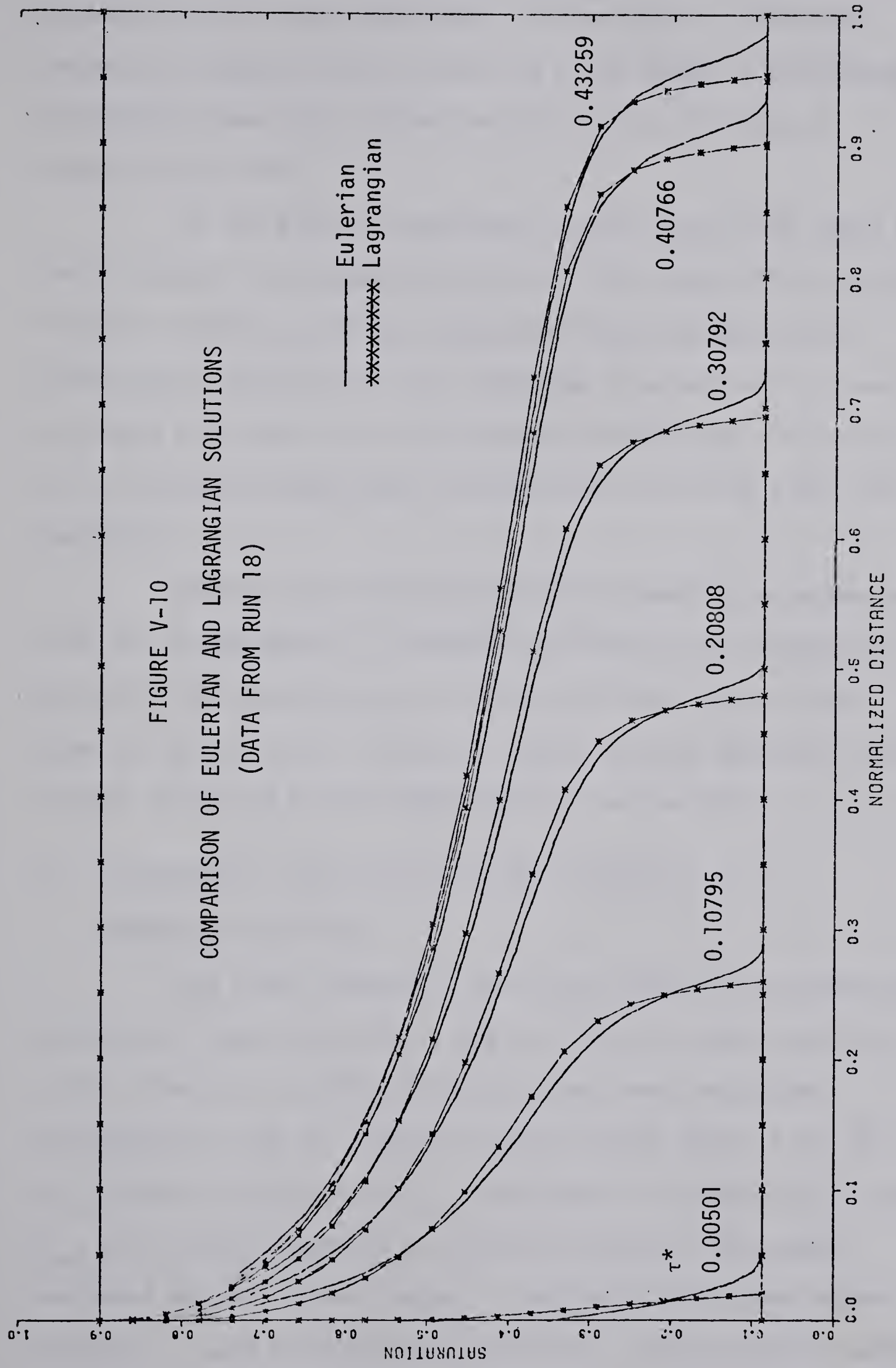


FIGURE V-10

COMPARISON OF EULERIAN AND LAGRANGIAN SOLUTIONS
(DATA FROM RUN 18)



balance check the area under these profiles was also calculated. The maximum material balance error was of the order of two percent. The profiles were then compared and the results are shown in Figure V-8 to V-10.

All the Eulerian saturation profiles show a less steep front and a reversal in curvature at the foot of the front. This resulted in early breakthrough of the displacing liquid and pessimistic breakthrough recoveries of oil as compared to experimental recoveries and those calculated using the Lagrangian formulation. The results of this comparison also agree with what was inferred by Fayers and Sheldon[17].

Based on these comparisons and the numerical experimentation done for the estimation of parameters in the relative permeability and capillary pressure models, it can be inferred that solutions based on the Lagrangian formulation should be used, when more realistic frontal shapes and breakthrough recoveries are desired.

V.7 COMPARISON OF EXPERIMENTAL SATURATION PROFILES AND LAGRANGIAN SOLUTIONS

Data bases required to support the numerical procedure were prepared for Runs 9, 23, 24, 11 and 18. For favourable viscosity ratios (Runs 9, 23 and 24) all the data sets were determined experimentally, but for adverse viscosity ratios (Runs 11 and 18), the residual oil saturation, S_{or}, and effective permeability to water, K_{wr}, at S_{or} were determined by using the extrapolation methods mentioned earlier in this chapter. The dimensionless pore volumes produced, τ, were corrected using Eq.(IV-3). These corrected values

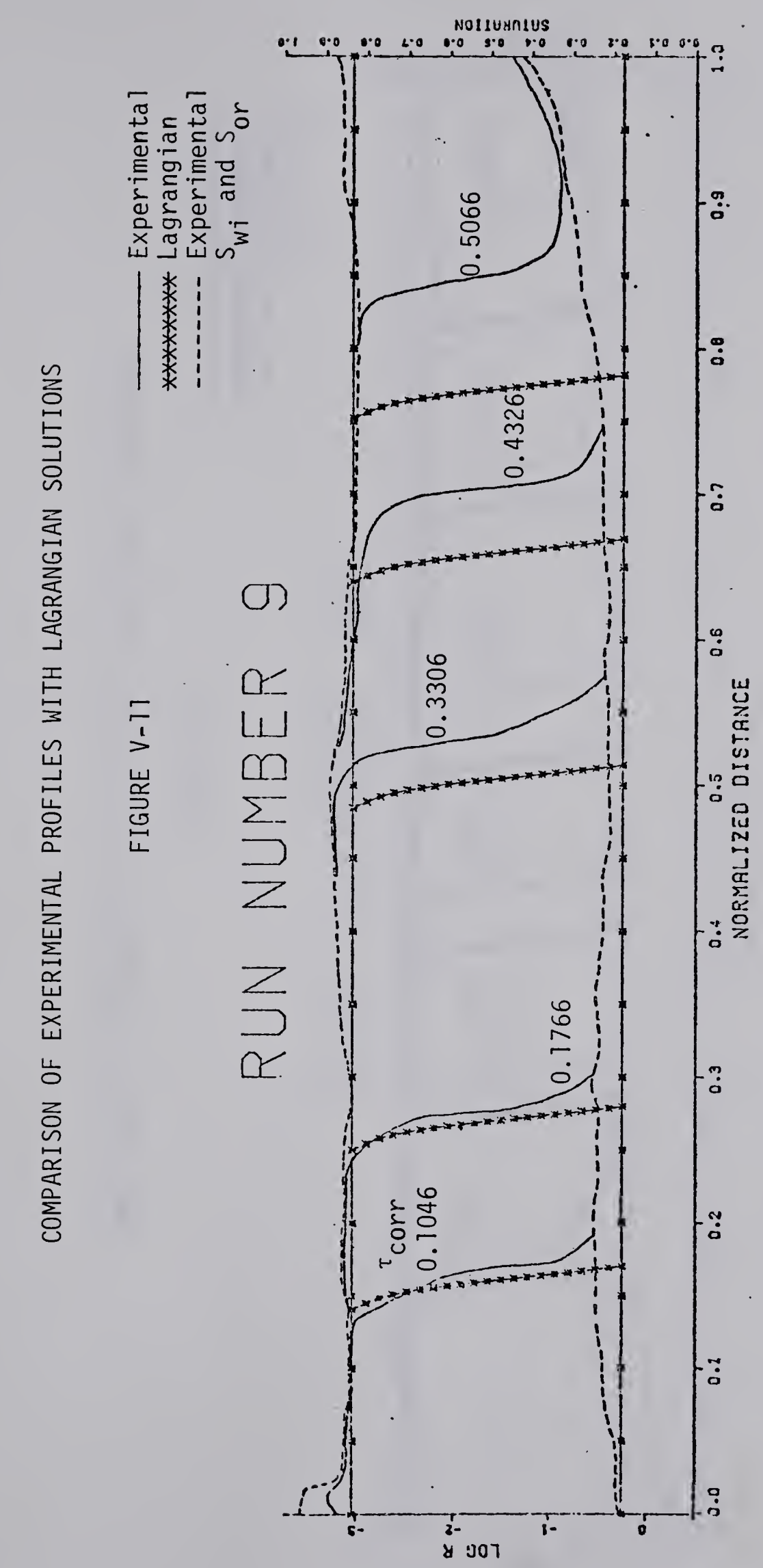
are written beside the saturation profiles shown in Figures V-II to V-15. In the experimental saturation profiles given in Appendix A, uncorrected values of dimensionless pore volumes produced, τ, are written beside the saturation profiles.

The relative permeability and capillary pressure models were taken from the literature[3,4] and preliminary estimates[23,35] for their parameters arrived at. Representative values for the parameters were obtained by numerical experimentation.

In Runs 9, 23 and 24 the oilflood {while establishing S_{wi}} was carried out at an adverse viscosity ratio. A saturation gradient in the established S_{wi} is evident in all three runs {Figs. V-11 to V-13}. In the data sets used to generate numerical saturation profiles an average initial water saturation, $\overline{S}_{wi}$, determined from material balance was used. The numerical procedure considered this value of $\overline{S}_{wi}$ as constant throughout the length of the core. This was not the case in the actual experiments. Although the average absolute errors, in the material balance, {Fig.IV-2} for Runs 9, 23 and 24 were 3.74%, 13.55% and 3.29% respectively, the experimental saturation profiles seem to run faster than the numerical profiles at the later stages of the waterflood. This can be attributed to the increasing $\overline{S}_{wi}$ towards the outlet end of the core. Otherwise, the slopes of the profiles, and the particular relative permeability and capillary pressure models chosen seem to prevail in conjunction with the immiscible displacement equation, in so far as the overall physics of the displacement is concerned.

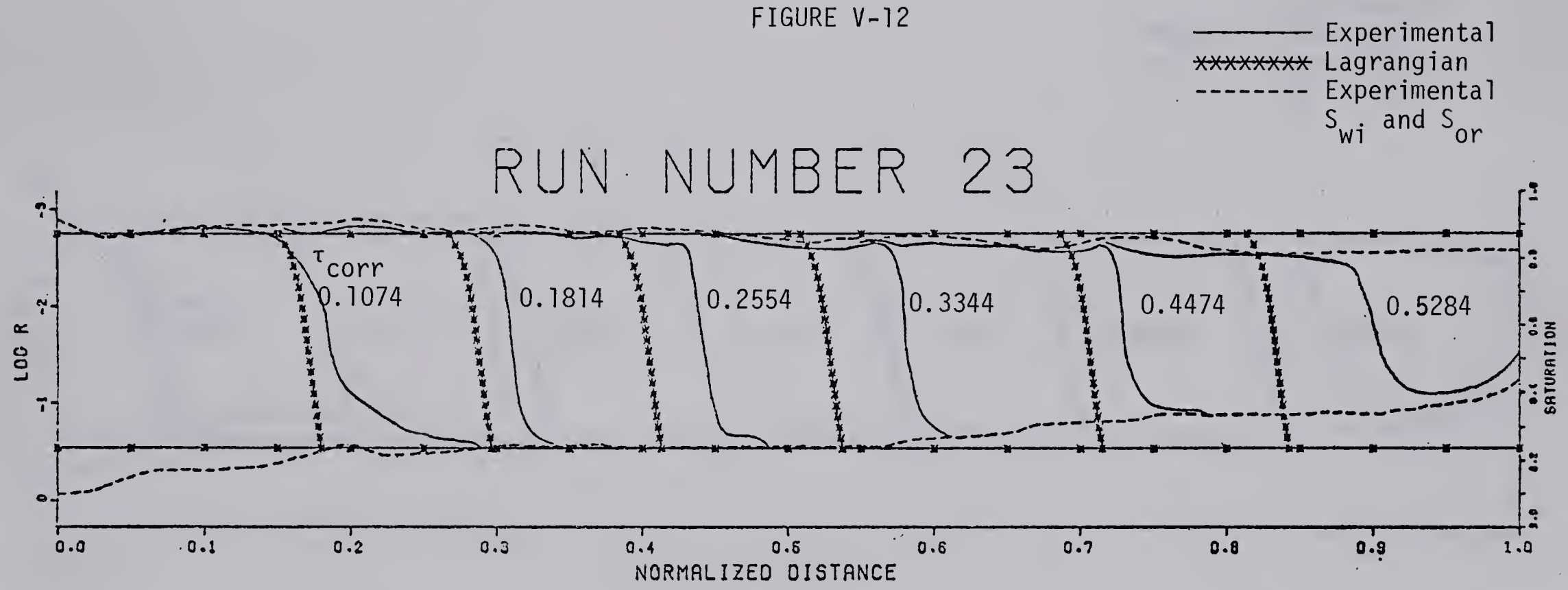
COMPARISON OF EXPERIMENTAL PROFILES WITH LAGRANGIAN SOLUTIONS

FIGURE V-11



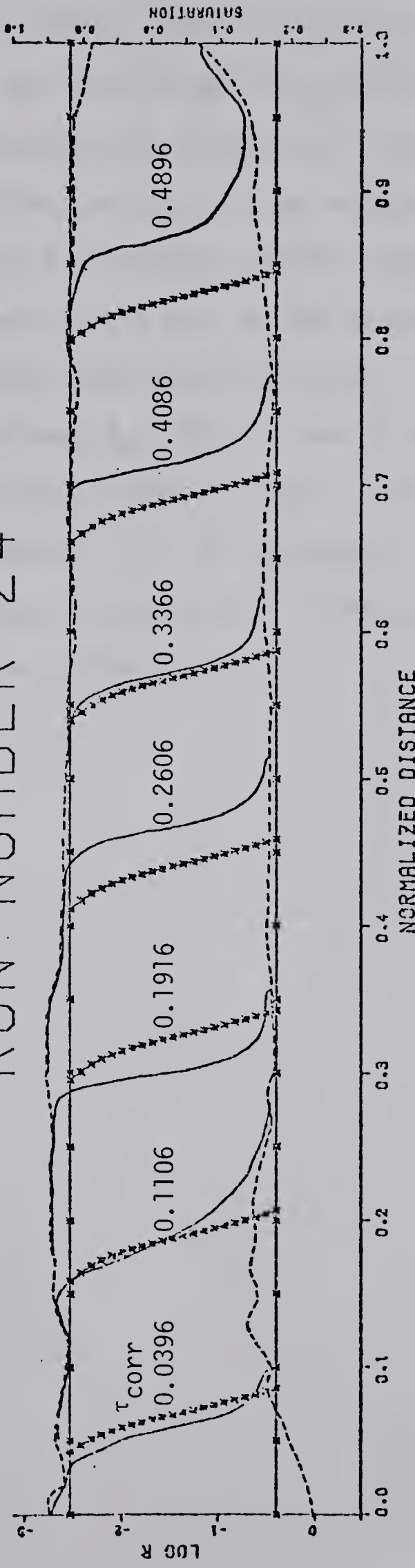
COMPARISON OF EXPERIMENTAL PROFILES WITH LAGRANGIAN SOLUTIONS

FIGURE V-12



COMPARISON OF EXPERIMENTAL PROFILES WITH LAGRANGIAN SOLUTIONS

FIGURE V-13

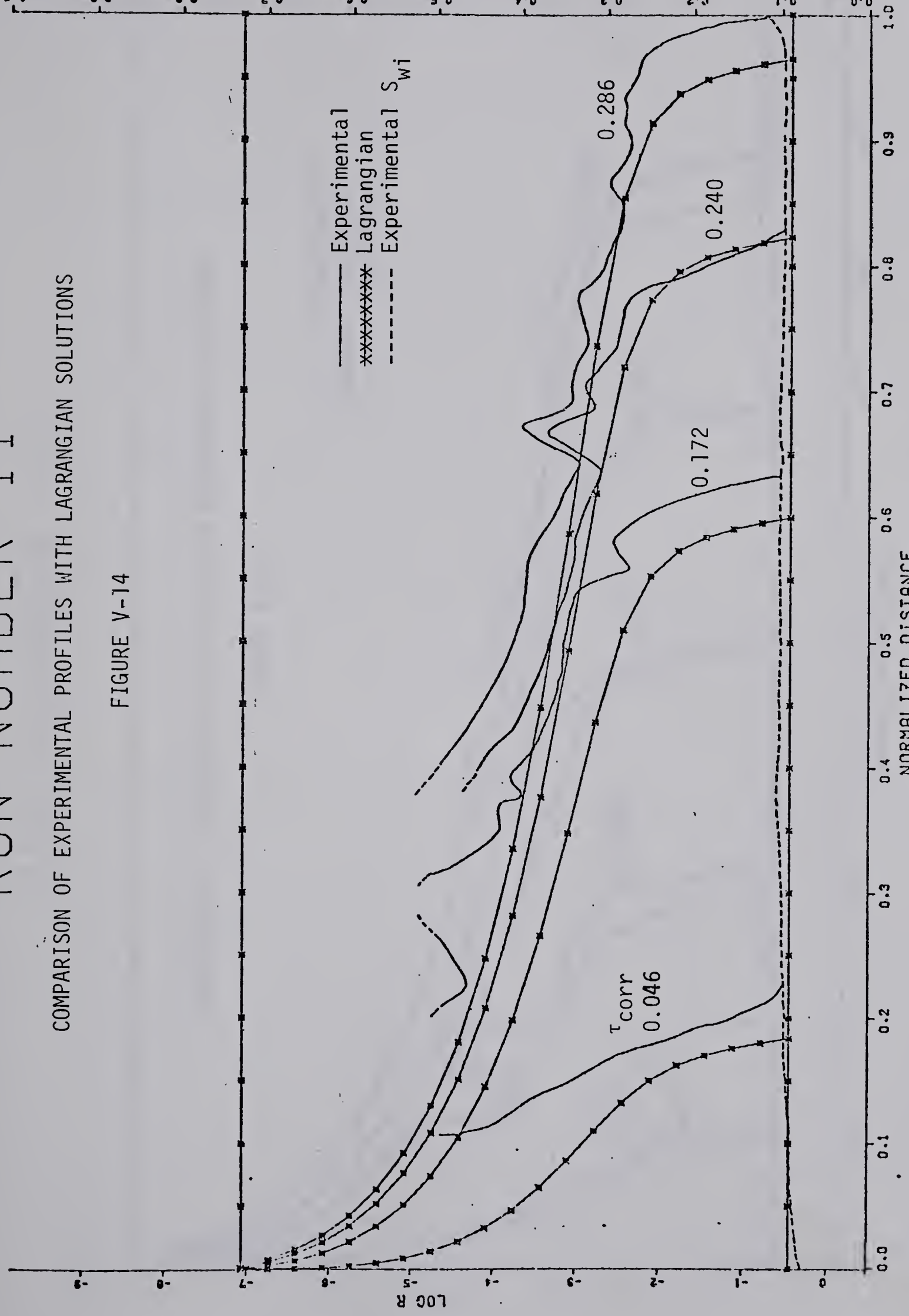


For the adverse viscosity ratios in Runs 11 and 18 the initial water saturation, S_{wi}, is more uniform and the experimental profiles tend to agree much more closely with the numerical results {Figs. V-14 to V-15}. Again, for those particular runs selected for numerical comparison, the immiscible displacement equation seems to apply. It may be worthwhile to mention here that as the immiscible displacement equation is solved using normalized saturations, S*, they have to be de-normalized to saturations, S_w. This is done by using Eq.(II-15). As a consequence the shape of the profiles is a strong function of the residual oil saturation, $\bar{S}_{or}$. An experimental determination of $\bar{S}_{or}$ would have given more confidence in the analysis of immiscible displacement theory undertaken here.

RUN NUMBER 11

COMPARISON OF EXPERIMENTAL PROFILES WITH LAGRANGIAN SOLUTIONS

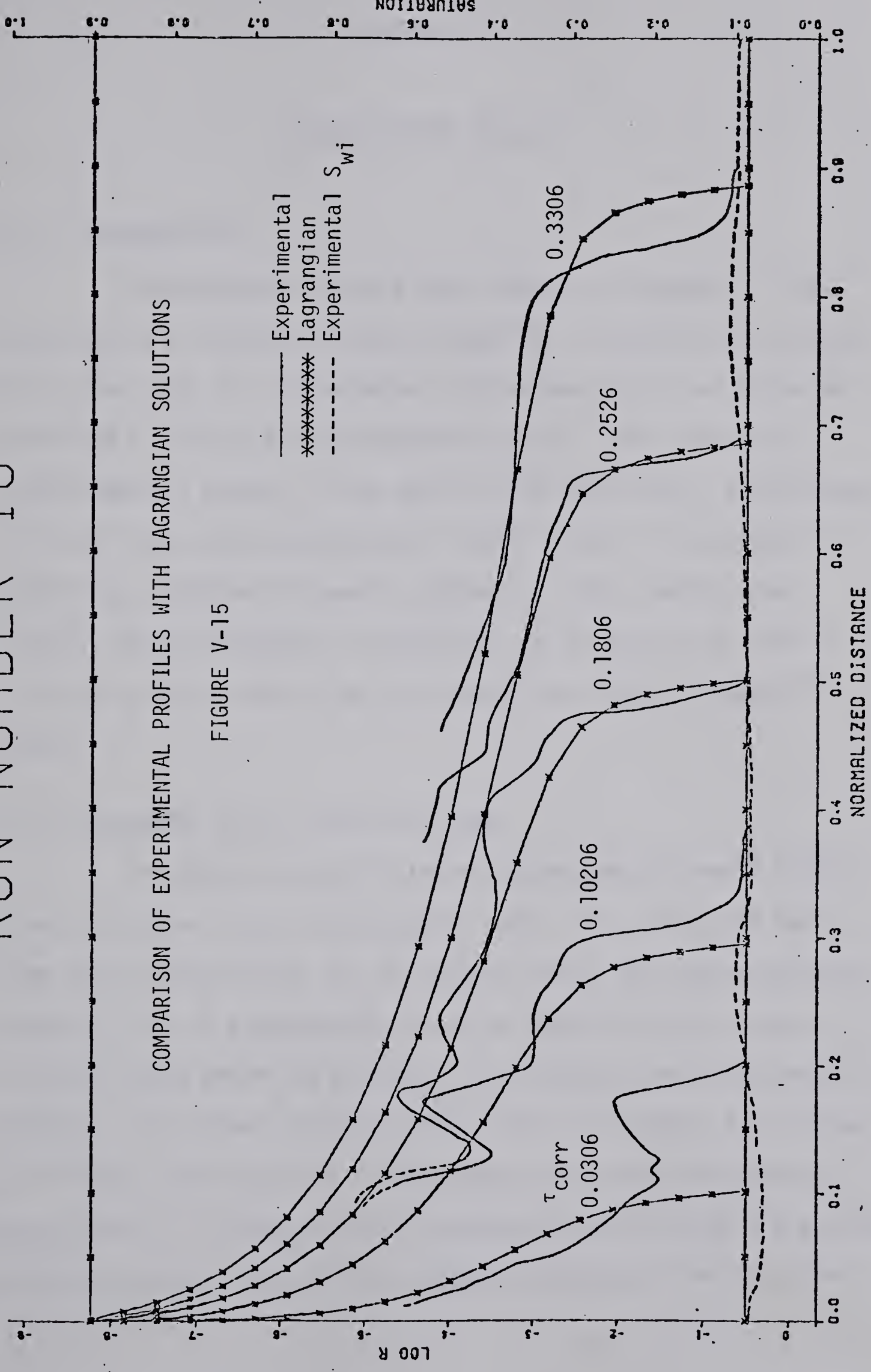
FIGURE V-14



RUN NUMBER 18

COMPARISON OF EXPERIMENTAL PROFILES WITH LAGRANGIAN SOLUTIONS

FIGURE V-15



CHAPTER VI

DISCUSSION OF RESULTS

VI.1 INTRODUCTION

Displacements may be either stable, or unstable. If the displacement is unstable, viscous fingering is completely dominating the process and, as a consequence, displacement behaviour cannot be predicted by solving the displacement equation. Even though the displacement is stable, it may not be fully stabilized. Displacements are said to be stabilized when the frontal region of the saturation profile has attained (or nearly attained) a fixed configuration. That is, the displacement is stabilized, if the saturation profile is close to that predicted by the conventional Buckley-Leverett[10] theory.

VI.2 ATTAINMENT OF THE STABILIZED ZONE

For adverse viscosity ratios, Warren and Calhoun[53] [1955] have reported on several displacement tests. They indicated that, when total pressure drop, ΔP, is plotted versus time, three distinct regions, prior to breakthrough, could be identified on the curve: a primary phase where the pressure is building up due to compressibility effects, a non-linear secondary phase where the pressure declines but the frontal region has not yet attained a stabilized configuration and, finally, a linear decline in pressure indicating that a stabilized zone has formed. Such plots for adverse viscosity ratios are shown

in Figure D-1 to D-3. Breakthrough points are also indicated on these plots.

Figure D-1 shows the plots for the displacement of Dow Corning oil (μ_o/μ_w = 9.34). Run 10 (100 cc/hr) indicates that a stabilized zone has not yet formed. But the plots for Run 8 (200 cc/hr) and Run 11 (300 cc/hr) are such that a straight line can be drawn through the pre-breakthrough data, suggesting that stabilization of the frontal region has been attained. Analysing the saturation profiles for this series of runs (Figures A-1 to A-3) leads to similar conclusions. The frontal regions in the profiles shown for Runs 8 and 11 (Figs. A-1 and A-3) seem to have a fixed configuration while the profiles in Run 10 (Fig. A-2) were still trying to stabilize, when breakthrough occurred.

In Figure D-2, ΔP versus τ_i plots are shown for Paraffin oil displacements(μ_o/μ_w = 73.33) conducted at different rates. Run 12 (25 cc/hr) and Run 15 (100 cc/hr) indicate that a stabilized zone may have been formed prior to breakthrough, while Run 13 (50 cc/hr) and Run 14 (80 cc/hr) do not depict stabilized behaviour. The saturation profiles {Figs. A-4 to A-7} for this series of runs, due to a larger adverse viscosity ratio, are obscured due to perturbations caused by microscopic heterogeneties in the porous medium. Hence no conclusion can be drawn regarding the attainment of a stabilized zone by only looking at the saturation profiles.

For the Mineral oil displacements, Figure D-3 shows the plots of ΔP versus τ_i. In this series of runs, all the plots indicate that the displacement is stabilized prior to breakthrough. The saturation profiles for Mineral oil displacements {Figs. A-8 to A-12} show that

for Runs 16, 18 and 19, all of them conducted at 100 cc/hr, the frontal region has formed a fixed configuration prior to breakthrough. The saturation profiles for Run 20 in Fig. A-11 have slopes less steep than, say, the profiles in Fig. A-9 for Run 18. The only difference in these two runs is the rate. Run 20 (200 cc/hr) should have steeper profiles than Run 18 (100 cc/hr), as dictated by immiscible displacement theory. But this was not observed. As Warren and Calhoun's[53] analysis of ΔP versus τ_i plots was based on the conventional immiscible displacement theory, which is violated by the profiles of Run 20, any deductions for Run 20 and Run 21 (which was conducted at an even higher rate of 300 cc/hr) regarding the attainment of a stabilized zone will be without any theoretical basis.

As is evident from the foregoing analysis, ΔP versus τ_i behaviour was not a very reliable test for determining whether stabilization had been attained. On the contrary, it suggested stabilized displacements even for those runs which did not conform to the immiscible displacement theory. Thus, a more robust method of attack was required to analyse the displacement tests conducted in this study.

VI.3 ANALYSIS WITH THE HELP OF DIMENSIONLESS GROUPS

Bentsen[3,6] has shown that two scaling groups, the mobility ratio, M_r, and the capillary number, N_c, are important. They are

$$M_r = \frac{\mu_o K_{wr}}{\mu_w K_{or}} \qquad \text{(VI-1)}$$

$$N_c = \frac{\sigma A K_{wr}}{q \mu_w L} \qquad \text{(VI-2)}$$

These scaling groups pertain if the displacement is dictated by immiscible displacement theory, and hence is stable, but not necessarily stabilized.

For unstable displacements [Chouke[13], Hagoort[23]], Peters[46] has proposed a stability criterion which, for rectangular co-ordinates, is

$$E_p = (M_r - 1)\frac{V\mu_w L_x^2 L_y^2}{C^*\gamma K_{wr}(L_x^2 + L_y^2)} \leq \pi^2 \qquad \text{(VI-3)}$$

When E_p is greater than π^2, the displacement is unstable and immiscible displacement equations do not apply. The capillary constant, C*, is unique for the fluids and porous medium used. In this study Runs 8 to 11 used the same oil {Dow Corning}, though of different viscosity, and the same type of sand {Ottawa sand} as used by Peters[46] in his experiments. For this system he estimated a value of 306.25 for C*, in connate water bearing displacements.

Bentsen[6] has suggested that a plot of breakthrough recovery versus reciprocal capillary number should approach asymptotically the Buckley-Leverett[10] steady state breakthrough recovery. For those relative permeability models which seem to apply in the runs conducted in this study, the steady state breakthrough recovery can be derived in a manner similar to that of Bentsen[3].

Consider the non-capillary fractional flow function

$$F_w(S^*) = \frac{M_r K_{rw}}{M_r K_{rw} + K_{ro}} \qquad \text{(VI-4)}$$

and the relative permeability models

$$K_{rw}(S^*) = S^{*2} \qquad \text{(VI-5)}$$

and

$$K_{ro}(S^*) = (1 - S^*) \qquad \text{(VI-6)}$$

Substitute for the relative permeability models from Eqs.(VI-5) and (VI-6) in Eq.(VI-4) to obtain

$$F_w(S^*) = \frac{M_r S^{*2}}{M_r S^{*2} + (1 - S^*)} \qquad \text{(VI-7)}$$

or

$$\frac{dF_w(S^*)}{dS^*} = \frac{M_r S^*(2 - S^*)}{\{M_r S^{*2} + (1 - S^*)\}^2} \qquad \text{(VI-8)}$$

By virtue of Welge's[54] tangent construction, the flood front saturation can be related to the fractional flow function as,

$$\left(\frac{dF_w(S^*)}{dS^*}\right)_{S_f^*} = \frac{F_w(S_f^*)}{S_f^*} \qquad \text{(VI-9)}$$

Substitute for $\left(\frac{dF_w(S^*)}{dS^*}\right)_{S_f^*}$ and $F_w(S_f^*)$ from Eqs.(VI-7) and (VI-8) in (VI-9) and solve for S_f^* to obtain

$$S_f^* = \frac{1}{\sqrt{M_r}}, \quad M_r > 1 \text{ ; and } \quad S_f^* = 1, \quad M_r \leq 1 \qquad \text{(VI-10)}$$

The average saturation at breakthrough, S_{abt}^*, can also be related to the flood front saturation as

$$S_{abt}^* = \frac{S_f^*}{F_w(S_f^*)} \qquad \text{(VI-11)}$$

The average saturation at breakthrough is numerically equal to the dimensionless pore volumes injected at breakthrough, τ_{bt}^*. Substitute for S_f^* and $F_w(S_f^*)$ in Eq.(VI-11) to obtain

$$\left.\begin{aligned} \tau_{bt}^* = S_{abt}^* &= \frac{1}{M_r}\{2\sqrt{M_r} - 1\} \qquad M_r > 1 \\ \tau_{bt}^* &= 1 \qquad\qquad\qquad\qquad M_r \leq 1 \end{aligned}\right\} \qquad \text{(VI-12)}$$

Breakthrough recoveries, τ^*_{bt} for Run 11 {M_r = 8.24} and Run 18 {M_r = 9.21}, using Eq.(VI-12), are 57.54% and 55.5%, respectively. These are shown as horizontal lines in Figure VI-1. A numerical experiment was undertaken, using the data bases for Runs11 and 18, in which τ^*_{bt} was plotted versus $1/N_c$. Maximum breakthrough recoveries can only be obtained when the flood is stabilized {Terwilliger[51] et al.}, that is, when steady state {Bentsen[6]} is approached asymptotically. The arrows in Fig.VI-1 indicate the points on the curve at which the two runs were actually conducted. It is obvious that a stabilized zone has not been attained, contrary to the analysis of ΔP versus τ_i curves in Figures D-1 and D-3.

The capillary constant, C*, for the Dow Corning - Ottawa sand system has been quantitatively determined by Peters[46] and the asymptotic approach to the steady state recovery has been illustrated in Fig.(VI-1) at a capillary number, N_c, of 0.01.

Limits on N_c for stable and stabilized displacements can be evaluated for this system. Re-writing Eq.(VI-3) in terms of N_c,

$$E_p = (M_r - 1)\frac{q\mu_w L}{\sigma A K_{wr}}\frac{\sigma}{L}\frac{L_x^2 L_y^2(10^7)}{C^*\gamma(L_x^2 + L_y^2)(9.87)} \qquad \text{(VI-13)}$$

or

$$E_p = \left\{\frac{M_r - 1}{N_c}\right\}\frac{\sigma}{L}\frac{L_x^2 L_y^2(10^7)}{C^*\gamma(L_x^2 + L_y^2)(9.87)} \qquad \text{(VI-14)}$$

Apply the stability criterion on E_p for rectangular co-ordinates,

$$\left\{\frac{M_r - 1}{N_c}\right\}\frac{\sigma}{L}\frac{L_x^2 L_y^2(10^7)}{(9.87)C^*\gamma(L_x^2 + L_y^2)} \leq \pi^2 \qquad \text{(VI-15)}$$

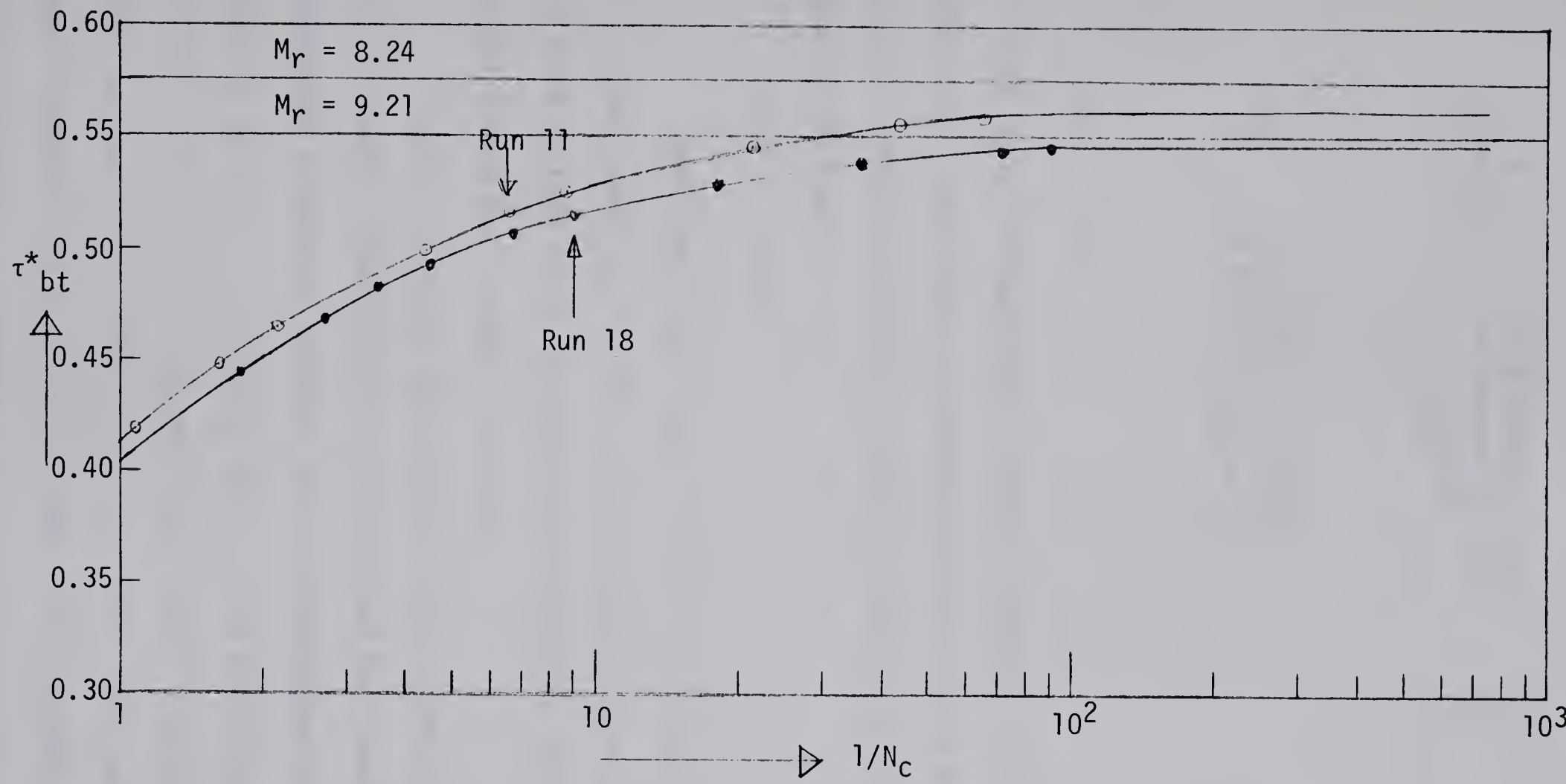


FIGURE VI-1

RECIPROCAL CAPILLARY NUMBER VERSUS BREAKTHROUGH RECOVERIES

or

$$\left\{\frac{N_c}{M_r - 1}\right\} \frac{L}{\sigma} \frac{(9.87)C^*\gamma(L_x^2 + L_y^2)}{L_x^2 L_y^2 (10^7)} \geq \frac{1}{\pi^2} \qquad \text{(VI-16)}$$

or

$$N_c \geq \frac{(10^7)(M_r - 1)\, L_x^2 L_y^2 \sigma}{(9.87\pi^2)C^*\gamma L(L_x^2 + L_y^2)} \qquad \text{(VI-17)}$$

Also

$$N_c \leq 0.01 \qquad \text{(VI-18)}$$

if a stabilized configuration is to be achieved within the confines of the core. Substitute the relevant values of the parameters in Eq.(VI-17) from the data set for Run 11 and obtain the limit on N_c for stable displacement

$$N_c \geq 0.0418 \qquad \text{(VI-19)}$$

Comparing inequalities (VI-18) and (VI-19) it is evident that for the geometry, fluids (Dow Corning) and porous medium (Ottawa sand) used in this study, a stabilized saturation configuration cannot be obtained within the length of the core.

Table VI-1 gives the values of the dimensionless groups, the experimental breakthrough recoveries and the steady state breakthrough recoveries using Eq.(VI-12) {but converting them to percent of initial oil in place} for all the runs conducted. For Runs 8 to 11, all have E_p much less than the maximum of π^2, indicating that these three runs were stable. The capillary number in each of the runs is more than 0.01 suggesting that stabilization has not been attained. This conclusion, which also

TABLE VI-1

VALUES OF DIMENSIONLESS GROUPS AND RECOVERIES
FOR THE RUNS CONDUCTED

Run No.	M_r	N_c	E_p	Recovery % IOIP	Steady State Recovery % IOIP	μ_o/μ_w
8	6.03	0.1453	1.47	51.3	72.8	
10	9.00	0.4140	0.82	39.6	63.6	9.34
11	8.24	0.1527	2.15	38.5	63.2	
12*	16.80	0.4930	1.27	18.5	47.1	
13*	40.16	0.6167	2.13	27.9	31.5	73.33
14*	43.90	0.4930	3.19	23.1	30.3	
15*	28.60	0.2248	4.27	24.4	37.0	
16	8.62	0.1209	2.09	51.8	63.2	
18	9.21	0.1113	2.30	48.6	60.2	
19	12.50	0.1815	2.01	41.9	51.8	12.25
20	11.89	0.0806	4.28	44.5	55.8	
21	10.73	0.0467	6.34	45.5	57.6	
9	0.3278	0.0234	**	79.0	80.0	
23	0.2920	0.0228	**	83.3	83.4	Favourable
24	0.2710	0.0424	**	78.4	78.5	

* σ for these series of runs was estimated as 0.017 atm
** these runs were unconditionally stable.

applies to Runs 8 and 11, is in contradiction with the analysis of ΔP versus τ_i curve where it was inferred that a stabilized zone had been formed.

The magnitude of E_p for the other two series of runs (Paraffin and Mineral oils) was determined using the same value of C* as estimated for Dow Corning oil - Ottawa sand system by Peters[46]. This allowed the calculation of relative values for E_p for each run. The absolute magnitudes of E_p may not be correct because an experimentally determined value of C* was not available for the Paraffin and Mineral oil systems.

For the Paraffin oil displacements the magnitude of the capillary numbers suggest that stabilization was not attained, but the estimated values of E_p indicate that the runs were stable. A similar analysis suggests that the same conclusions can be drawn with respect to the Mineral oil displacements in Runs 16, 18 and 19. That is, they are stable but stabilization has not been attained. Runs 20 and 21 have a lower N_c but a relatively higher value for E_p. The recoveries are also less than those obtained in Runs 16 and 18. This suggests an unstable displacement. The saturation profiles {Figs. A-11 and A-12} further substantiate this belief.

Thus it is possible to put bounds on C* for the Mineral oil - Ottawa sand system. As Run 18 (100 cc/hr) is stable (see saturation profiles in Fig.A-9), E_p should be less than π^2, while Run 20 is unstable (Fig.A-11) indicating E_p should be greater than π^2 which suggests that the capillary constant, C*, must lie within the range given below

$$77.22 < C^* < 141.45 \qquad \text{(VI-20)}$$

VI.4 EXPERIMENTAL SATURATION PROFILES AND BREAKTHROUGH RECOVERIES

The stable immiscible displacement theory suggests that there should be an increase in recovery with decreasing capillary number, for the same mobility ratio, till a stabilized displacement is attained. The definition of the capillary number, Eq.(VI-2) shows that an increase in length of the core will decrease the capillary number, N_c. Jones-Parra[32] et al. have reported that when they increased the length of the core, for the same rate, the recovery was increased.

The capillary number is also a function of the capillary pressure normalizing parameter, σ, and effective permeability to water at residual oil saturation, K_{wr}. These two variables were not measured experimentally. Their estimates were obtained by the procedure described in Chapter V. Similarly, mobility ratio is a function of K_{wr}. The estimates of effective permeability at residual oil saturation, K_{wr}, suggested that it was influenced by rate. As a consequence the mobility ratio would also be influenced by rate. It may also be that the K_{wr} was estimated at different residual oil saturations. If this is the case then S_{or} could be a function of rate. Because of these uncertainties in estimating K_{wr}, its value should, ideally, have been determined experimentally.

In the Dow Corning oil displacements, Run 8 (200 cc/hr) gave higher recoveries as compared to Run 10 (100 cc/hr) and Run 11 (300 cc/hr). A lower estimate of mobility ratio for Run 8 explains the higher recovery and also suggests a higher floodfront saturation, S_f^* {Eq.(VI-10)}. This difference in S_f^* is evident when the saturation profiles for Run 8 (Fig.A-1) and Run 11 (Fig.A-3) are compared. An outlet end-effect was observed in Run 10. The recovery

would have been much lower without the end-effect. Run 10 has a higher N_c and hence the frontal region is far from attaining a stabilized configeration. This is in contrast to Run 8 and 11 which are closer to stabilization. This is substantiated by the saturation profiles shown in Figs. A-1 to A-3.

On the basis of E_p values {Table VI-1} the Mineral oil displacements {Figs. A-8 to A-10}, Run 16, Run 18 and Run 19 are considered to be stable. Their breakthrough recoveries are consistent with the magnitudes of N_c and M_r. Runs 20 and 21 were found to be unstable with a high E_p and lower breakthrough recoveries. The significant difference in the slopes of the saturation profiles, when Run 18 and Run 20 are compared {Figs. A-9 and A-11}, indicates that a different mechanism is operating in each run.

Bentsen's[6] contention that the larger the value of M_r the earlier steady state is approached is substantiated when comparing the runs for the Paraffin oil displacements. Run 13 (50 cc/hr) and Run 15 (100 cc/hr) have different mobility ratios and capillary numbers. Run 15, with a lower N_c should be closer to steady state, but is not (compare the experimental and steady state breakthrough recoveries for each run), because of the lower M_r. Run 12 and Run 14 have exactly the same N_c but Run 12 is farther away from steady state than Run 14, because Run 14 has a much higher M_r.

VI.5 COMMENTS ON EXTERNAL DRIVE TECHNIQUES FOR THE DETERMINATION OF RELATIVE PERMEABILITIES

The graphical techniques proposed by Jones and Roszelle[30] were used to generate the relative permeability-saturation relationships depicted in Chapter V. Relative permeability curves were

determined for Runs 11 and 18. The basis for external drive techniques is the non-capillary Buckley-Leverett[10] theory. To strictly follow the theory and use displacement data to generate K_{eo}/K and K_{ew}/K curves the displacement should have achieved steady state prior to breakthrough. That is to say that N_c should have been less than 0.01, which was not the case. This may explain the scatter in the data of K_{eo}/K versus S_w curve {Figs. V-2 and V-3}.

Nevertheless the graphical techniques were used. These techniques require that effective viscosity, $\bar{\lambda}^{-1}$, and pore volumes produced, τ, be plotted versus pore volumes injected, τ_i. Moreover the after breakthrough portions of these curves are used for the determination of relative permeabilities. A close inspection of the $\bar{\lambda}^{-1} - \tau_i$ and $\tau - \tau_i$ curves indicate {Figs. D-5 to D-7 and Figs D-9 to D-11} that there is no substantial difference in the behaviour of these curves, for the same viscosity ratio, after breakthrough of the displacing liquid. The only exceptions to this argument are the Dow Corning oil displacements {Figs. D-5 and D-9} in which Runs 10 and 11 are similar but Run 8 is different. This implies that essentially the same relative permeability curves will be generated for a particular viscosity ratio. But when the saturation profiles of any two runs, in the same series, say, Run 18 and Run 20 are compared {Figs. A-9 and A-11}, it is apparent that substantially different relative permeability curves would be needed to match the saturation profiles.

The drawbacks of the external drive technique were also reported by Archer[1] [1973] and Sigmund and McCaffery[49] [1977].

Archer[1] suggested the use of a numerical simulator to match the oil production and pressure histories with a suitable choice of relative permeability models. His contention was that smooth relative permeability curves will be obtained, in contrast to the anomalous ones generated using the JBN[29] method. As found in this study, even if the recoveries and pressure histories are matched for a particular set of relative permeability curves this does not imply that the saturation profiles will also be matched using the same set of relative permeability curves.

VI.6 ANALYSIS OF RUNS AT FAVOURABLE MOBILITY RATIOS

The capillary numbers for Run 9, Run 23 and Run 24 {Table VI-1} have values closer to 0.01 implying that these displacement runs were nearly stabilized.

Figure D-4 shows the plots of pressure versus pore volumes injected for each of the three runs conducted at favourable mobility ratios. The plots do exhibit a non-linear secondary phase and then a linear stabilized zone, prior to breakthrough. The saturation profiles also suggest {Figs. A-13 to A-15} that after some time they do attain a stabilized configuration.

Runs 23 and 24 have essentially the same mobility ratio but Run 24 has twice the capillary number of Run 23. Both are nearly stabilized but the slope of the stabilized front at the lower N_c is steeper. This is consistent with the immiscible displacement theory which suggests that as capillary forces increase {higher N_c} the frontal region becomes more diffuse.

The non-linear secondary phase on the ΔP versus τ_i plot, and the saturation profiles corresponding to that phase, are in accordance with the transient behaviour of the fractional flow function shown in Fig.II-4.

The breakthrough recoveries in Run 9, Run 23 and Run 24 are consistent with the magnitudes of M_r and N_c. It could be said that these runs, conducted at favourable mobility ratio, validate the arguments for ΔP versus τ_i curve put forward by Warren and Calboun[53], and substantiate Bentsen's[6] contention that steady-state solution is an acceptable approximation to the displacement equation at low N_c.

It is appropriate to mention that external drive techniques cannot be applied here as oil production ceased immediately after breakthrough. This is evident from $\bar{\lambda}^{-1}$ and τ versus τ_i curves in Figs. D-8 and D-12, respectively.

CHAPTER VII

CONCLUSIONS AND RECOMMENDATIONS

VII.1 SUMMARY AND CONCLUSIONS

An attempt has been undertaken to obtain a better understanding of the immiscible displacement process by measuring saturations as a function of time and distance using a relatively new technique based on the principle of microwave attenuation. The measured saturation profiles were compared with numerical solutions of a Lagrangian formulation of the displacement equation to yield a quantitative measure of the theory.

An overall analysis in the light of published scaling groups and a stability criterion was also undertaken on saturation profiles, pressure plots and breakthrough recoveries.

The experimental and numerical results of this study, together with the analysis undertaken, led to the following conclusions:

1. The solution to the Lagrangian formulation of the immiscible displacement equation compared more favourably with the experimental saturation profiles than did the solution based on the Eulerian formulation.
2. The one-dimensional, immiscible displacement theory unconditionally represents displacements carried out at a favourable mobility ratio. For adverse mobility ratio displacements in horizontal systems, a stability criterion must be satisfied before the theory can be said to represent the

displacement process.

3. A stabilized configuration of the frontal region was not attained in the adverse mobility ratio displacements carried out in this study.
4. In the Dow Corning oil displacements, a stable displacement together with a stabilized configuration of the frontal region was not possible, for the core dimensions and the sand used in this study. That is, the bounds on the capillary number, N_c, for stabilized and stable displacements were mutually exclusive.
5. The capillary constant, C*, was found to lie in the range

$$77.22 < C^* < 141.45$$

for the Mineral oil - Ottawa sand system.

6. The capillary pressure normalizing parameter was estimated by a history match of the saturation profiles. The slope of the front depended on the magnitude of the capillary pressure normalizing parameter, σ.
7. This study experimentally verified that, for the same capillary number, N_c, the difference between steady state and transient breakthrough recoveries is higher for lower mobility ratios.
8. The experimental results obtained in this study suggest that the displacement process, at favourable mobility ratio, can be approximated by the steady state solution of the displacement equation, provided the capillary number is sufficiently small.
9. The scatter in the data for the oil relative permeability curve, calculated using the external drive technique, may be due to the fact that the runs were not stabilized. This suggests that a stabilized displacement is necessary, if the external drive

technique for the determination of relative permeabilities is used.

10. It may be difficult, if not impossible to infer the correct relative permeability curves from effective viscosity and cumulative oil production histories by applying the external drive technique used in this study. This is so because, while the saturation profiles differed substantially in a given series of runs (suggesting different relative permeability curves), the effective viscosity and cumulative oil production histories only differed slightly for a given viscosity ratio.

VII.2 RECOMMENDATIONS

The following suggestions may help in improving upon the results of this study:

1. The oscillator/RF unit used in this study did not provide sufficient power to measure water saturations over the entire range. It is recommended that a higher microwave power output unit, such as a Klystron, be used in future studies.
2. Raw microwave data were converted to saturation profiles by manually taking the logarithm of the power measured. In order to reduce the manual work required in this conversion, it is recommended that a log amplifier be placed in the circuit.
3. An extrapolation technique was used to obtain S_{or} and K_{wr}. As there is some question as to the accuracy of values obtained in this way, it is recommended that S_{or} and K_{wr} be experimentally determined in future studies.
4. It was found that the limits on the capillary number for a

stabilized and stable displacement were mutually exclusive in some of the runs conducted at adverse viscosity ratios. It is recommended, therefore, that some care be taken to design a flood where both criteria can be met, if external drive techniques are used to estimate relative permeability curves.

5. Runs 16, 18 and 19 were replicates. Run 19 was considerably different than the other two. While this difference may be attributed to the difference in absolute permeability, it may also be attributed to heterogeneous wettability. It is recommended that the sand packs used in future studies be treated so as to assure homogeneous wettability.
6. Parameters used in the capillary pressure and relative permeability models were obtained by matching numerically derived profiles with those obtained experimentally. In future studies, it is recommended that these parameters be estimated independently.
7. The microwave technique used in this study is based on the decrease in amplitude which occurs when a microwave signal passes through the core. Saturations can also be estimated by measuring phase shifts in the microwave signal. It is recommended that an investigation be undertaken with a view to ascertaining which of these two methods is better, and whether they may be used together to study three-phase flow, for example.
8. It was estimated that only 68% of the sample height was intercepted by microwaves in the vertical plane, which may not be true. It is recommended that an experiment be carried out to study the variation in microwave response when the core is scanned in the vertical plane. This experiment may suggest that improvements

in the design of the horn-lens antenna are necessary if a completely representative cross-section of the core is to be measured. For example, a larger aperture or a narrower microwave beam may be necessary.

9. Gravitational segregation may be a problem at lower displacement rates. If such is the case, it is recommended that the smaller dimension of the core cross-section be placed in the vertical plane. As a consequence, the transmitting and receiving horn antennas have to be placed above and below the mobile core-holder.

REFERENCES

1. Archer, J.S.: "Use of a Reservoir Simulator to Interpret Laboratory Waterflood Data", S.P.E. J., (December, 1973), p.343.

2. Baker, P.E.: "Discussion", S.P.E. J., (August, 1975), p.309.

3. Bentsen, R.G.: "Scaled Fluid Flow Models with Permeabilities Differing from That of the Prototype", Journal of Canadian Petroleum Technology, (July-September, 1976), Vol.15, No.3, p.46.

4. Bentsen, R.G. & Anli, J.: "A New Displacement Capillary Pressure Model", Journal of Canadian Petroleum Technology, (July-September, 1976), Vol.15, No.3, p.75.

5. Bentsen, R.G. & Anli, J.: "Using Parameter Estimation Techniques to Convert Centrifuge Data into a Capillary Pressure Curve", S.P.E. J., (February, 1977), p.57.

6. Bentsen, R.G.: "Conditions Under Which the Capillary Term May Be Neglected", Journal of Canadian Petroleum Technology, (October-December, 1978), Vol.17, No.4, p.25.

7. Bail, P.T. & Marsden, S.S.: "Saturation Distribution in a Linear System During Oil Displacement", Producers Monthly, (June, 1957), p.22.

8. Blair, P.M. & Weinaug, C.F.: "Solution of Two-Phase Flow Problems Using Implicit Difference Equations", S.P.E. J., (December, 1969), p.417.

9. Brown, J.: "Microwave Lenses", John Wiley & Sons, Inc., (1953).

10. Buckley, S.E. & Leverett, M.C.: "Mechanism of Fluid Displacement in Sands", Trans. AIME, Vol.146, (1942), p.107.

11. Cardwell, Jr., W.T.: "The Meaning of the Triple Value in Non-Capillary Buckley-Leverett Theory", Trans. AIME, Vol.216, (1959), p.271.

12. Chu, L.J. & Barrow, W.L.: "Electromagnetic Horn Design", Trans. Electrical Engineering, (July, 1939), Vol.58, p.333.

13 Chuoke,R.L., van Meurs, P. & van der Poel, C.: "The Instability of Slow, Immiscible, Viscous Liquid-Liquid Displacements in Permeable Media", Trans. AIME, Vol.216, (1959), p.188.

14. Dardaganian, S.G.: "The Application of the Buckley-Leverett Frontal Advance Theory to Petroleum Recovery", Trans. AIME, Vol.213, (1958), p.365.

15. Dekker, A.J.: "Solid State Physics", Prentice-Hall, Inc., Englewood Cliffs, N.J., (1957).

16. Douglas, Jr., J., Blair, P.M. & Wagner, R.J.: "Calculation of Linear Waterflood Behavior Including the Effects of Capillary Pressure", Trans. AIME, Vol.213, (1958), p.96.

17. Fayers, F.J. & Sheldon, J.W.: "The Effect of Capillary Pressure and Gravity on Two-Phase Fluid Flow in a Porous Medium", Trans. AIME, Vol.216, (1959), p.147.

18. Fradin, A.Z.: "Microwave Antennas", Translated from the Russian by Morton Nadler, Edited by R.C. Glass, Pergamon Press, N.Y. (1961).

19. Flock, D.L., Peters, E.J., Baird, H., Wiborg, R. & Kloepfer, J.: "The Influence of Frontal Instabilities During Viscous Oil Displacement", Proceedings, Canada-Venezuela Oil Sands Symposium, (1977), p.380.

20. Geffen, T.M. & Gladfelter, R.E.: "A Note on the X-ray Absorption Method of Determining Fluid Saturation in Cores", Trans. AIME, Vol.195, (1952), p.322.

21. Gladfelter, R.E.: "Private Communication", Amoco Production Company, Tulsa, Oklahoma, (February, 1978).

22. Gottfried, B.S., Guilinger, W.H. & Snyder, R.W.: "Numerical Solutions of the Equations for One-Dimensional Multi-Phase Flow in Porous Media", S.P.E. J., (March, 1966), p.62.

23. Hagoort, J.: "Displacement Stability of Water Drives in Water-Wet Connate-Water-Bearing Reservoirs", S.P.E. J., (February, 1974), p.63.

24. Harrison, G.R., Lord, R.C. & Loofbourow, J.R.: "Practical Spectroscopy", Prentice-Hall, Inc., Englewood Cliffs, N.J., (1948).

25. Harvey, A.F.: "Microwave Engineering", Academic Press, London & N.Y. (1963).

26. Hasted, J.B. & El Sabeh, S.H.M.: "The Dielectric Properties of Water in Solutions", Trans. Faraday Society, (1953), p.103.

27. Hellums, J.D. and Churchill, S.W.: "Dimensionless Analysis and Natural Circulation", Chem. Eng. Prog. Symposium Series, (1961), No.32, Vol.57, p.75.

28. Hovanessian, S.A. & Fayers, F.J.: "Linear Water Flood with Gravity and Capillary Effects", S.P.E. J., (March, 1961), p.32.

29. Johnson, E.F., Bossler, D.P. & Naumann, V.O.: "Calculation of Relative Permeability from Displacement Experiments", Trans. AIME, Vol.216, (1959), p.370.

30. Jones, S.C. & Roszelle, W.O.: "Graphical Techniques for Determining Relative Permeability from Displacement Experiments", J.P.T., (May, 1978), p.807.

31. Jones-Parra, J. & Calhoun, Jr., J.C.: "Computation of a Linear Flood by the Stabilized Zone Method", Trans. AIME, Vol.198, (1953), p.335.

32. Jones-Parra, J., Stahl, C.D. & Calhoun, J.C.: "A Theoretical and Experimental Study of Constant Rate Displacements in Water Wet Systems", Producers Monthly, (January, 1954), p.18.

33. Kufus, H.B. & Lynch, E.J.: "Linear Frontal Displacement in Multilayered Sands", Producers Monthly, (December, 1959), p.32.

34. Leverett, M.C.: "Flow of Oil-Water Mixtures through Unconsolidated Sands", Trans. AIME, Vol.132, (1939), p.149.

35. Leverett, M.C.: "Capillary Behavior in Porous Solids", Trans. AIME, Vol.142, (1941), p.152.

36. Levine, J.S.: "Displacement Experiments in a Consolidated Porous System", Trans. AIME, Vol.201, (1954), p.57.

37. Lipson, B.L.: "Theoretical Note on Linear Absorption Methods of Determination of Fluid Saturation in Porous Media", Trans. AIME, Vol.192, (1951), p.375.

38. McEwen, C.R.: "A Numerical Solution of the Linear Displacement Equation with Capillary Pressure", Trans. AIME, Vol.216, (1959), p.412.

39. Van Koughnett, A.L.: "Fundamentals of Microwave Heating", Transactions of the International Microwave Power Institute, Vol.1, (1973), Editors: Voss, W.A.G. and Tinga, W.R.

40. Parsons, R.W.: "Microwave Attenuation -- A New Tool for Monitoring Saturations in Laboratory Flooding Experiments", S.P.E. J., (August, 1975), p.302.

41. Parsons, R.W. & Jones, S.C.: "Linear Scaling in Slug-Type Processes -- Application to Micellar Flooding", S.P.E. J., (February, 1977), p.11.

42. Parsons, R.W.: "Private Communication", Marathon Oil Company, Littleton, Colorado, (1977-78).

43. Perkins, F.M.: "An Investigation of the Role of Capillary Forces in Laboratory Water Floods", Trans. AIME, Vol.210, (1957), p.409.

44. Perkins, Jr., F.M. & Collins, R.E.: "Scaling Laws for Laboratory Flow Models of Oil Reservoirs", Trans. AIME, Vol.219, (1960), p.383.

45. Perkins, T.K. & Johnson, O.C.: "A Study of Immiscible Fingering in Linear Models", S.P.E. J., (March, 1969), p.39.

46. Peters, E.J.: "Stability Theory and Viscous Fingering in Porous Media", Ph.D. dissertation, Department of Mineral Engineering, University of Alberta, Edmonton, Alberta. (1979).

47. Rapoport, L.A. & Leas, W.J.: "Properties of Linear Waterfloods", Trans. AIME, Vol.198, (1953), p.139.

48. Rose, W.D.: "Some Problems Connected with the Use of Classical Description of Fluid/Fluid Displacement Processes", Fundamentals of Transport Phenomena In Porous Media, Elsevier Publishing Co., (1972).

49. Sigmund, P.M. & McCaffery, F.G.: "An Improved Unsteady State Procedure for Determining the Relative Permeability Characteristics of Heterogeneous Porous Media", Paper No. SPE 6720, presented at 52nd Annual Fall Meeting of SPE of SIME in Denver, Colorado, (October 9-12, 1977).

50. Steber, J.D. & Marsden, S.S.: "The Determination of Liquid Saturations in a Porous Medium by a Method of Matched Refractive Indices", Producers Monthly, (April, 1956), p.48.

51. Terwilliger, P.L., Wiley, L.E., Hall, H.N., Bridges, P.M. & Morse, R.A.: "An Experimental and Theoretical Investigation of Gravity Drainage Performance", Trans. AIME, Vol.192, (1951), p.285.

52. Tinga, W.R.: "Interaction of Microwaves with Materials", Proceedings of IMPI Short Course for Users of Microwave Power, (November, 1970), p.19.

53. Warren, J.E. & Calhoun, Jr., J.C.: "The Inlet Saturation Distribution Transient in a Water Flood", Producers Monthly, (June, 1955), p.34.

54. Welge, H.J.: "A Simplified Method for Computing Oil Recovery by Gas or Water Drive", Trans. AIME, Vol.195, (1952), p.91.

55. Wyckoff, R.D. & Botset, H.G.: "The Flow of Gas-Liquid Mixtures Through Unconsolidated Sands", Physics, Vol.7, (September, 1936), p.325.

BIBLIOGRAPHY

1. Bagley, F.J. & Menzie, D.E.: "A Test of Connate Water Mobility", Producers Monthly, (July, 1958), p.21.

2. Batycky, J.P. & McCaffery, F.G.: "Low Interfacial Tension Displacement Studies", Paper No. 78-29-26, presented at the 29th Annual Technical Meeting of the Petroleum Society of CIM in Calgary, (June 13-16, 1978).

3. Boyer, R.L., Morgan, F. & Muskat, M.: "A New Method for Measurement of Oil Saturation in Cores", Trans. AIME, Vol.170, (1947), p.15.

4. Brinkman, H.C.: "Calculations on the Flow of Heterogeneous Mixtures Through Porous Media", App. Sci. Res., Vol.A1, (1949), p.333.

5. Brown, H.W.: "Capillary Pressure Investigations", Trans. AIME, Vol.192, (1951), p.67.

6. Calhoun, Jr., J.C. & LaRue, J.W.: "The Effect of Velocity in Water Flooding", Producers Monthly, (April, 1951), p.20.

7. Calhoun, Jr., J.C.: "A Discussion of Pressure Gradients on Oil Recovery by Water Flooding", Producers Monthly, (May, 1951), p.18.

8. Coley, F.H., Marsden, S.S. & Calhoun, J.C.: "A Study of the Effect of Wettability on the Behavior of Fluids in Synthetic Porous Media", Producers Monthly, (June, 1956), p.29.

9. Craig, Jr., F.F.: "The Reservoir Engineering Aspects of Waterflooding", Monograph Volume 3, AIME, Henry L. Doherty Series (1971), p.20.

10. Craig, Jr., F.F., Sanderlin, J.L., Moore, D.W. & Geffen, T.M.: "A Laboratory Study of Gravity Segregation in Frontal Drives", Trans. AIME, Vol.210, (1957), p.275.

11. Croes, G.A. & Schwarz, N.: "Dimensionally Scaled Experiments and the Theories on the Water Drive Process", Trans. AIME, Vol.204, (1955), p.35.

12. Dale, C.B., Macfarlane, R.M. & Hughes, R.V.: "The Effect of Pore Size on Oil Recovery when Flooding Long Unconsolidated Cores", Producers Monthly, (May, 1950), p.8.

13. De Haan, H.J.: "Effect of Capillary Forces in the Water-Drive Process", Proceedings, Fifth World Petroleum Congress, (1959), Section II, Paper No.25.

14. Dietz, D.N.: "A Theoretical Approach to the Problem of Encroaching and By-Passing Edge Water", Konikl Ned. Akad. Wetenschap, (1953), Proc. B56, 83.

15. Engelberts, W.F. & Klinkenberg, L.J.: "Laboratory Experiments on the Displacement of Oil by Water from Packs of Granular Material", Proceedings, Third World Petroleum Congress, Section II, (1951), p.544.

16. Fayers, F.J. & Perrine, R.L.: "Mathematical Description of Detergent Flooding in Oil Reservoirs", Trans. AIME, Vol.216, (1959), p.277.

17. "Flow Through Porous Media", Edited by Roger J.M. De Wiest. Academic Press, New York & London, (1969), p.455.

18. Gatenby, W.A. & Marsden, S.S.: "Some Wettability Charecteristics of Synthetic Porous Media", Producers Monthly, (November, 1957), p.5.

19. Hadley, G.F. & Handy, L.L.: "A Theoretical and Experimental Study of the Steady State Capillary End Effect", Paper No.707-G, presented at the 31st Annual Fall Meeting of SPE of AIME held in Los Angeles, (October 14-17, 1976).

20. Handy, L.L.: "Determination of Effective Capillary Pressures for Porous Media from Imbibition Data", Trans. AIME, Vol.219, (1960), p.75.

21. Handy, L.L. & Datta, P.: "Fluid Distributions During Immiscible Displacements in Porous Media", S.P.E. J., (September, 1966), p.261.

22. Hawthorne, R.G.: "Two-Phase Flow in Two-Dimensional System-Effects of Rate, Viscosity and Density on Fluid Displacement in Porous Media", Trans. AIME, Vol.219, (1960), p.81.

23. Jennings, H.Y.: "Effect of Laboratory Core Cleaning on Water-Oil Relative Permeability", Producers Monthly, (August, 1958), p.26.

24. Jordan, E.C. & Balman, K.G.: "Electromagnetic Waves and Radiating Systems", Prentice Hall, Inc., New Jersey, (1950).

25. Kern, L.R.: "Displacement Mechanism in Multi-Well Systems", Trans. AIME, Vol.195, (1952), p.39.

26. Kinney, P.T. & Nielson, R.F.: "The Role of Wettability in Oil Recovery", Producers Monthly, (January, 1950), p.29.

27. Kyte, J.R. & Rapoport, L.A.: "Linear Waterflood Behavior and End Effects in Water-Wet Porous Media", Trans. AIME, Vol.213, (1958), p.423.

28. Lefebvre du Prey, E.J.: "Factors Affecting Liquid-Liquid Relative Permeabilities of a Consolidated Porous Medium", S.P.E. J., (February, 1973), p.39.

29. Loomis, A.G. & Crowell, D.C.: "Relative Permeability Studies: II. Water-Oil Systems", Producers Monthly, (August, 1959), p.18.

30. Maguss, H. & Flock, D.L.: "Laboratory Model Flow Tests", Journal of Canadian Petroleum Technology, (Spring, 1962), Vol.1, No.1.

31. Martin, J.C.: "The Theory of One-Dimensional Two-Phase Flows of Incompressible Fluids", Producers Monthly, (July, 1960), p.18.

32. Melrose, J.C.: "Interfacial Phenomena as Related to Oil Recovery Mechanisms", Canadian Journal of Chemical Engineering, Vol.48, (December, 1970), p.638.

33. Moore, T.F. & Slobod, R.L.: "The Effect of Viscosity and Capillarity on the Displacement of Oil by Water", Producers Monthly, (August, 1956), p.20.

34. Morgan, F., McDavell, J.M. & Doty, E.C.: "Improvements in the X-Ray Saturation Technique of Studying Fluid Flow", Trans. AIME, Vol.189, (1950), p.183.

35. Morrow, N.R.: "Interplay of Capillary, Viscous and Bouyancy Forces in the Mobilization of Residual Oil", Paper No.78-29-24, presented at the 29th Annual Technical Meeting of the Petroleum Society of CIM in Calgary, (June 13-16, 1978).

36. Muskat, M. & Meres, M.W.: "The Flow of Heterogeneous Fluids Through Porous Media", Physics, Vol.7, (September, 1936), p.346.

37. Paez, J., Read, P. & Calhoun, Jr., J.C.: "Relationship Between Oil Recovery, Interfacial Tension, Pressure Gradient in Water Wet Porous Media", Producers Monthly, (May, 1955), p.34.

38. Rachford, Jr., H.H.: "Numerical Calculation of Immiscible Displacement By a Moving Reference Point Method", S.P.E. J., (June, 1966), p.87.

39. Richardson, J.G. & Perkins, F.M.: "A Laboratory Investigation of the Effect of Rate on Recovery of Oil by Water Flooding", Trans. AIME, Vol.210, (1957), p.114.

40. Richardson, J.G.: "The Calculation of Waterflood Recovery From Steady-State Relative Permeability Data", Trans. AIME, Vol.210, (1957), p.373.

41. Rust, C.F.: "Electrical Resistivity Measurements on Reservoir Rock Samples by the Two-Electrode and Four-Electrode Methods", Trans. AIME, Vol.195, (1952), p.217.

42. Salathiel, R.A.: "Oil Recovery by Surface Film Drainage in Mixed-Wettability Rocks", J.P.T., (October, 1973), p.1216.

43. Settari, A. & Aziz, K.: "A Computer Model for Two-Phase Coning Simulation", S.P.E. J., (June, 1974), p.221.

44. Sheldon, J.W. & Cardwell, Jr., W.T.: "One-Dimensional, Incompressible, Noncapillary, Two-Phase Fluid Flow in a Porous Medium", Trans. AIME, Vol.216, (1959), p.290.

45. Sincovec, R.F.: "Numerical Reservoir Simulator Using an Ordinary Differential-Equations Integrator", S.P.E. J., (June, 1975), p.255.

46. Sincovec, R.F.: "Generalized Collocation Methods for Time-Dependent, Nonlinear, Boundary-Value Problems", S.P.E. J., (October, 1977), p.345.

47. Vossoughi, Shapour: "Viscous Fingering in Immiscible Displacement", Ph.D. dissertation, Department of Chemical Engineering, University of Alberta, Edmonton, Alberta, (1976).

48. Warren, J.E.: "A Study of Waterflood Efficiency in Oil-Wet Systems", Trans. AIME, Vol.204, (1955), p.22.

APPENDIX A

EXPERIMENTALLY MEASURED SATURATION PROFILES

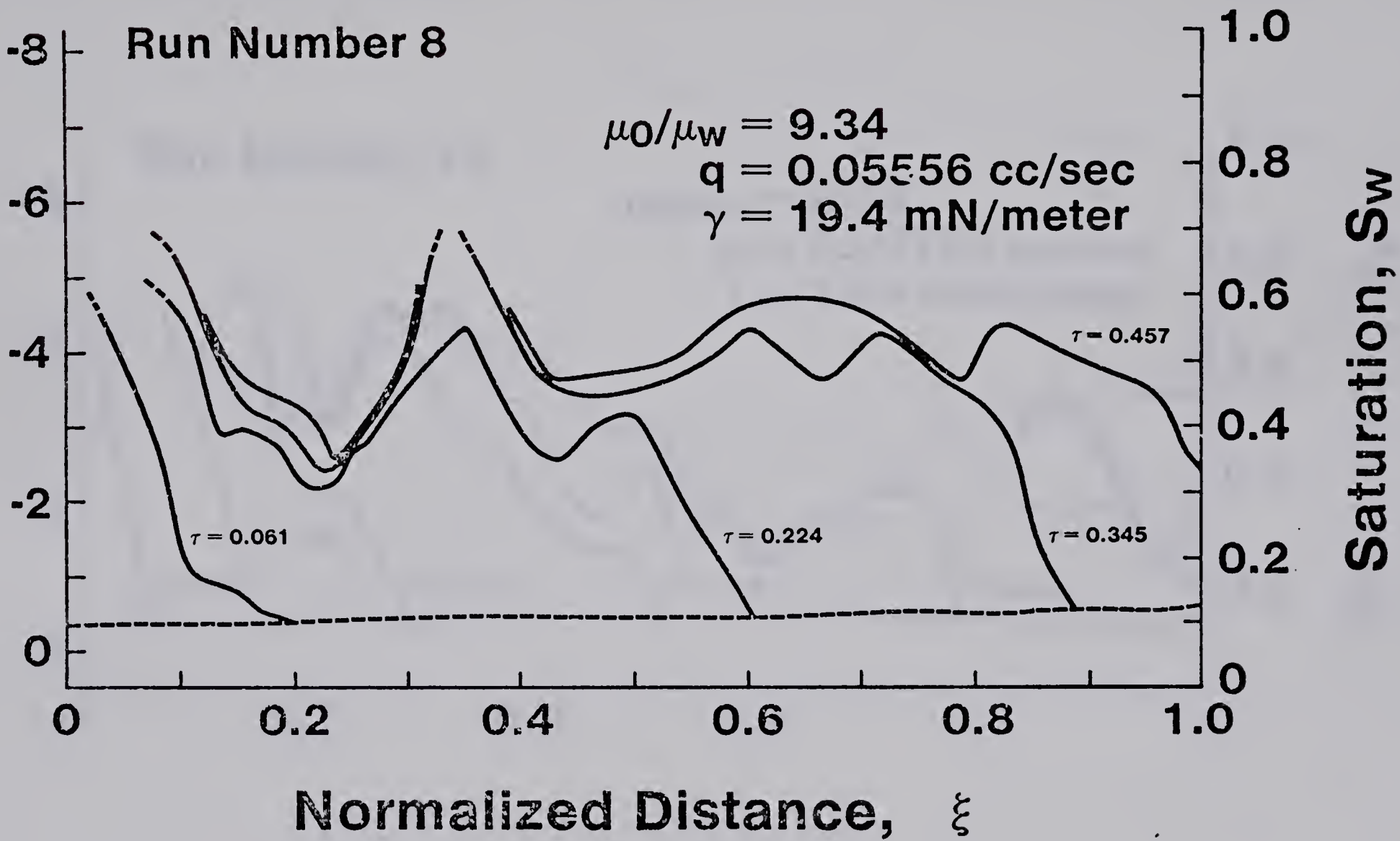


FIGURE A-1 EXPERIMENTAL SATURATION PROFILES

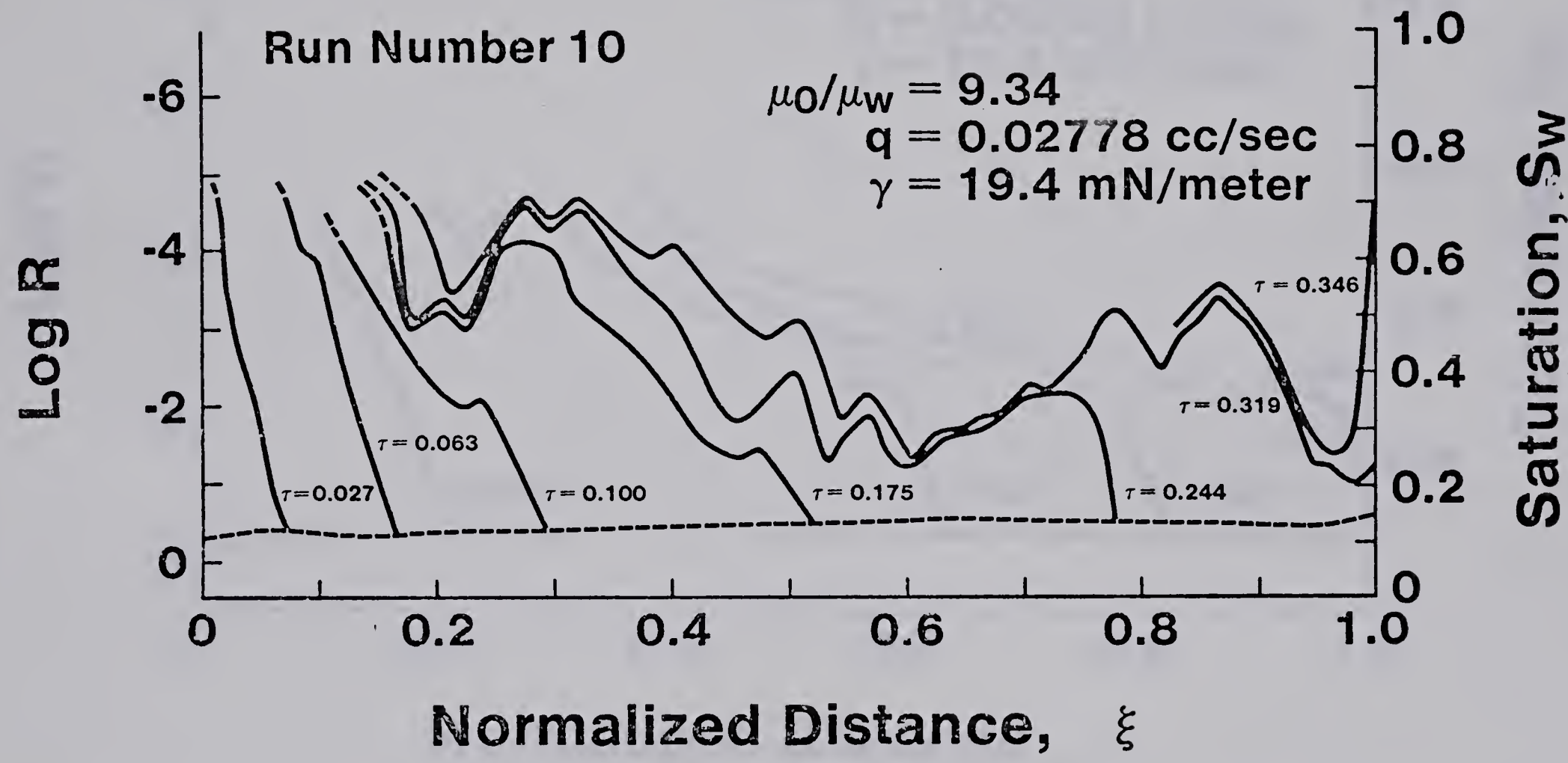


FIGURE A-2 EXPERIMENTAL SATURATION PROFILES



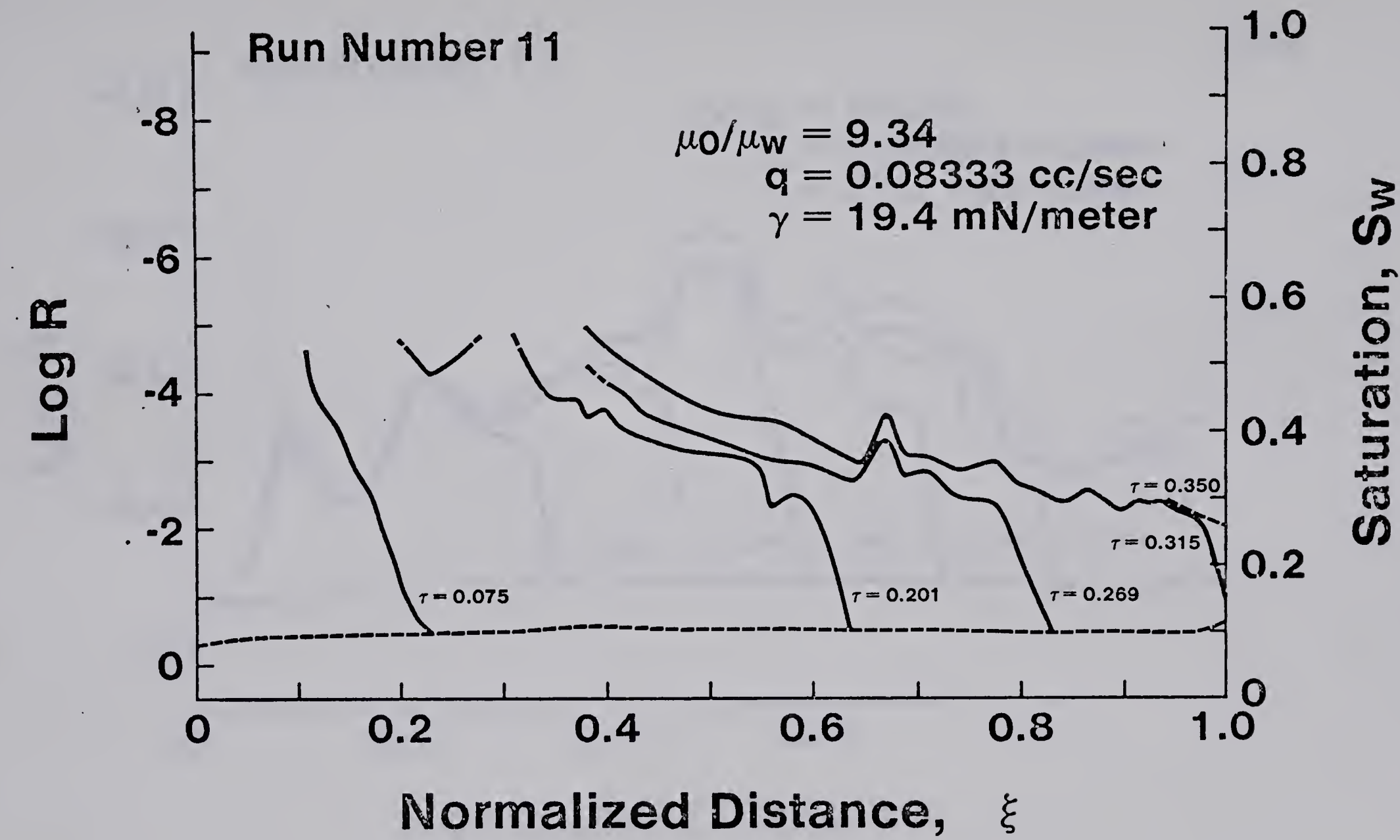


FIGURE A-3 EXPERIMENTAL SATURATION PROFILES



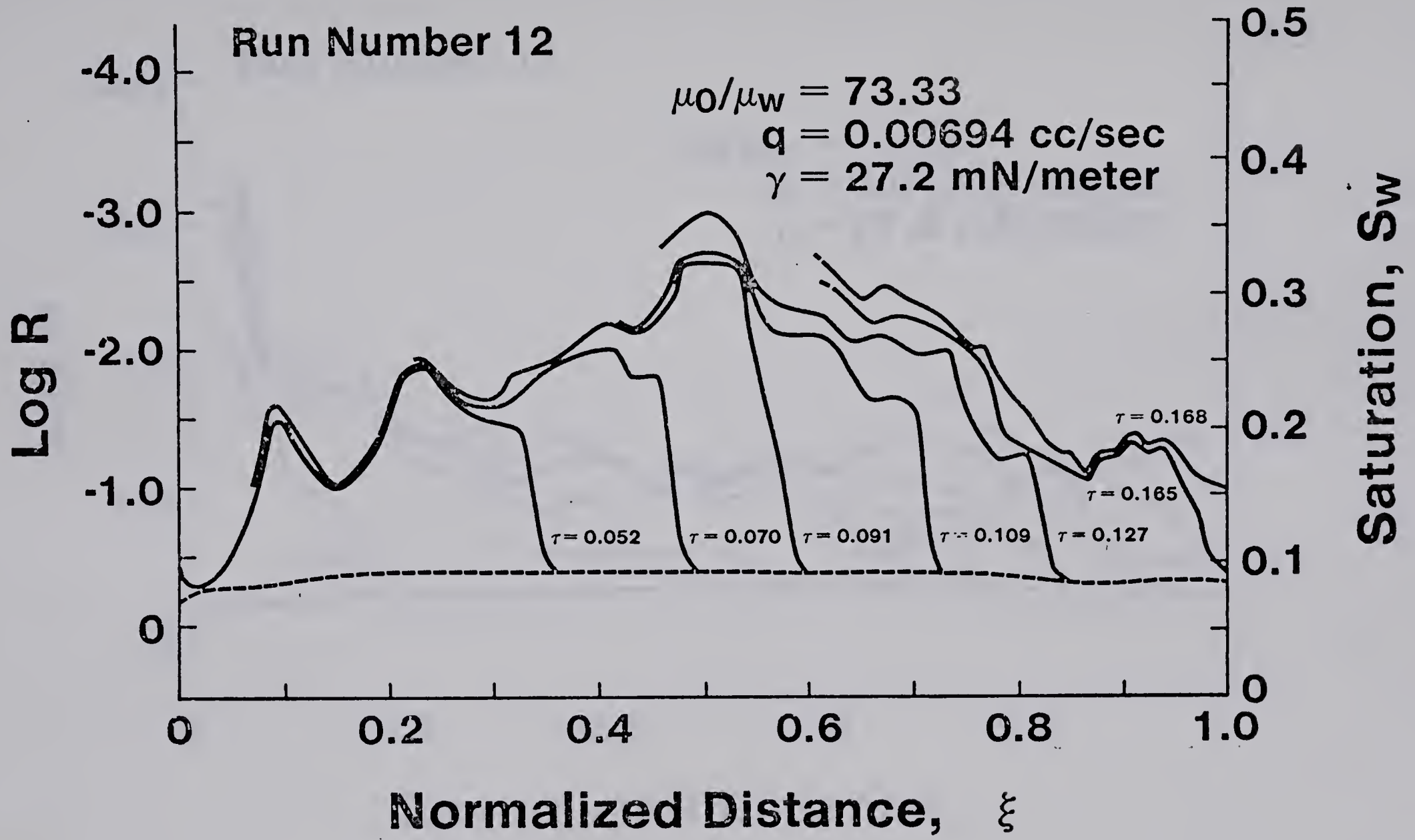


FIGURE A-4 EXPERIMENTAL SATURATION PROFILES



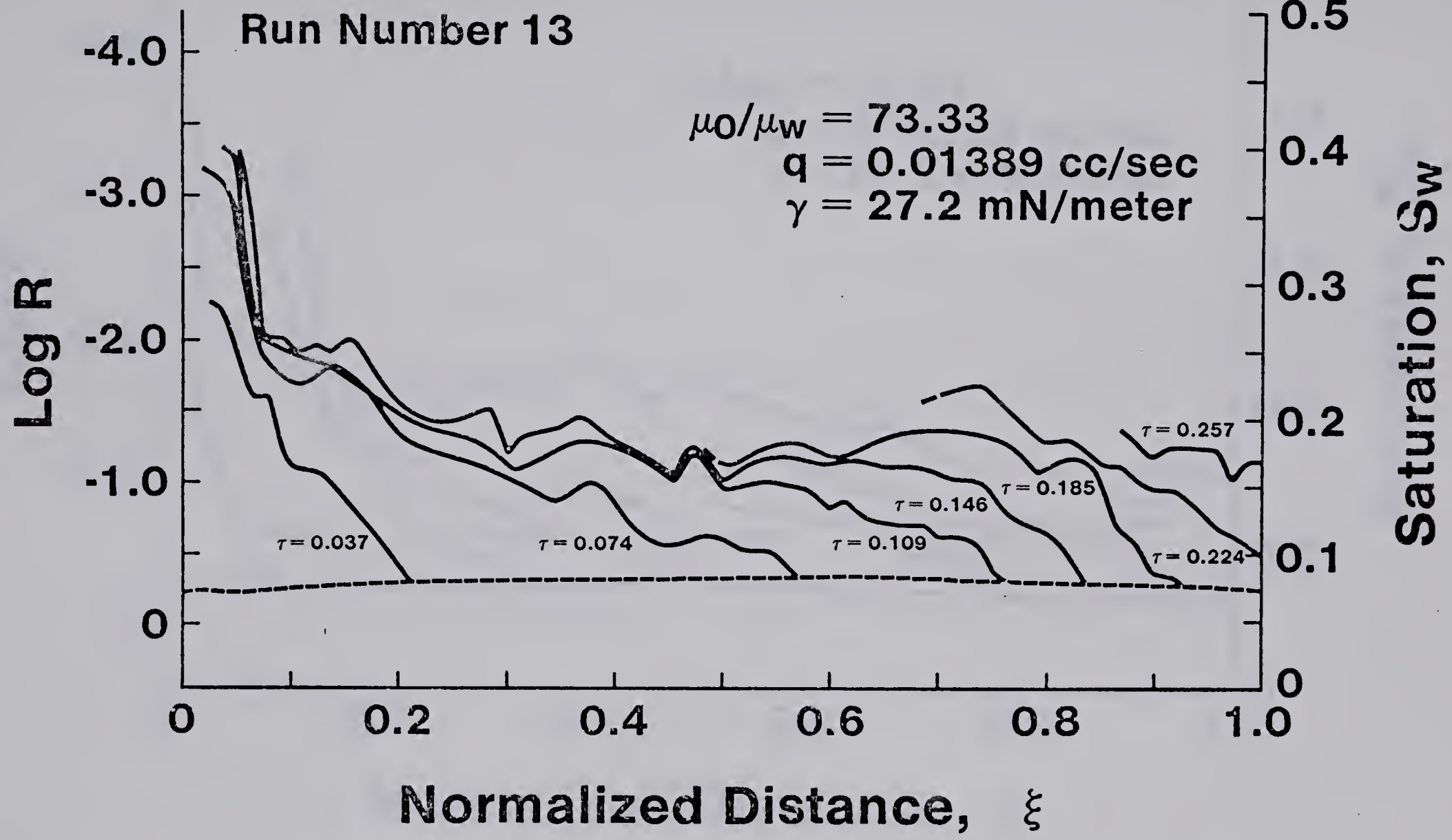


FIGURE A-5 EXPERIMENTAL SATURATION PROFILES



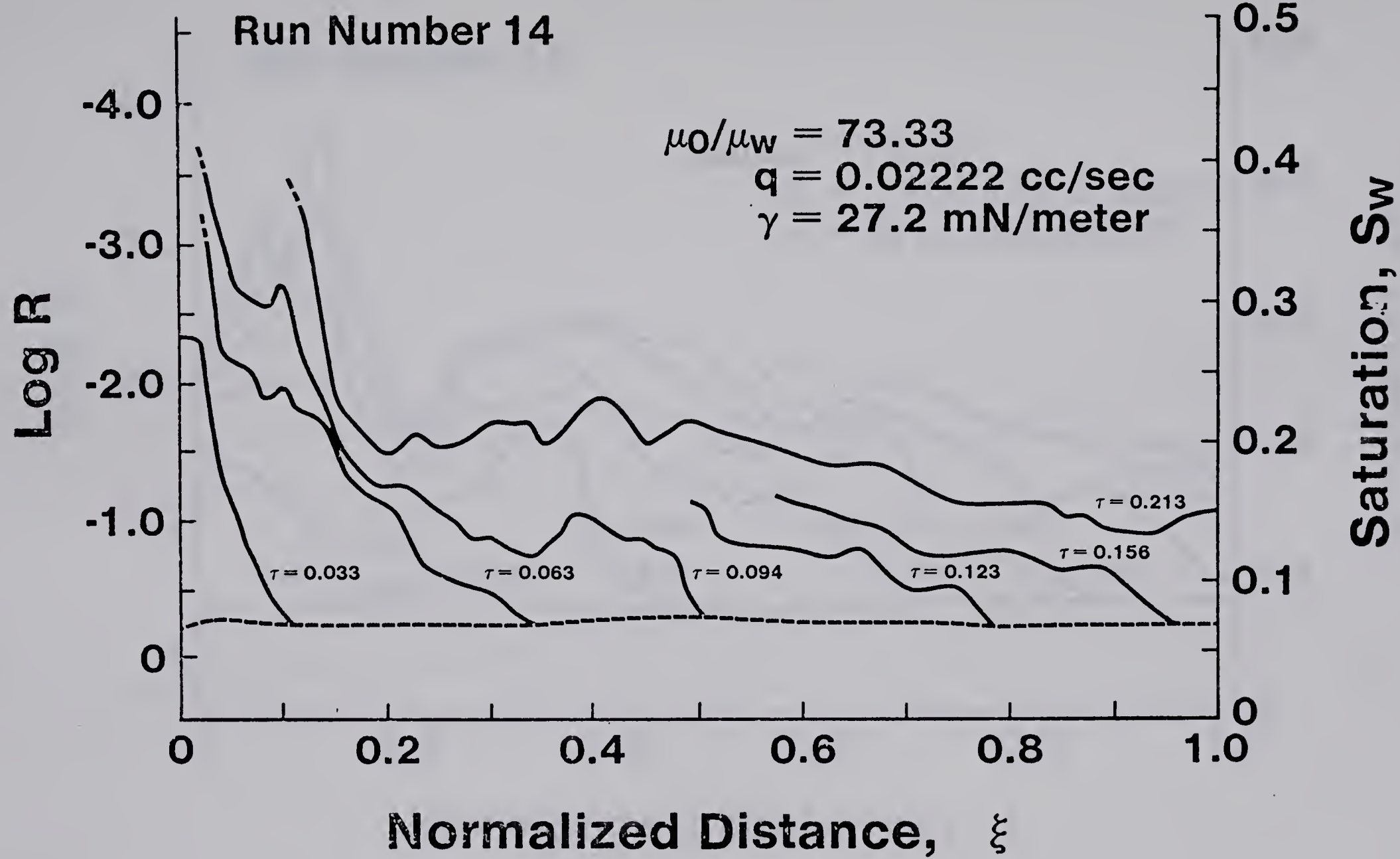


FIGURE A-6 EXPERIMENTAL SATURATION PROFILES



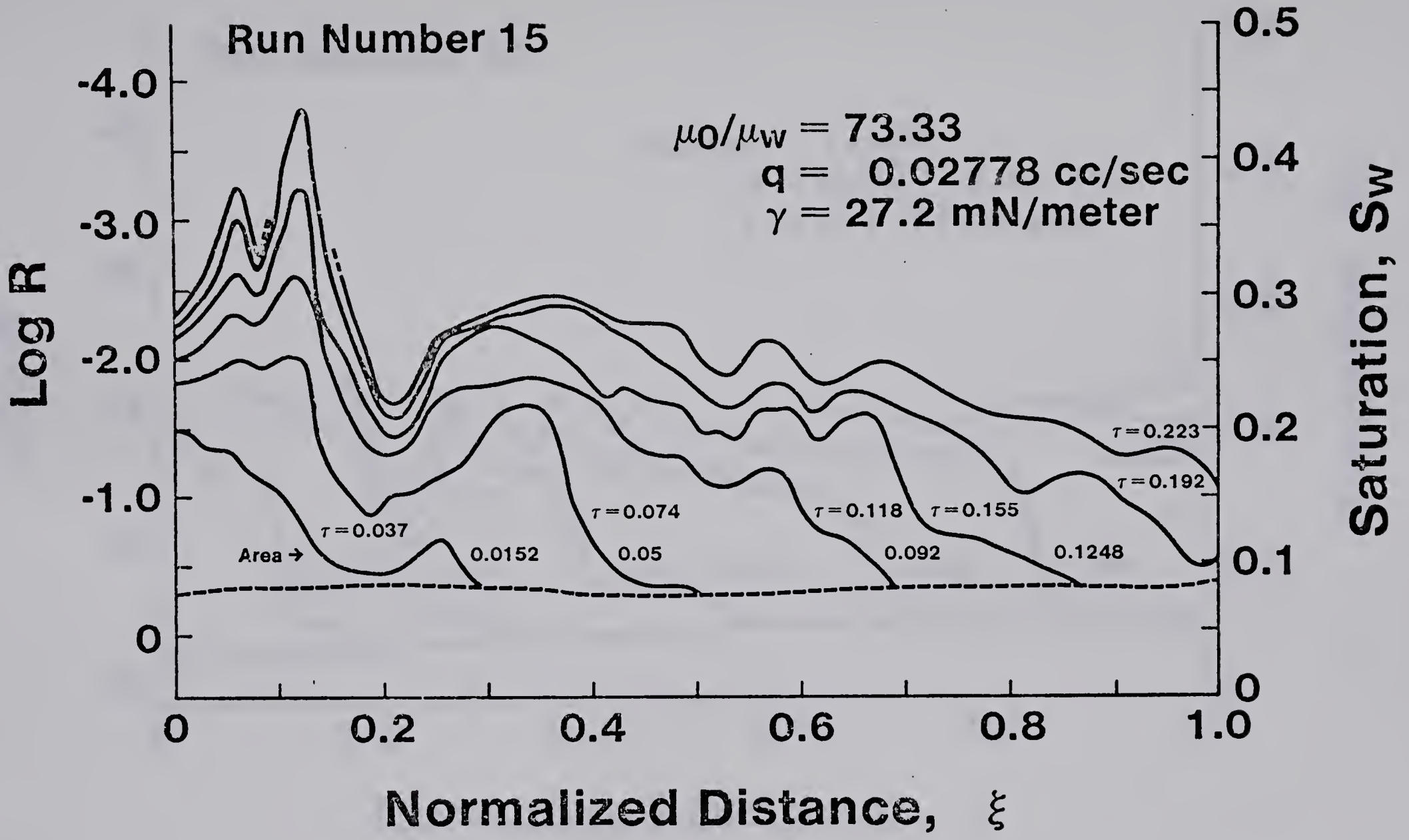


FIGURE A-7 EXPERIMENTAL SATURATION PROFILES



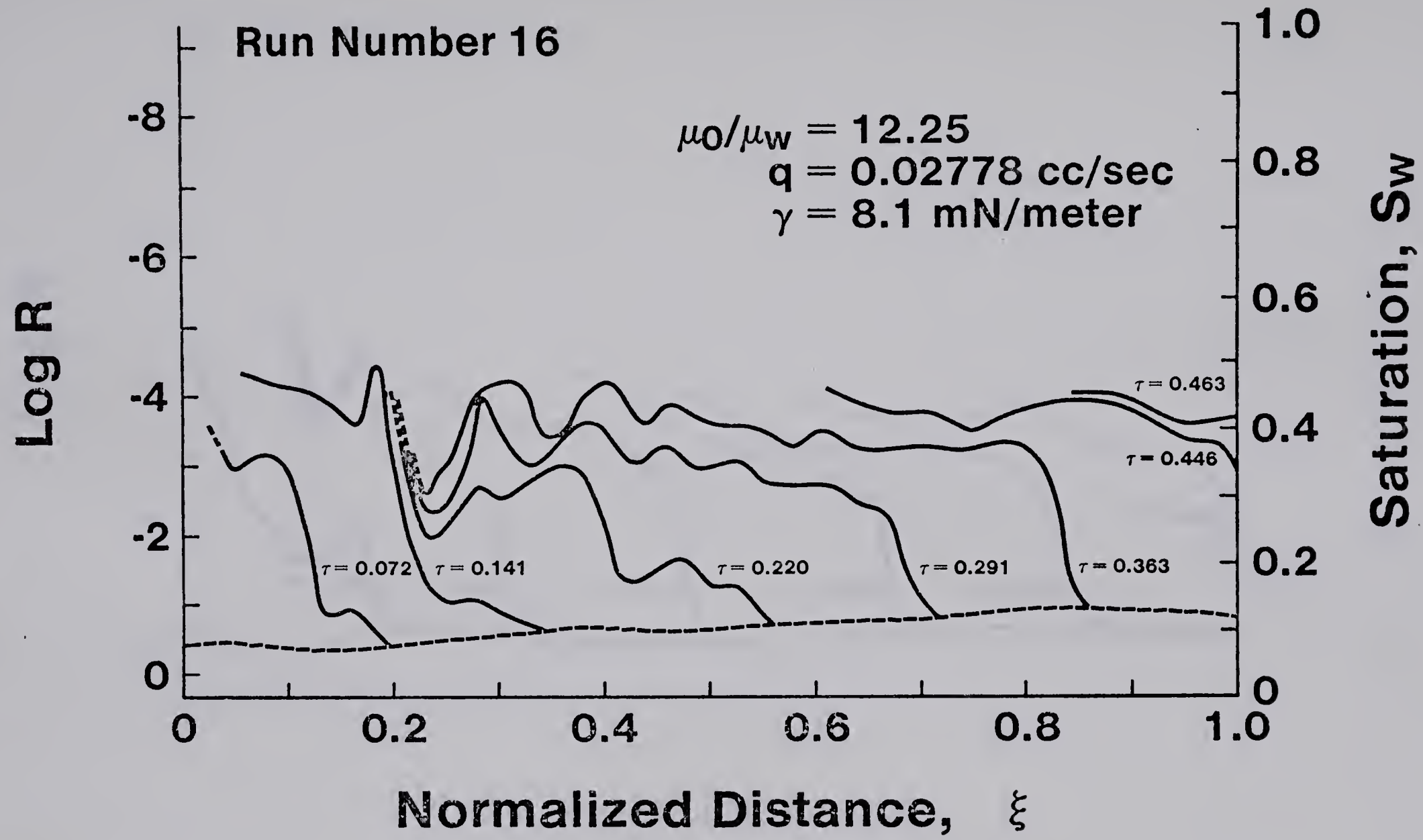


FIGURE A-8 EXPERIMENTAL SATURATION PROFILES



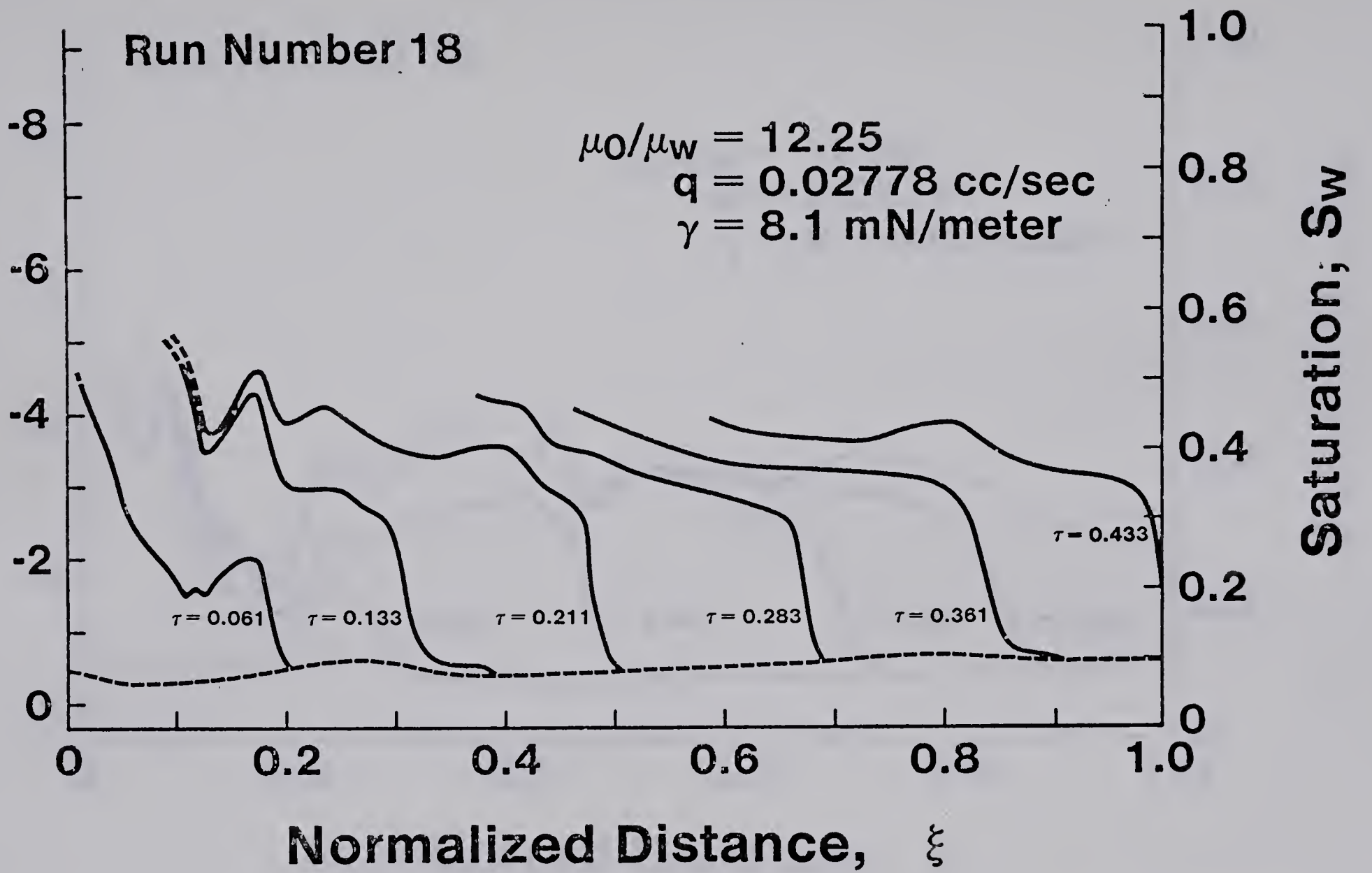


FIGURE A-9 EXPERIMENTAL SATURATION PROFILES

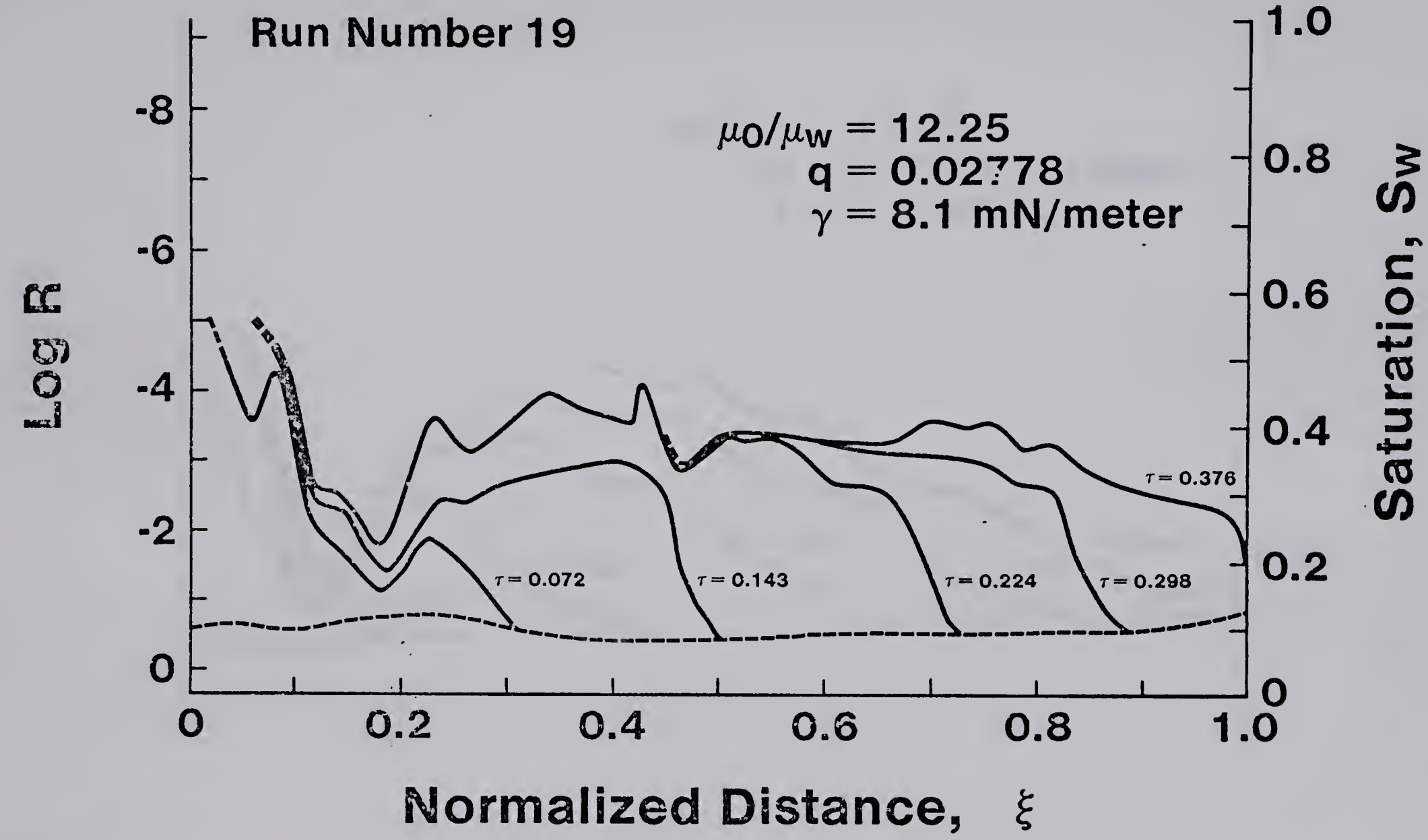


FIGURE A-10 EXPERIMENTAL SATURATION PROFILES



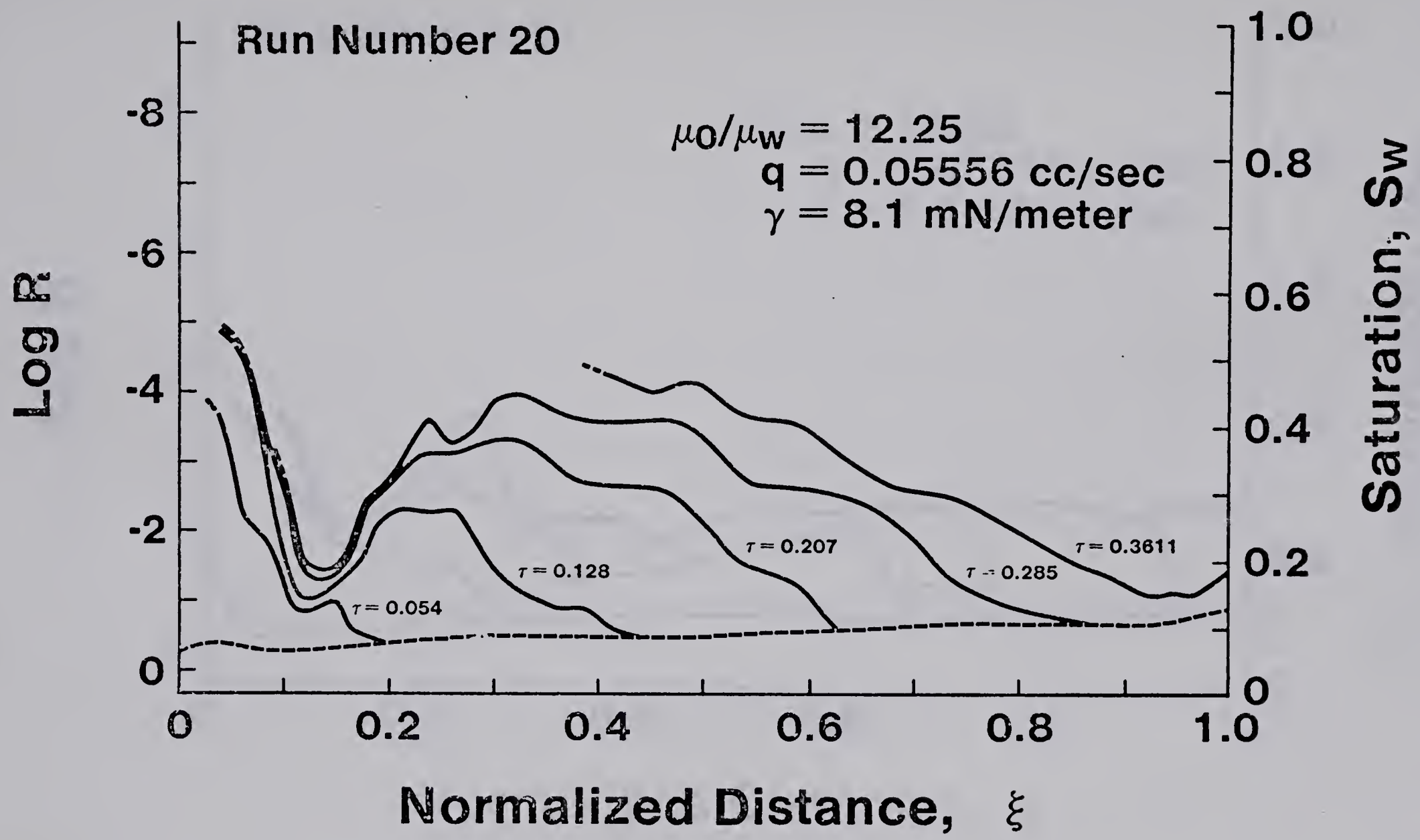


FIGURE A-11 EXPERIMENTAL SATURATION PROFILES

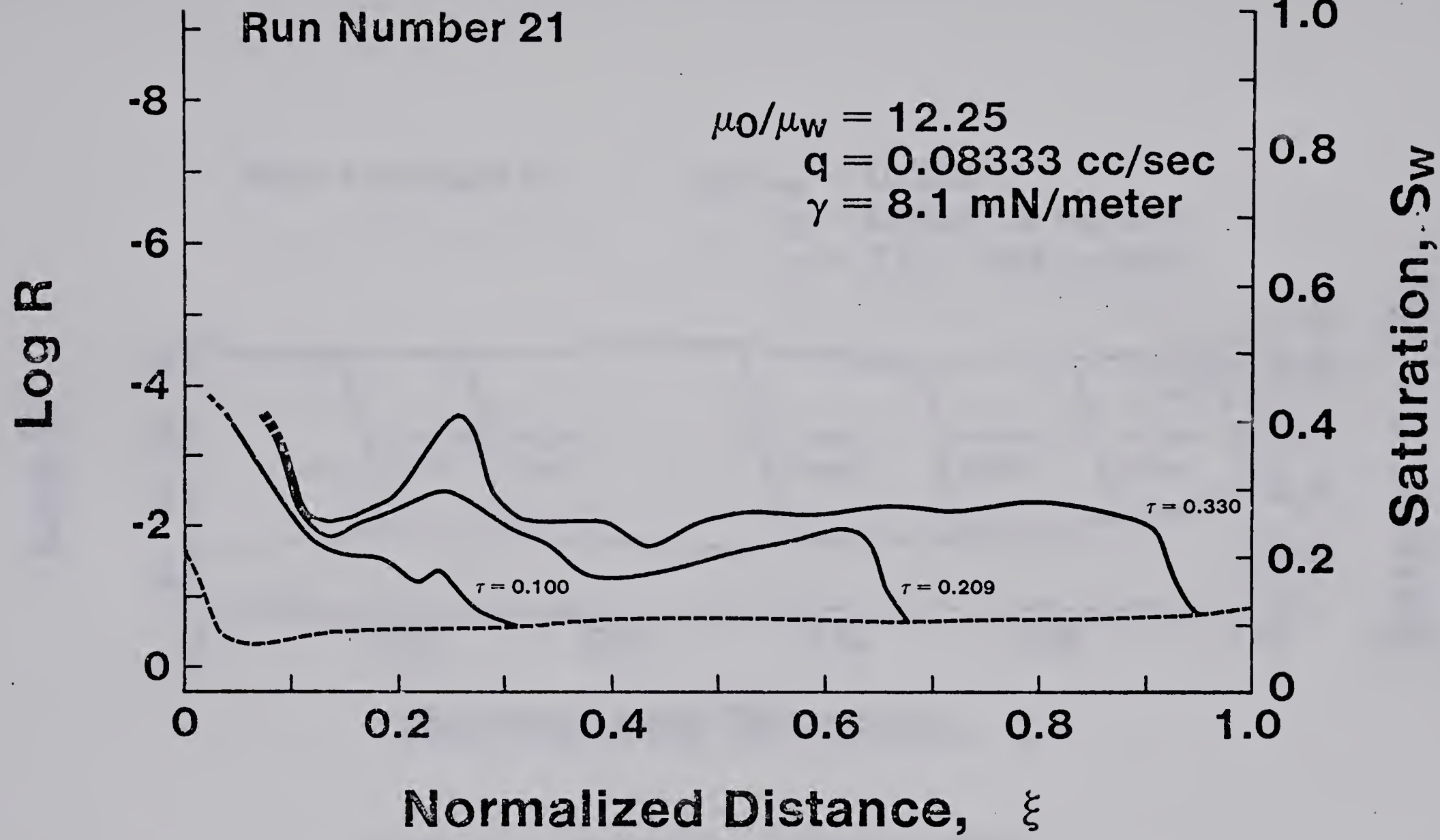


FIGURE A-12 EXPERIMENTAL SATURATION PROFILES

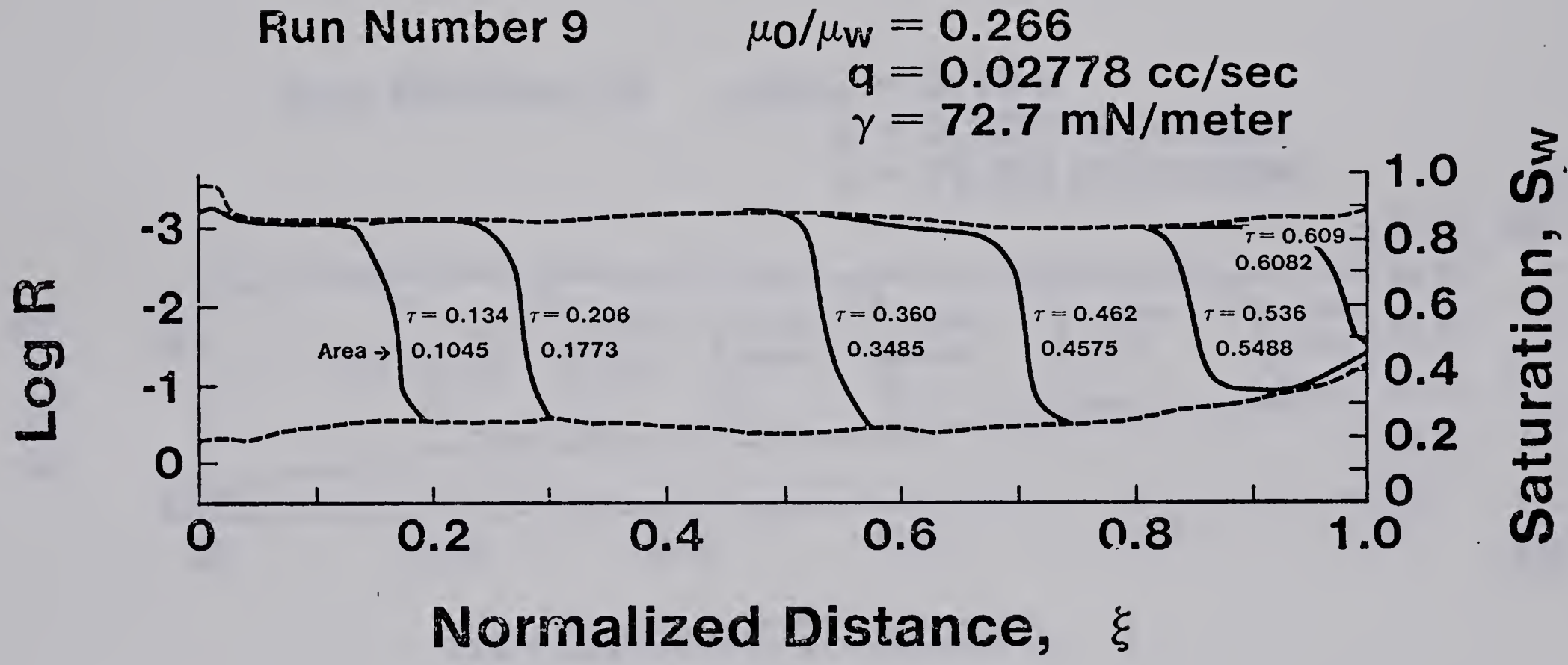


FIGURE A-13 EXPERIMENTAL SATURATION PROFILES



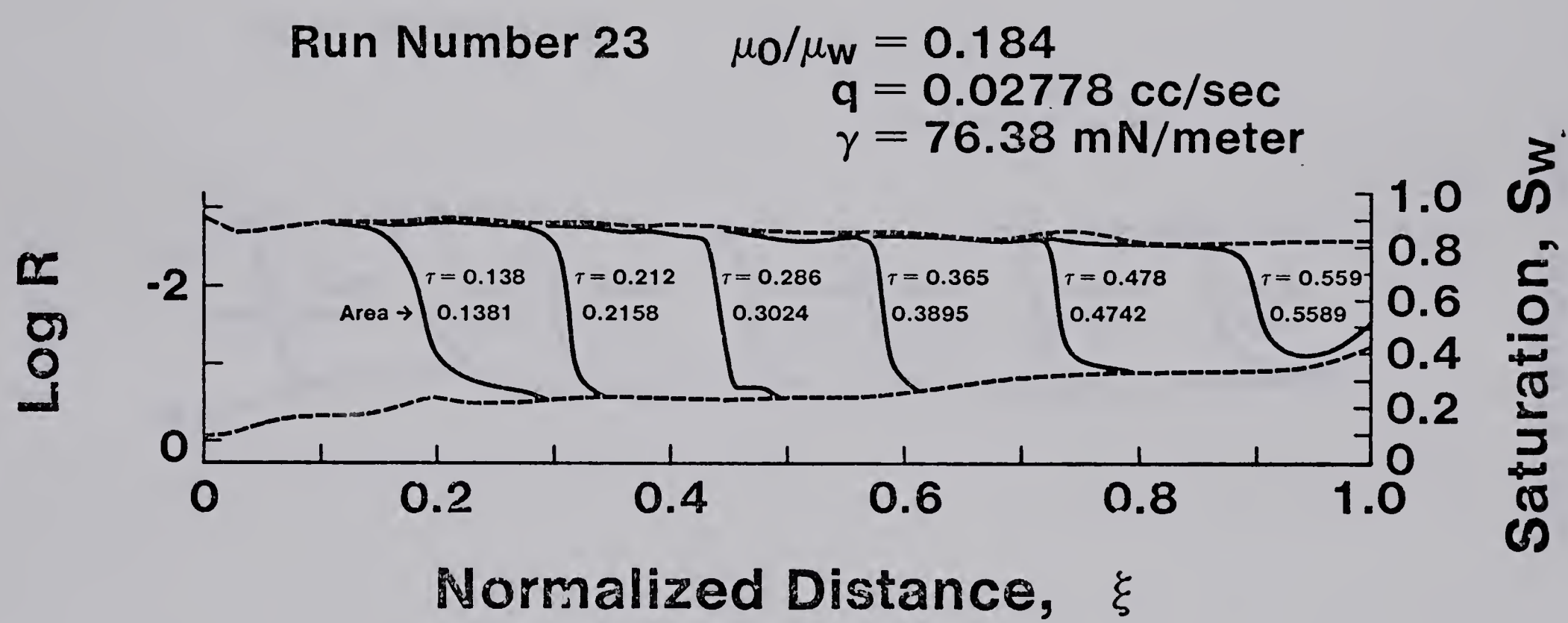


FIGURE A-14 EXPERIMENTAL SATURATION PROFILES



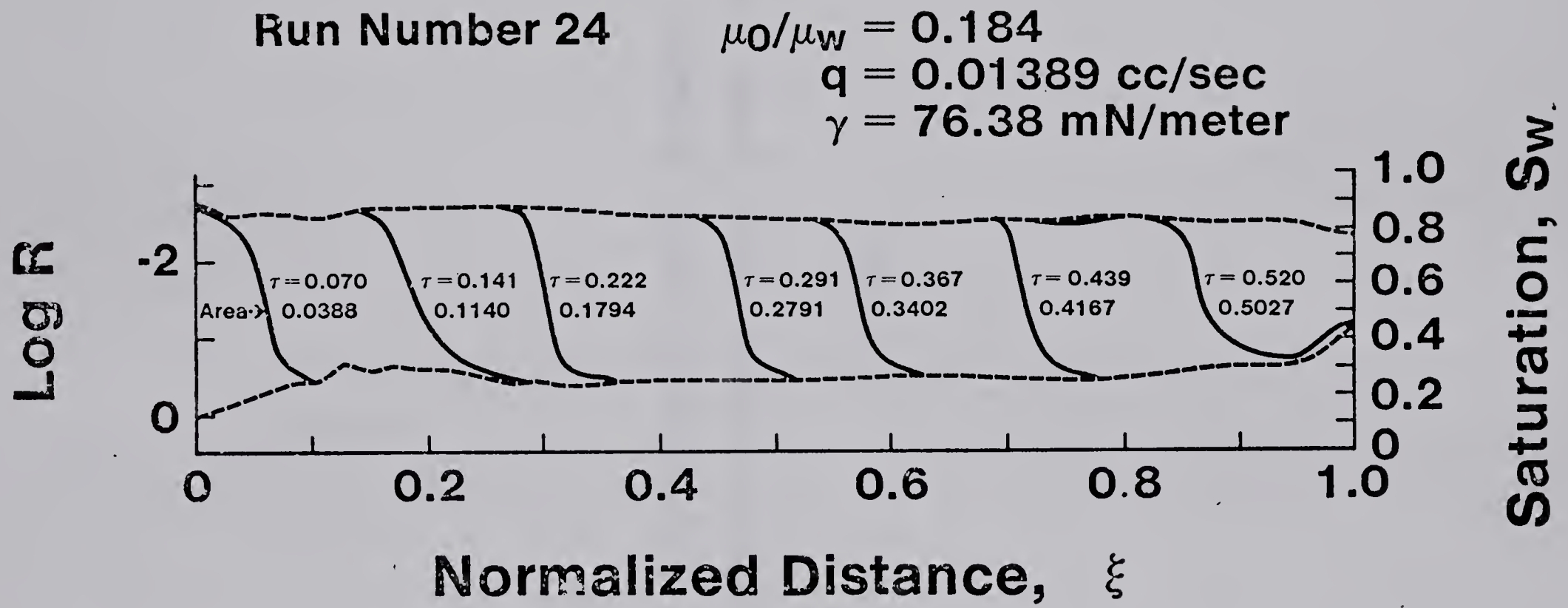


FIGURE A-15 EXPERIMENTAL SATURATION PROFILES



APPENDIX B

TABLES SHOWING PHYSICAL PROPERTIES AND OTHER PARAMETERS FOR THE EXPERIMENTAL RUNS

TABLE B-1

CORE HOLDER #1

OIL: DOW-CORNING

μ_o = 9.34 mPa-sec

ρ_o = 934 kg/m^3

L = 91.44 cm

μ_w = 1.0 mPa-sec

q (oil flood) = 0.05556 cc/sec (while establishing S_{wi})

ρ_w = 1000 kg/m^3

A = 6.859 cm^2

γ = 19.4 mN/meter

Run No.	q (water flood) cc/sec	K μm^2	P.V. cc	$\bar{S}_{wi}$ %	K_{or} μm^2	K_{wr} μm^2	$\bar{S}_{or}$ %
8	0.05556	12.08	245.0	10.82	8.33	5.38*	**
10	0.02778	10.78	240.0	12.60	7.97	7.67*	**
11	0.08333	12.29	241.2	9.00	9.61	8.48*	27.00*

* estimated using extrapolation technique [Ref. Ch.V]
** not estimated

TABLE B-2

CORE HOLDER #1

OIL: PARAFFIN

μ_o = 73.33 mPa-sec

ρ_o = 862.7 kg/m^3

L = 91.44 cm

μ_w = 1.0 mPa-sec

q (oil flood) = 0.02778 cc/sec (while establishing S_{wi})

ρ_w = 1000 kg/m^3

A = 6.859 cm^2

γ = 27.2 mN/meter

Run No.	q (water flood) cc/sec	K μm^2	P.V. cc	$\bar{S}_{wi}$ %	K_{or} μm^2	K_{wr} μm^2	$\bar{S}_{or}$ %
12	0.00694	10.75	230.0	9.10	11.69†	2.68*	**
13	0.01389	12.79	243.5	7.90	12.27	6.72*	**
14	0.02222	13.71	239.8	7.90	14.37†	8.60*	**
15	0.02778	12.79	242.0	8.47	12.54	4.89*	**

† The effective permeability to oil at initial water saturation, K_{or}, is larger than the absolute permeability, K, which may not be. The exact reason for this could not be ascertained.

** not estimated.

* estimated using extrapolation technique [Ref. Ch.V]

TABLE B-3

CORE HOLDER #2

OIL: MINERAL (HEPTANE + PARAFFIN)

μ_o = 12.25 mPa-sec q (oil flood) = 0.05556 cc/sec (while establishing S_{wi})

ρ_o = 833 kg/m^3 ρ_w = 1000 kg/m^3

L = 91.93 cm A = 6.477 cm^2

μ_w = 1.0 mPa-sec γ = 8.1 mN/meter

Run No.	q (water flood) cc/sec	K μm^2	P.V. cc	$\bar{S}_{wi}$ %	K_{or} μm^2	K_{wr} μm^2	$\bar{S}_{or}$ %
16	0.02778	14.48	230.0	10.65	13.54	9.53*	**
18	0.02778	13.15	230.0	8.70	11.53	8.78*	10.00*
19	0.02778	15.05	230.0	6.10	14.02	14.31*	**
20	0.05556	14.12	230.0	11.10	13.10	12.71*	**
21	0.08333	14.30	230.0	10.18	12.62	11.05*	**

* estimated using extrapolation technique [Ref. Ch.V]
** not estimated

TABLE B-4

CORE HOLDER #1

OIL: KEROSINE

DISPLACING FLUID: GLYCERINE + WATER

μ_o = 1.367 mPa-sec q (oil flood) = 0.05556 cc/sec (while establishing S_{wi})

ρ_o = 794.6 kg/m^3 ρ_w = 1079 kg/m^3

L = 91.44 cm A = 6.859 cm^2

μ_w = 5.14 mPa-sec γ = 72.7 mN/meter

Run No.	q (water flood) cc/sec	K μm^2	P.V. cc	$\bar{S}_{wi}$ %	K_{or} μm^2	K_{wr} μm^2	$\bar{S}_{or}$ %
9	0.02778	12.42	238.0	17.90	5.76	6.36	16.34

TABLE B-5

CORE HOLDER #2

OIL: KEROSINE

DISPLACING FLUID: GLYCERINE + WATER

μ_o = 1.22 mPa-sec q (oil flood) = 0.05556 cc/sec (while establishing S_{wi})

ρ_o = 798 Kg/m^3 ρ_w = 1100 kg/m^3

L = 91.93 cm A = 6.477 cm^2

μ_w = 6.62 mPa-sec γ = 76.38 mN/meter

Run No.	q (water flood) cc/sec	K μm^2	P.V. cc	$\bar{S}_{wi}$ %	K_{or} μm^2	K_{wr} μm^2	$\bar{S}_{or}$ %
23	0.02778	14.02	229.0	23.80	5.37	8.51	12.66
24	0.01389	14.59	230.0	24.35	5.37	7.90	16.30

APPENDIX C

MICROWAVE LENS ANTENNA DESIGN

MICROWAVE SIGNAL-WATER SATURATION CALCULATION

C.1 DESIGN OF THE LENS ANTENNA

C.1.1 Basis

The design of the lens antenna is based on the principle of refraction in optics. A spherical or cylindrical wave has to be incident on the excited side of the lens and emerges into free space according to the equation

$$n = \frac{c}{v_\phi} = \frac{3(10^{10})}{v_\phi} \qquad \text{(C-1)}$$

$n = \frac{\sin\Phi}{\sin\psi}$ = refractive index $\neq$ 1

c = velocity of light cm/sec

v_ϕ = phase velocity

Φ = angle of incidence

ψ = angle of refraction

In this work the radiator was a pyramidal horn and a point source was taken at the throat of the horn or at the focal point, F {Fig.C-1}.

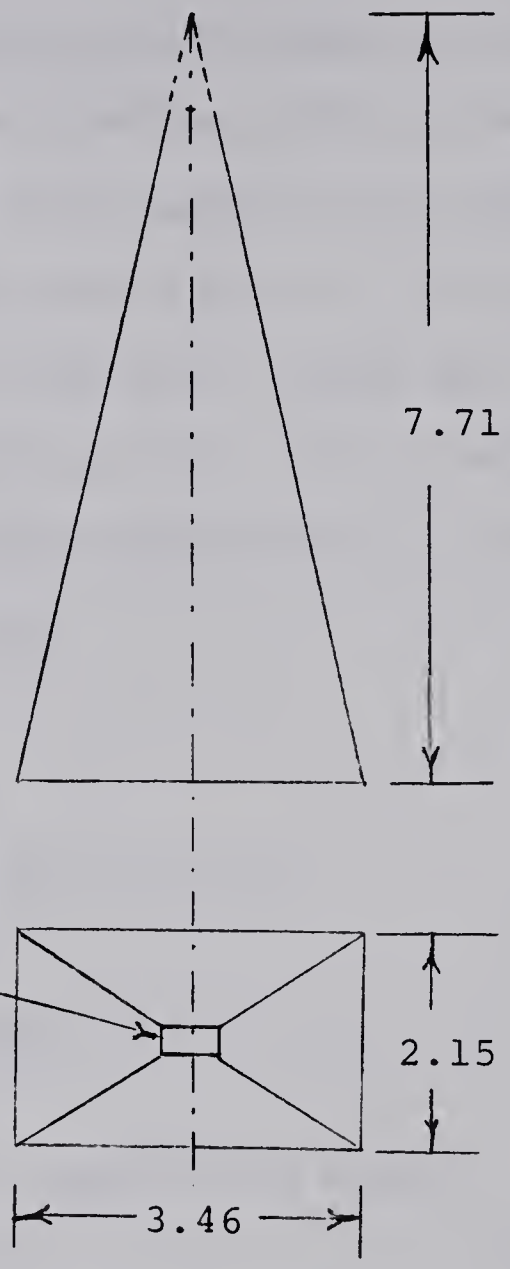
A spherical wave travels through the horn and is incident on the excited (curved) side of the convex lens {Fig.C-2}, and is transformed into a plane wave.

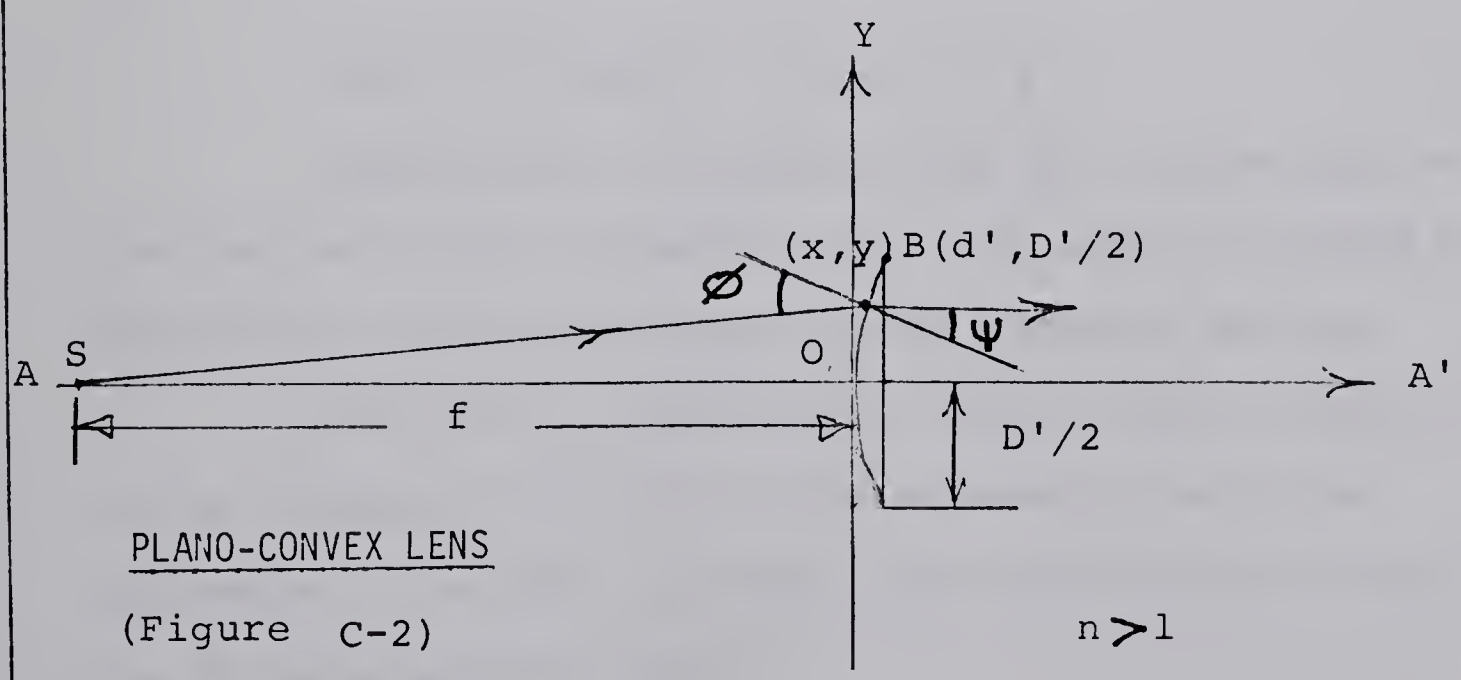
The design of the lens antennas having plane apertures (as in this case) largely consists of calculating the profile of the excited side of the lens, permitting a plane wave to be obtained for given values of the refractive index of the medium, n, and the focal length, f.

PYRAMIDAL HORN

(Figure C-1)

(all dimensions in cm)





PLANO-CONVEX LENS

(Figure C-2)

$n > 1$

(ref: Fradin, pg. 264)

C.1.2 Thickness and Radius of Curvature of the Plano-Convex Lens

The plane wave in the lens signifies, firstly, that any ray emerging from the source, incident on the surface of the lens, propagates further parallel to the x-axis {Fig.C-2}. And secondly, that the time of passage of the ray over such a broken path from the source to the aperture is the same for all rays. For a refractive index of more than unity, a plane wave characteristic is given by

$$\frac{f}{c} + \frac{x}{v_\phi} = \frac{\sqrt{(f + x)^2 + y^2}}{c} \qquad \text{(C-2)}$$

f = focal length, cm

and

x, y are the co-ordinate axes {Fig.C-2}

or

$$f + \frac{cx}{v_\phi} = \sqrt{(f + x)^2 + y^2} \qquad \text{(C-3)}$$

Substitute n for c/v_ϕ from Eq.(C-1) into Eq.(C-3) to get

$$f + nx = \sqrt{(f + x)^2 + y^2}$$

or

$$x^2(n^2 - 1) + 2fx(n - 1) - y^2 = 0 \qquad \text{(C-4)}$$

From Eq.(C-4) it is evident that for n greater than unity the lens profile has a hyperbolic form. The source is located at the focus of the hyperbola furthest from the surface of the lens.

As Eq.(C-4) is valid for any point on the curve then (x, y) can be replaced by (d', D'/2) the co-ordinates of one of the extremeties of the lens. By doing so and solving Eq.(C-4) for d', the following equation results,

$$d' = -\frac{f}{n+1} + \sqrt{\left(\frac{f}{n+1}\right)^2 + \frac{(D'/2)^2}{(n^2 - 1)}} \qquad \text{(C-5)}$$

given

n (for polystyrene) = 1.60

f (focal length) = 7.71 cm

D' (aperture) = 3.46 cm

the thickness of the lens d' is calculated as 0.3076 cm.

Radius of curvature for a plano-convex lens can be determined by the relationship,

$$\frac{1}{f} = (n - 1)(1/\gamma_1) \qquad \text{(C-6)}$$

γ_1 = radius of curvature.

For n = 1.6 and f = 7.71 cm, the radius of curvature is calculated as 4.626 cm.

C.2 SAMPLE CALCULATION OF POWER EMERGING FROM THE CORE HOLDER AT DIFFERENT WATER SATURATIONS

Re-writing Eq.III-7 as

$$\log_{10} \frac{I_x}{I_o} = \frac{-4\pi fhk\phi S_w}{2.303c} \qquad \text{(III-7)}$$

Given that

k = 2.9 (value given in Ch.III)

ϕ = 0.37 (say)

f = $27(10^9)$ Hz

h = 1.27 cm (thickness of core)

c = $3(10^{10})$ cm/sec

and substituting in Eq.(III-7)

$$\log_{10} \frac{I_x}{I_o} = - \frac{4(\pi)(27)(10^9)(1.27)(2.9)(0.37)S_w}{2.303(3)(10^{10})}$$

or

$$\log_{10} \frac{I_x}{I_o} = 6.7\ S_w \qquad \text{(C-7)}$$

Taking I_o as 3 mW, the power incident on the core holder, and assuming that all the attenuation occurs in the water, then Eq.(C-7) becomes,

$$\log_{10} I_x = \log_{10} I_o - 6.7\ S_w$$

or

$$\log_{10} I_x = 0.48 - 6.7\ S_w \qquad \text{(C-8)}$$

In this simplified calculation for the power measured, I_x, the following values result when solving for measured power at different water saturations,

TABLE C-1

WATER SATURATIONS AND THEORETICAL MICROWAVE POWER RECEIVED

S_w (fraction)	I_x (or R) (mW)
0.0	3.00
0.2	0.14
0.4	0.01
0.6	$2.88\ (10^{-4})$
0.8	$1.32\ (10^{-5})$
1.0	$6.03\ (10^{-7})$

This calculation was undertaken to have an idea of the powers that are to be measured. The calibration for the experimental runs was done using the values measured.

APPENDIX D

PLOTS OF TOTAL PRESSURE DROP, PORE VOLUMES PRODUCED AND EFFECTIVE VISCOSITIES VERSUS PORE VOLUMES INJECTED

DATA IN TABULAR FORM FOR THESE PLOTS

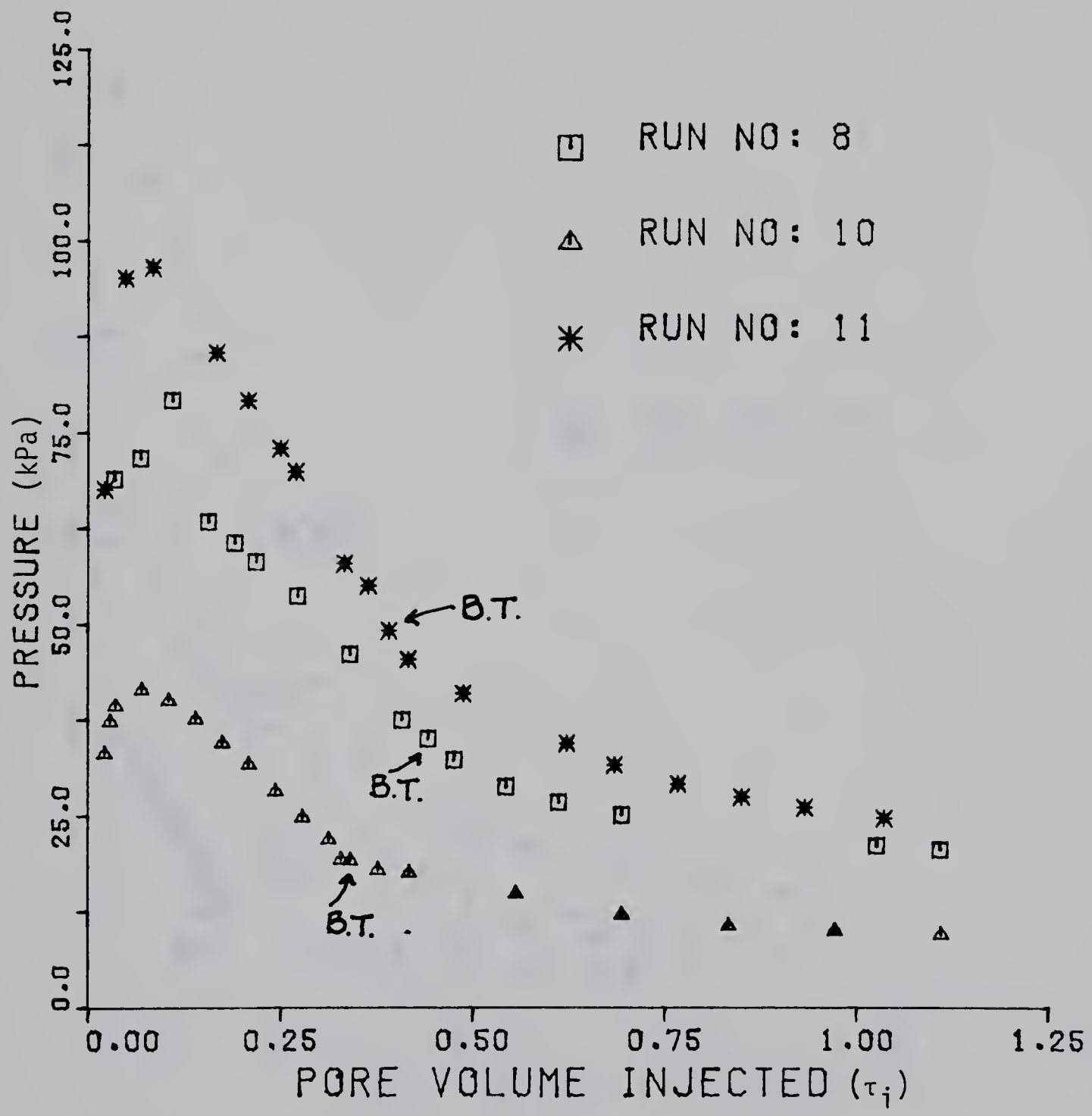


FIGURE D-1 TOTAL PRESSURE DROP HISTORY



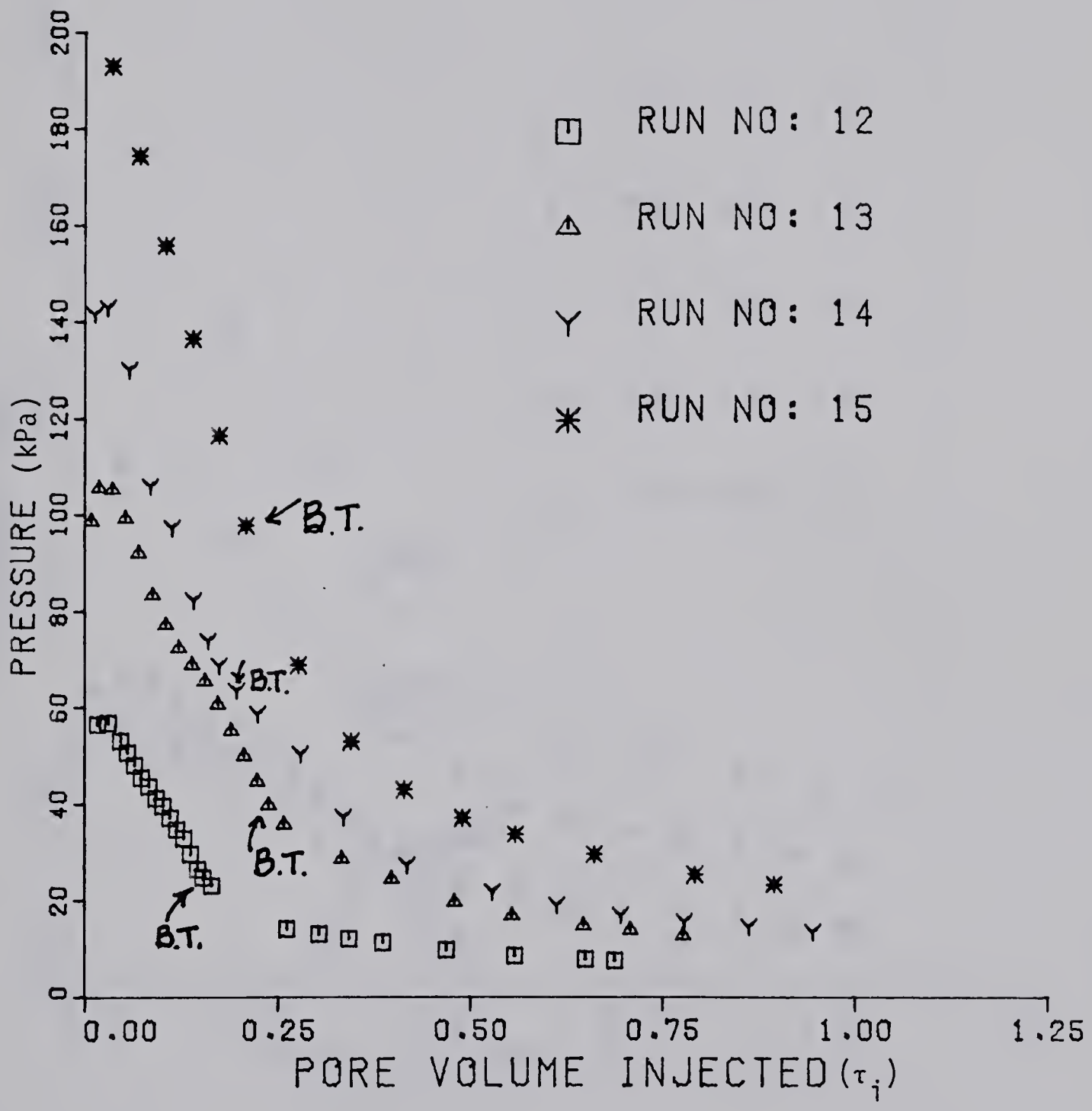


FIGURE D-2 TOTAL PRESSURE DROP HISTORY

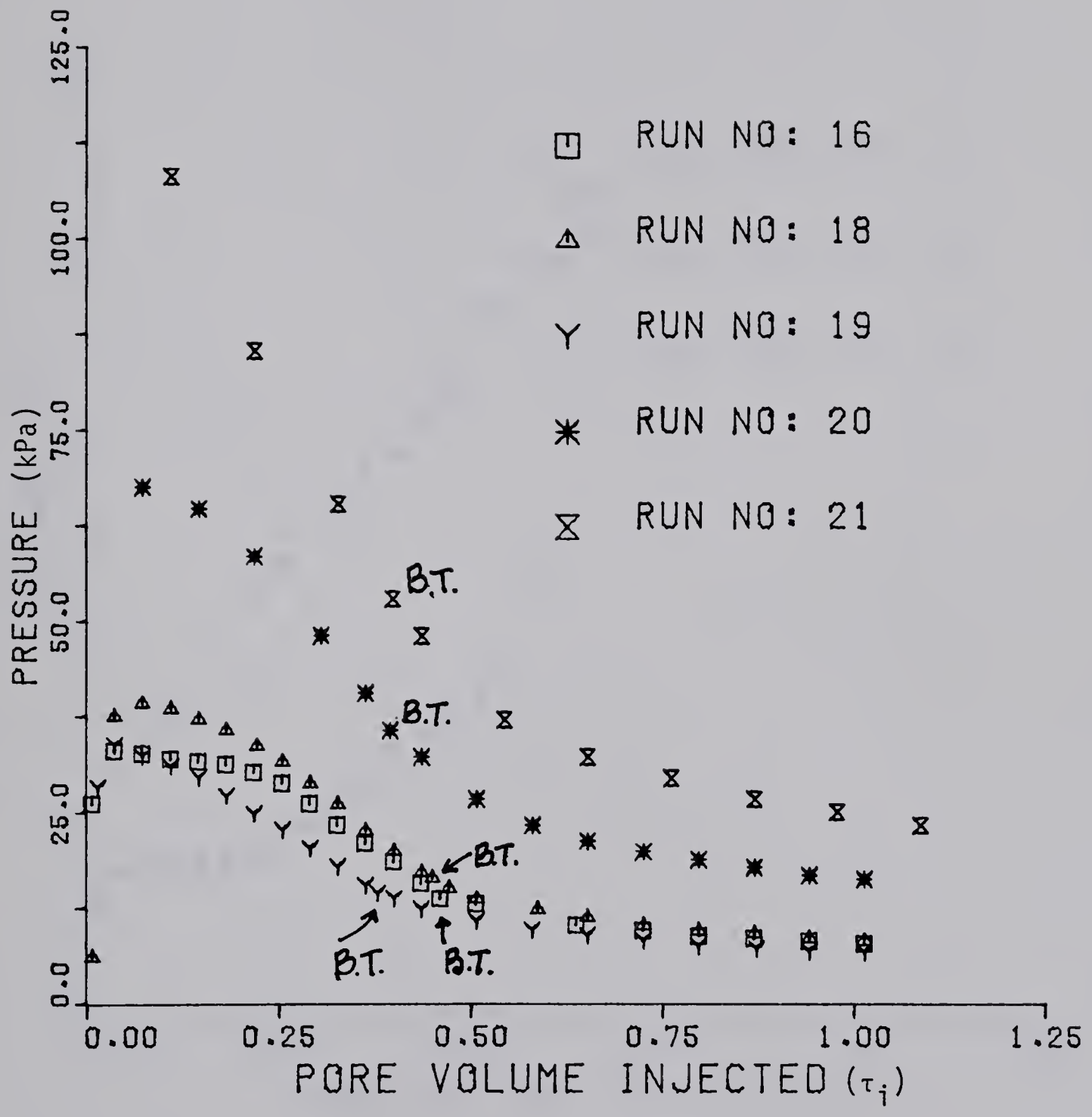


FIGURE D-3 TOTAL PRESSURE DROP HISTORY

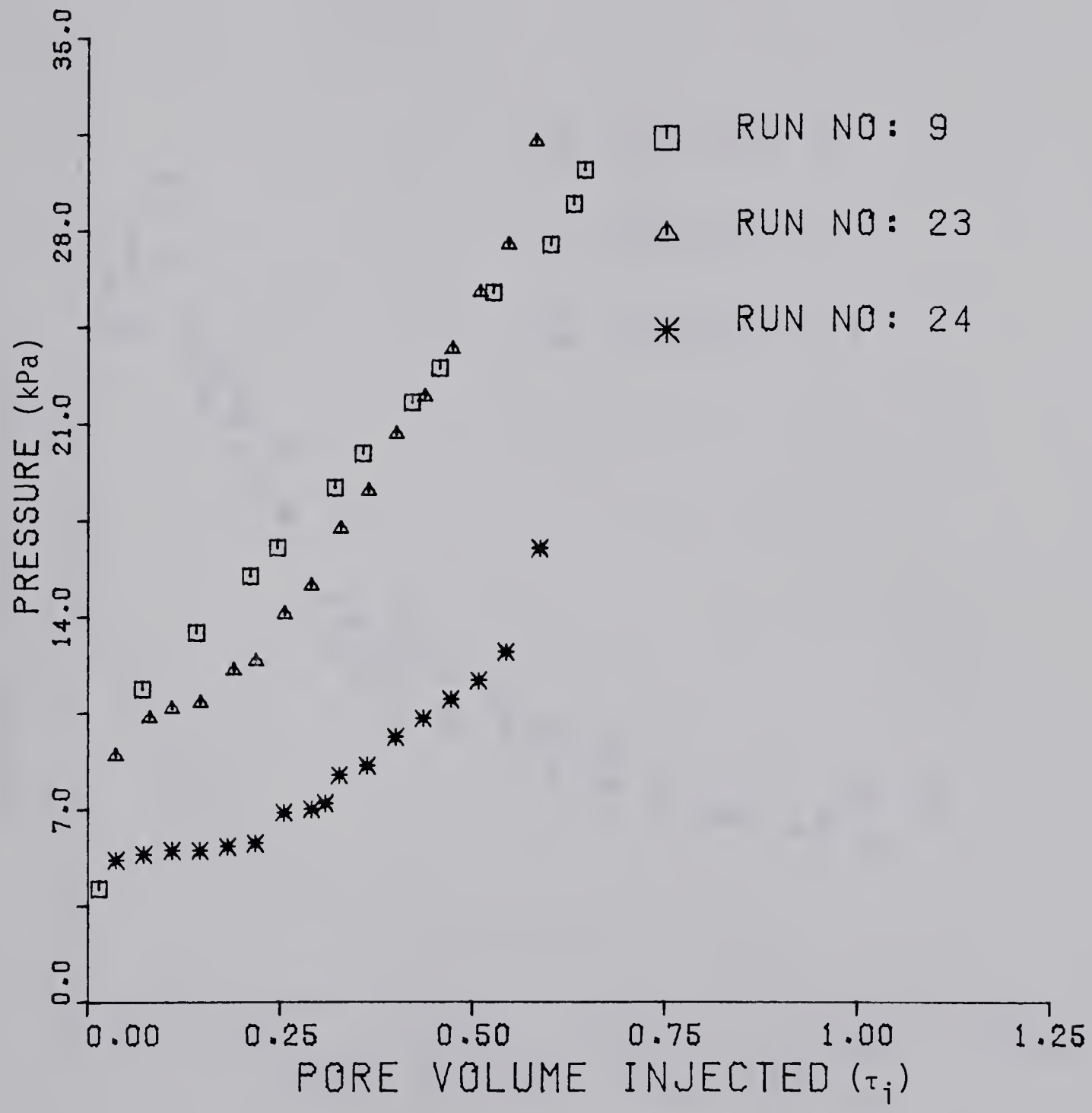


FIGURE D-4 TOTAL PRESSURE DROP HISTORY

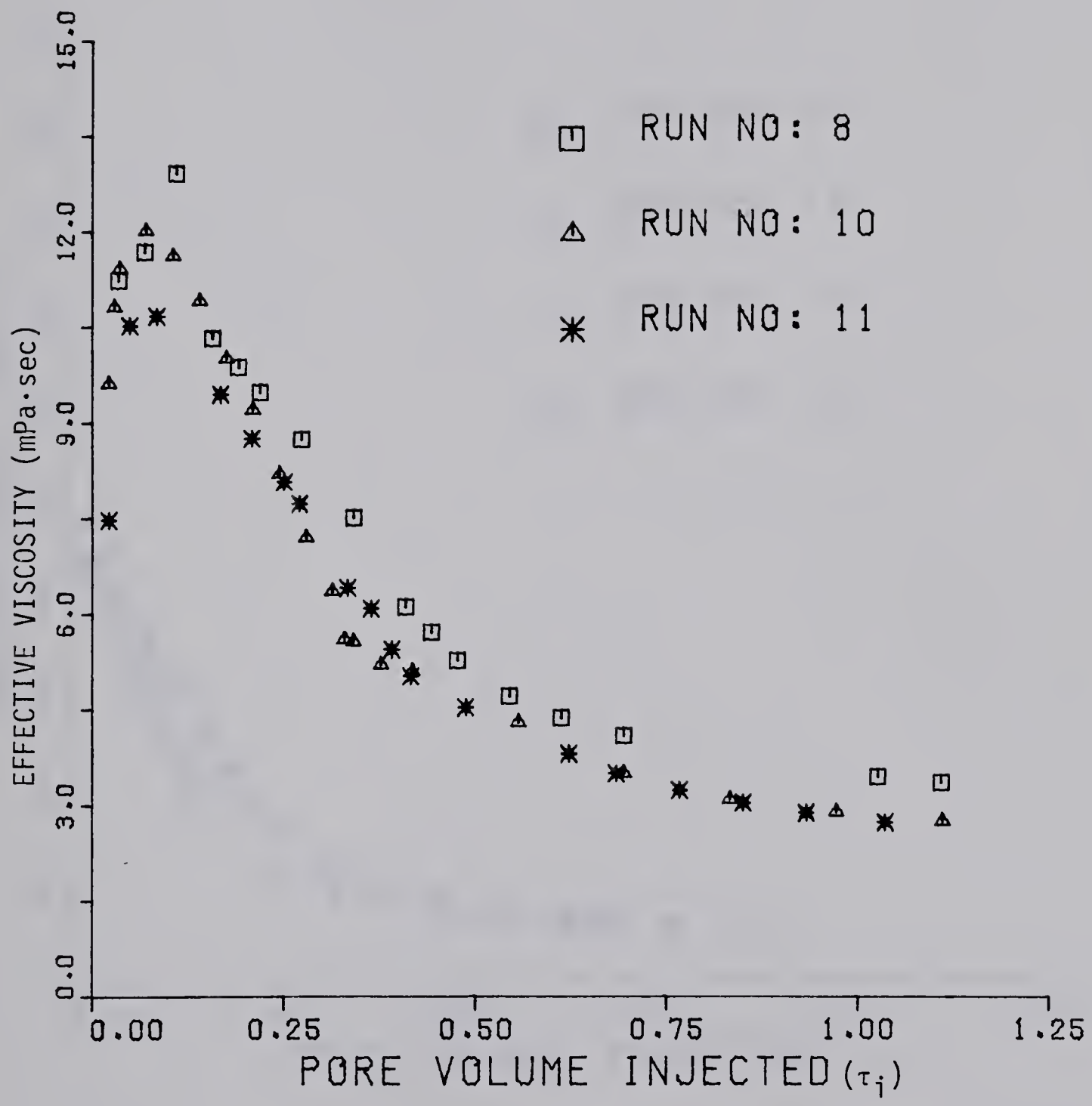


FIGURE D-5 EFFECTIVE VISCOSITY HISTORY

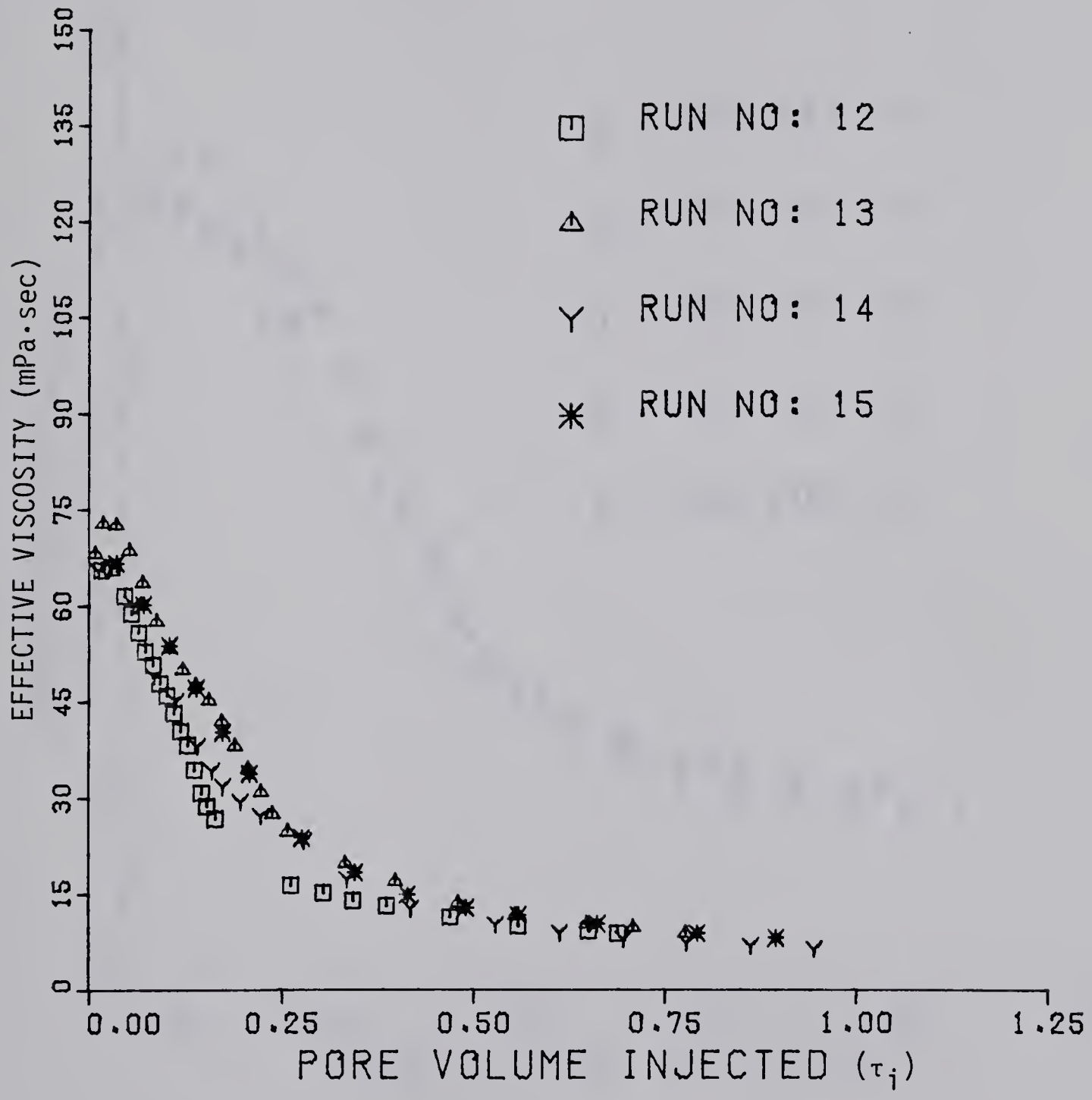


FIGURE D-6 EFFECTIVE VISCOSITY HISTORY

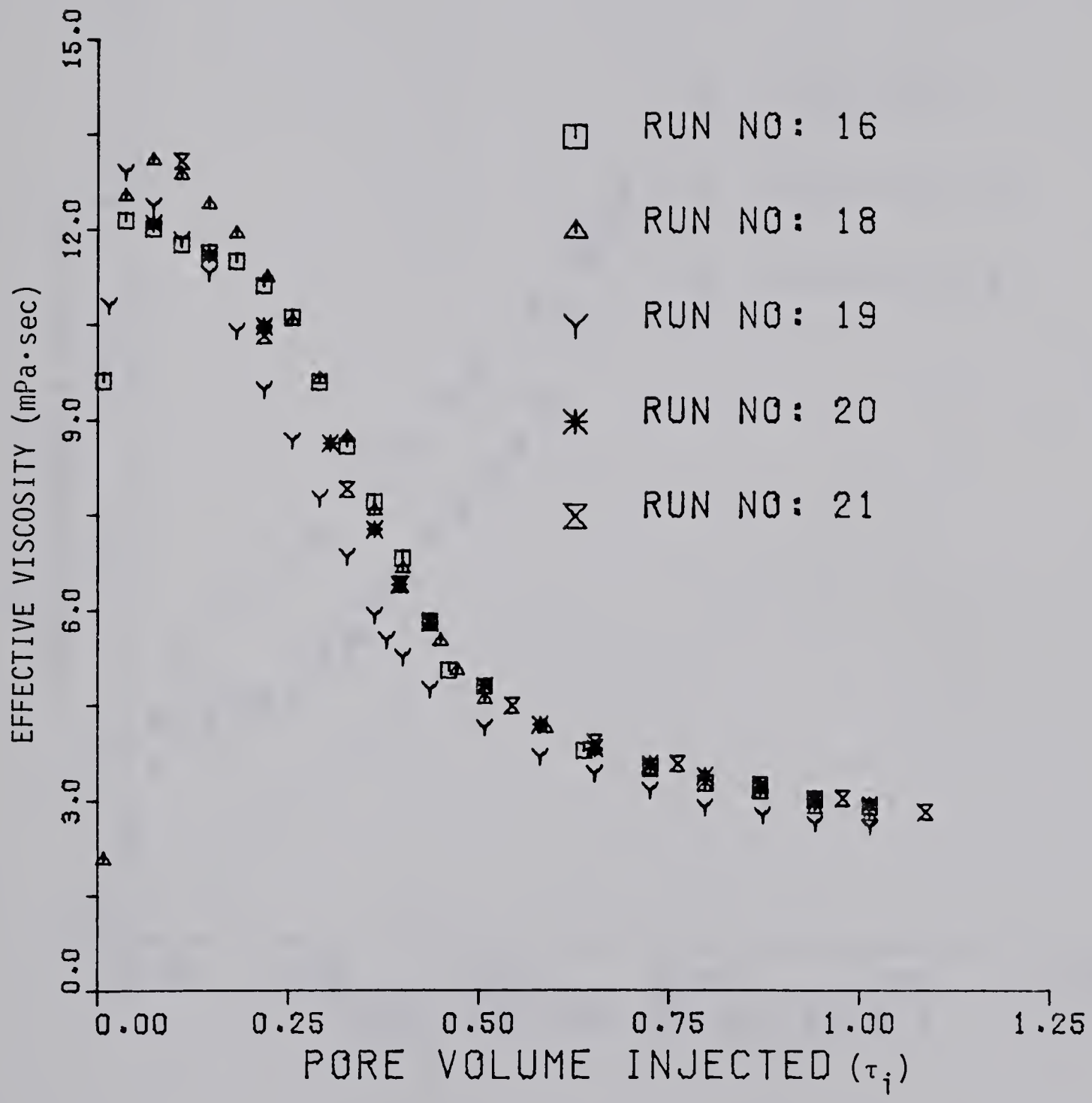


FIGURE D-7 EFFECTIVE VISCOSITY HISTORY



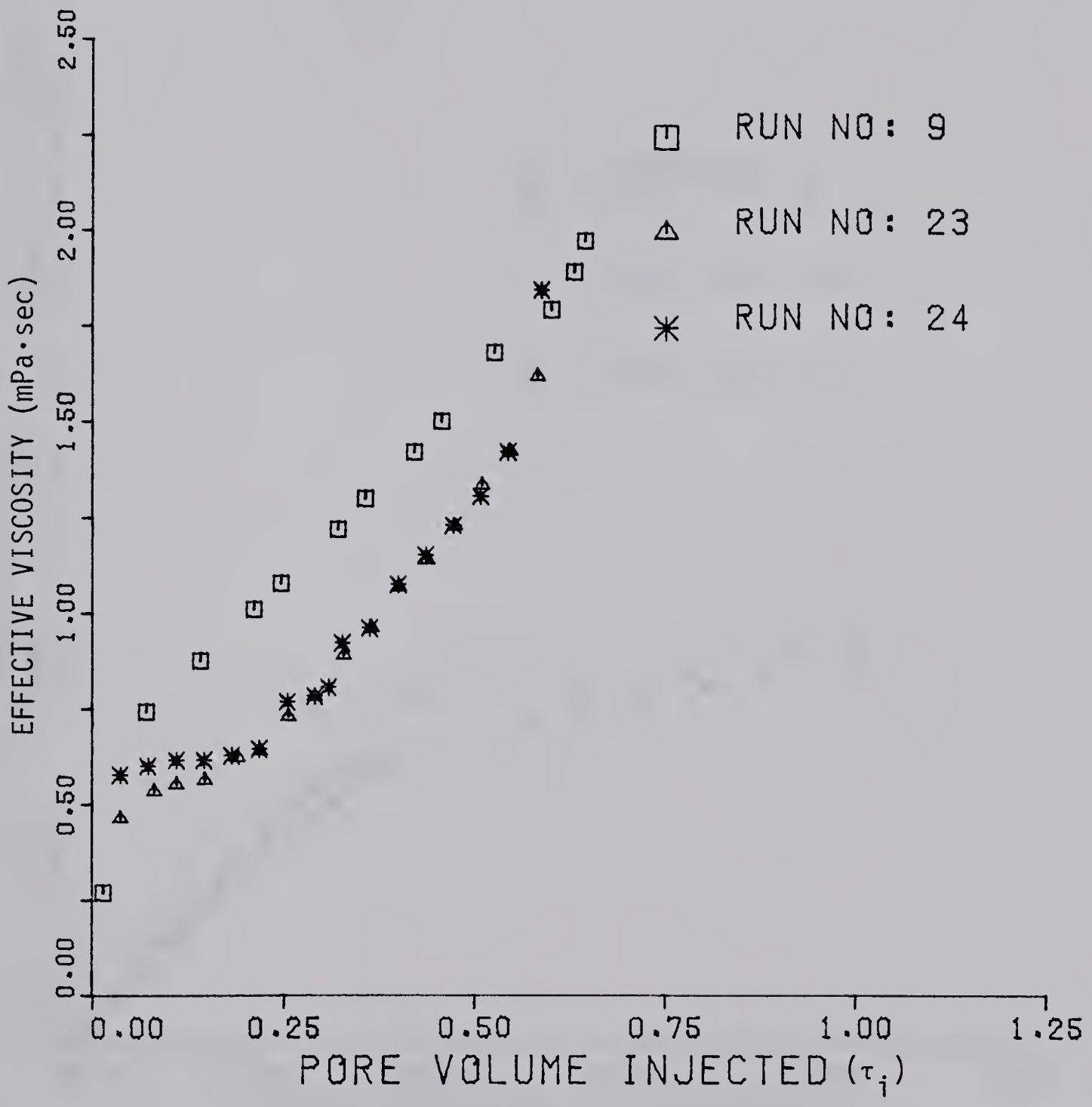


FIGURE D-8 EFFECTIVE VISCOSITY HISTORY



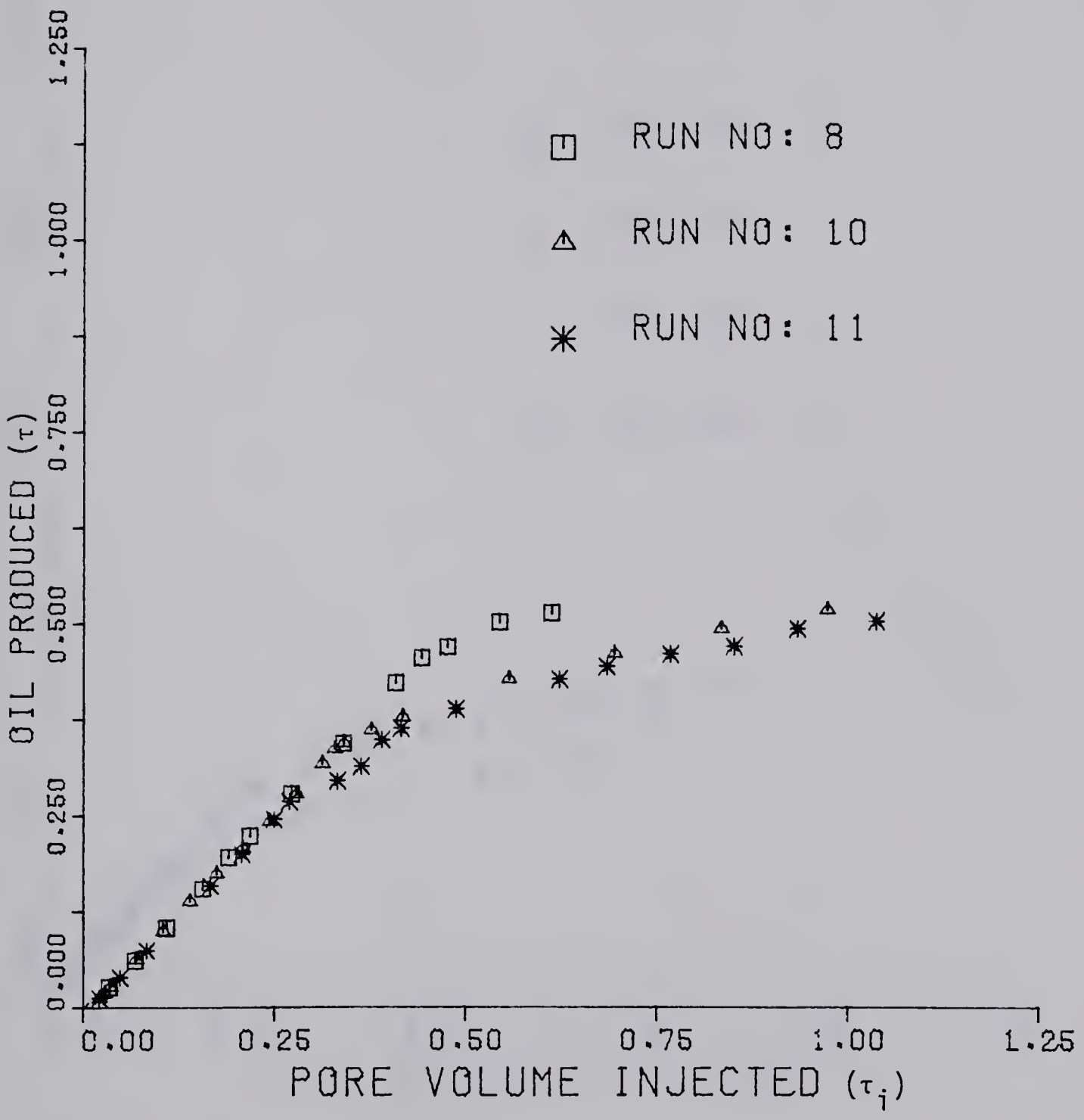


FIGURE D-9 OIL PRODUCTION HISTORY

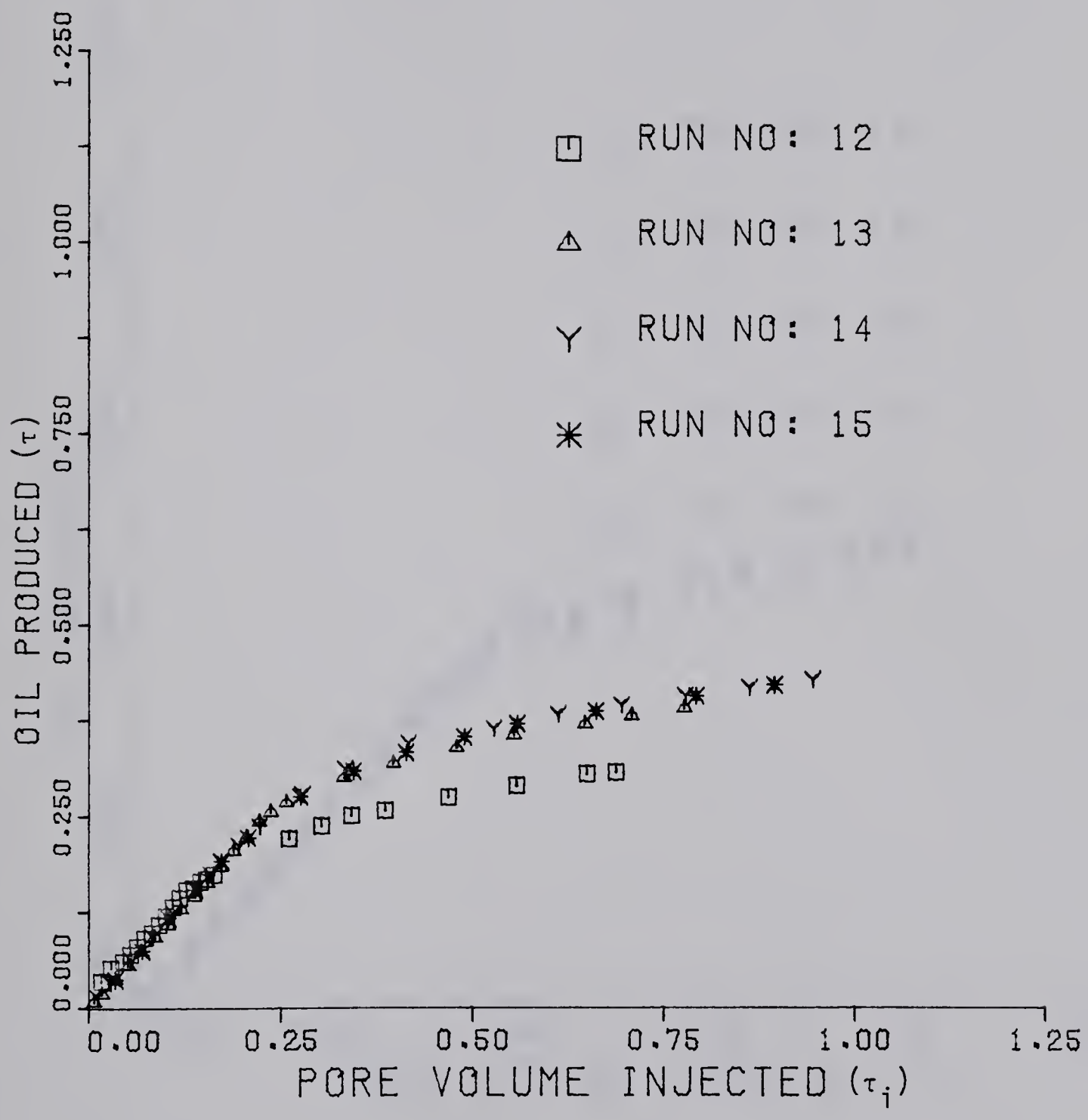


FIGURE D-10 OIL PRODUCTION HISTORY

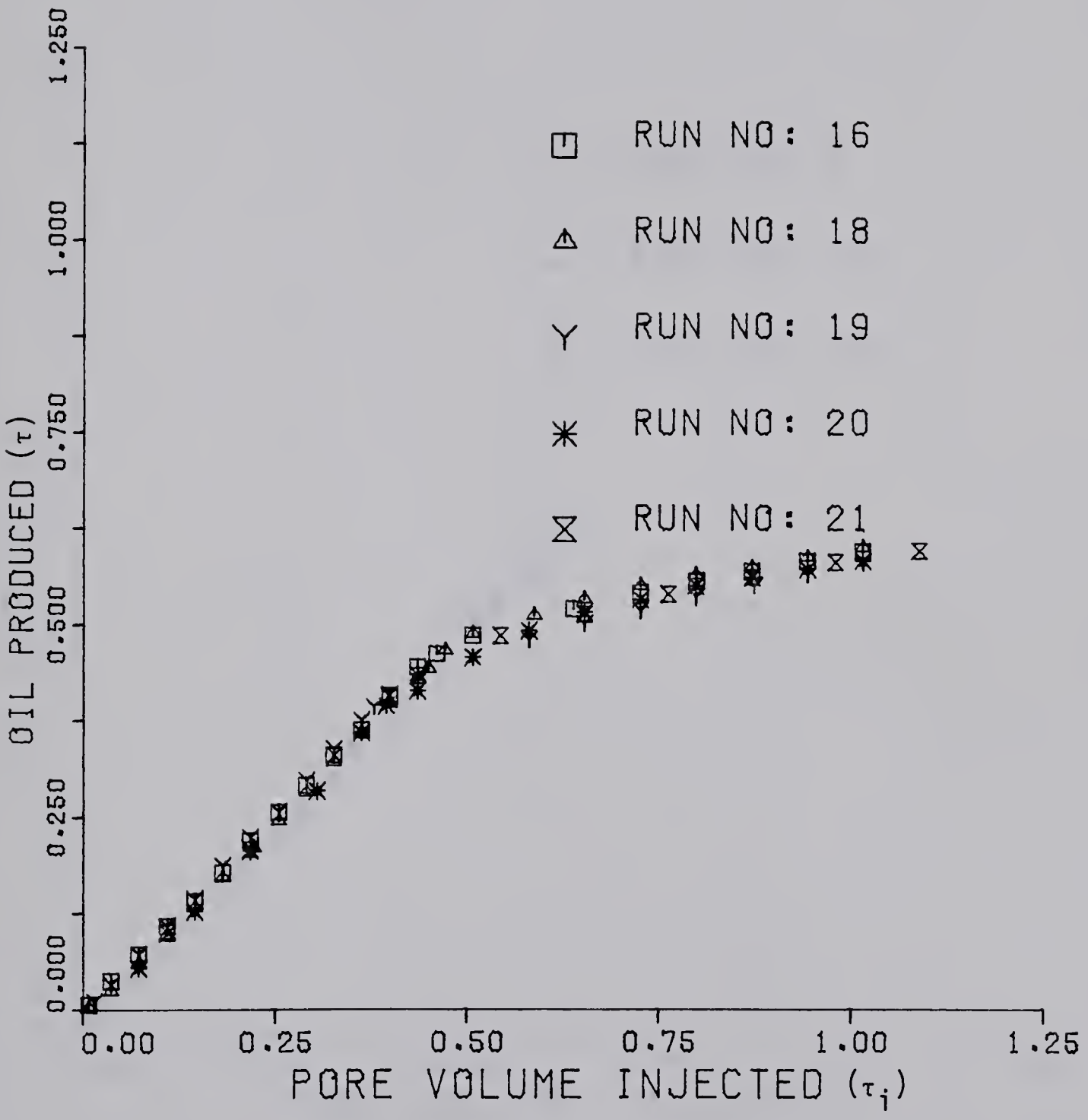


FIGURE D-11 OIL PRODUCTION HISTORY

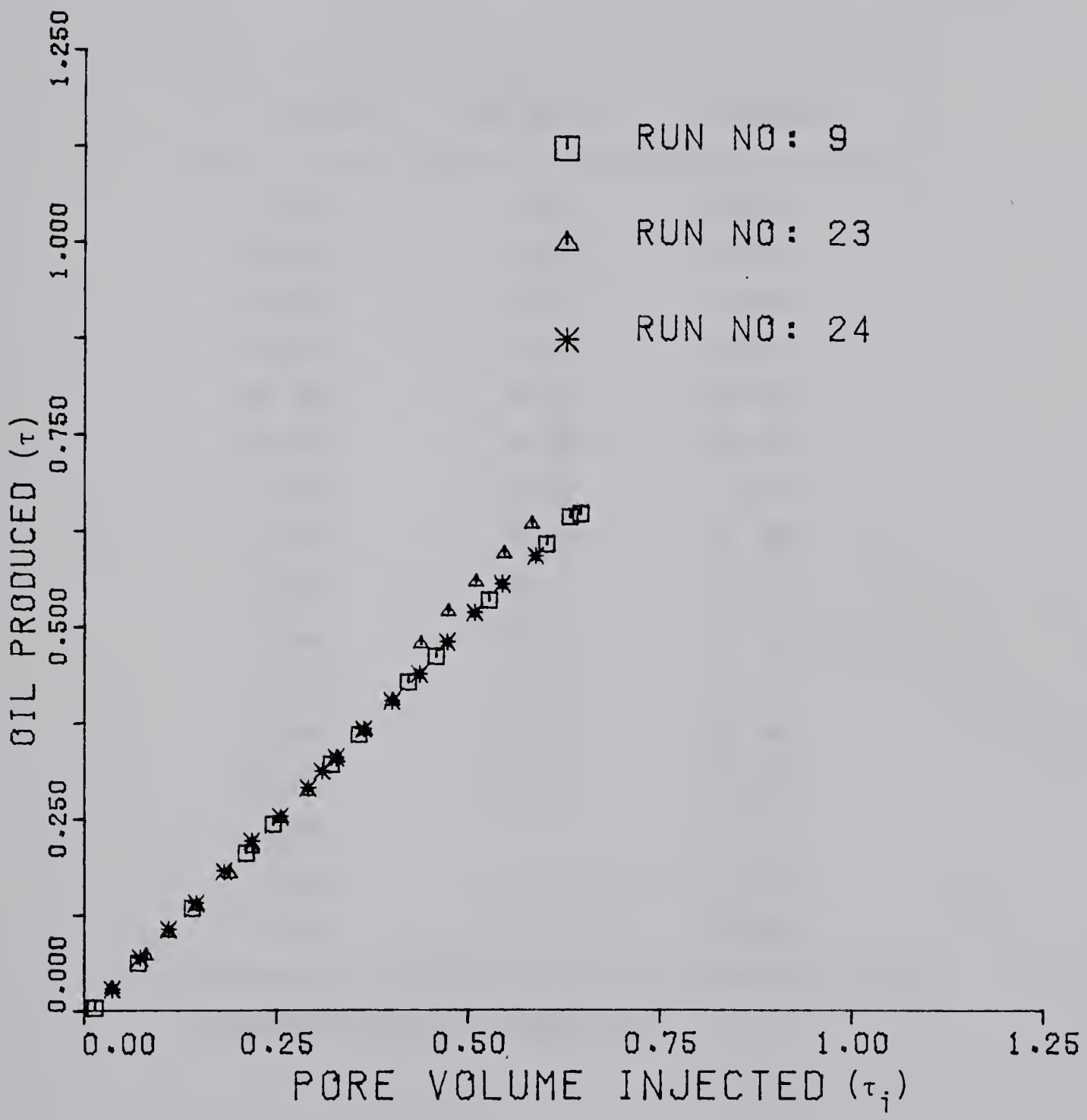


FIGURE D-12 OIL PRODUCTION HISTORY

TABLE D-1

OIL PRODUCTION AND PRESSURE HISTORY

RUN NUMBER 8

$\tau_i = qt/\phi AL$	Np (cc)	ΔP (kPa)
0.034	6.5	68.95
0.068	15.0*	71.71
0.109	25.5	79.29
0.156	38.0	63.43
0.190	48.0	60.68
0.218	55.0*	58.26
0.272	68.5	53.78
0.340	84.5*	46.20
0.408	104.0	37.58
0.442	112.0*	35.16 (B.T.)
0.476	115.5	32.41
0.544	123.5	28.96
0.612	126.5	26.89
0.694		25.17
1.026		21.24
1.109		20.69

* Saturation profile available

TABLE D-2

OIL PRODUCTION AND PRESSURE HISTORY

RUN NUMBER 10

$\tau_i = qt/\phi AL$	Np (cc)	ΔP (kPa)
0.021	3.0	33.10
0.028	4.5	37.23
0.035	6.5*	39.30
0.069	15.0*	41.37
0.104	24.0*	40.00
0.139	33.25	37.58
0.174	42.0*	34.48
0.208	50.0	31.72
0.243	58.5*	28.27
0.278	67.0	24.82
0.312	76.5*	21.93
0.328	81.0	19.31
0.340	83.0*	19.17 (B.T.)
0.376	87.0	17.93
0.417	91.0	17.58
0.556	103.0	14.82
0.694	111.0	12.07
0.833	119.0	10.69
0.972	125.0	10.00
1.111		9.52

* Saturation profile available

TABLE D-3

OIL PRODUCTION AND PRESSURE HISTORY

RUN NUMBER 11

$\tau_j = qt/\phi AL$	Np (cc)	ΔP (kPa)
0.021	3.0	67.57
0.048	9.5	95.15
0.083	18.0*	96.53
0.166	38.5	85.50
0.207	48.5*	79.29
0.249	59.5	73.09
0.269	65.0*	69.98
0.332	71.5	58.06
0.363	76.0*	55.16
0.390	84.5*	49.30 (B.T.)
0.415	88.0	45.51
0.487	94.0	41.03
0.622	103.5	34.48
0.684	107.5	31.72
0.767	111.5	29.30
0.850	114.0	27.58
0.933	119.5	26.20
1.036	122.0	24.82

* Saturation profile available

TABLE D-4

OIL PRODUCTION AND PRESSURE HISTORY

RUN NUMBER 12

$\tau_i = qt/\phi AL$	Np (cc)	ΔP (kPa)
0.016	8.0	56.54
0.029	12.0*	56.88
0.045	14.0	53.09
0.054	16.0*	50.68
0.063	18.5	48.13
0.072	21.0*	45.58
0.082	22.5	43.78
0.091	25.0*	41.23
0.100	27.5	39.65
0.109	30.25*	37.23
0.118	33.0	34.82
0.127	35.5*	32.96
0.136	36.0	29.65
0.145	38.0*	26.55
0.152	38.75*	24.82 (B.T.)
0.163	40.0	23.10
0.261	50.9	14.13
0.303	54.75	13.10
0.342	57.9	12.07
0.386	59.4	11.38
0.469	63.4	9.86
0.558	66.9	8.62
0.650	70.4	7.93
0.688	70.9	7.58

* Saturation profile available



TABLE D-5

OIL PRODUCTION AND PRESSURE HISTORY

RUN NUMBER 13

$\tau_j = qt/\phi AL$	Np (cc)	ΔP (kPa)
0.007	2.0	98.60
0.017	4.5	105.50
0.034	9.0*	105.15
0.051	13.5	99.29
0.068	18.0*	92.05
0.086	22.5	83.43
0.103	26.5*	77.22
0.120	31.5	72.40
0.137	35.5*	68.95
0.154	40.0	65.50
0.171	45.0*	60.68
0.188	50.0	55.16
0.205	54.5*	49.99
0.222	59.5	44.82
0.237	62.5*	39.85 (B.T.)
0.257	65.5	35.85
0.332	73.5	28.61
0.397	78.0	24.48
0.479	83.0	19.58
0.554	87.0	16.89
0.647	90.5	14.82
0.708	93.0	13.93
0.777	95.5	12.76

* Saturation profile available

TABLE D-6

OIL PRODUCTION AND PRESSURE HISTORY

RUN NUMBER 14

$\tau_i = qt/\phi AL$	Np (cc)	ΔP (kPa)
0.011	3.5	141.35
0.028	8.0*	142.73
0.056	15.0*	129.97
0.083	22.5*	105.84
0.111	29.5*	97.22
0.139	37.5*	82.05
0.158	42.0	73.78
0.172	46.0	68.61
0.195	51.0*	63.43 (B.T.)
0.222	57.0	58.61
0.278	67.0	50.33
0.334	75.0	37.23
0.417	83.0	27.24
0.528	87.5	21.72
0.612	92.0	18.96
0.695	95.0	16.89
0.778	98.0	15.51
0.862	100.5	14.48
0.945	103.0	13.45

* Saturation profile available

TABLE D-7

OIL PRODUCTION AND PRESSURE HISTORY

RUN NUMBER 15

$\tau_i = qt/\phi AL$	Np (cc)	ΔP (kPa)
0.034	9.0	193.06
0.069	19.0	174.44
0.103	28.5*	155.83
0.138	37.5*	136.52
0.172	46.5*	116.53
0.207	54.0*	97.91 (B.T.)
0.275	67.0	68.95
0.344	75.0	53.09
0.413	81.0	43.09
0.489	86.0	37.23
0.558	90.0	33.79
0.661	94.0	29.65
0.792	99.0	25.51
0.895	102.5	23.44

* Saturation profile available

TABLE D-8

OIL PRODUCTION AND PRESSURE HISTORY

RUN NUMBER 16

$\tau_i = qt/\phi AL$	Np (cc)	ΔP (kPa)
0.007	1.5	26.20
0.036	8.5	33.10
0.072	16.5*	32.75
0.109	25.0	32.06
0.145	32.5*	31.72
0.181	41.0	31.37
0.217	50.5*	30.34
0.254	59.0	28.96
0.290	67.0*	26.20
0.326	76.0	23.44
0.362	83.5*	21.03
0.399	93.5	18.62
0.435	102.5*	15.86
0.460	106.5*	13.79 (B.T.)
0.507	112.0	13.10
0.638	120.0	10.34
0.725	124.75	9.65
0.798	128.25	8.96
0.870	131.25	8.62
0.942	134.25	8.27
1.014	137.25	7.93

* Saturation profile available

TABLE D-9

OIL PRODUCTION AND PRESSURE HISTORY

RUN NUMBER 18

$\tau_i = qt/\phi AL$	Np (cc)	ΔP (kPa)
0.007	0.6	6.21
0.036	5.5	37.58
0.072	14.0*	39.30
0.109	22.5	38.61
0.145	30.5*	37.23
0.181	39.5	35.85
0.221	48.5*	33.79
0.254	56.5	31.72
0.290	65.0*	28.96
0.326	74.0	26.20
0.362	83.0*	22.75
0.399	91.5	20.00
0.435	99.5*	17.24
0.449	102.0	16.55 (B.T.)
0.471	107.5	15.17
0.507	112.5	13.79
0.587	118.0	12.41
0.652	123.0	11.38
0.725	127.0	10.34
0.797	130.2	9.65
0.870	132.45	9.31
0.942	135.45	8.62
1.014	138.45	8.27

* Saturation profile available

TABLE D-10

OIL PRODUCTION AND PRESSURE HISTORY

RUN NUMBER 19

$\tau_i = qt/\phi AL$	Np (cc)	ΔP (kPa)
0.014	2.5	28.27
0.036	7.5	33.79
0.072	16.5*	32.41
0.109	25.0	31.03
0.145	33.0*	29.65
0.181	43.0	27.24
0.217	51.5*	24.82
0.254	59.0	22.75
0.290	68.5*	20.34
0.326	78.0	17.93
0.362	86.5*	15.51
0.378	90.5	14.48 (B.T.)
0.399	94.5	13.79
0.435	98.5	12.41
0.507	105.5	10.86
0.580	110.75	9.65
0.652	115.5	8.96
0.725	119.5	8.27
0.797	123.5	7.58
0.873	127.0	7.24
0.942	130.25	6.90
1.014	133.75	6.76

* Saturation profile available

TABLE D-11

OIL PRODUCTION AND PRESSURE HISTORY

RUN NUMBER 20

$\tau_j = qt/\phi AL$	Np (cc)	ΔP (kPa)
0.072	12.5*	67.57
0.145	29.5*	64.81
0.217	47.5*	58.61
0.304	65.5*	48.27
0.362	83.0*	40.68
0.394	91.0	35.85 (B.T.)
0.435	95.5	32.41
0.507	105.5	26.89
0.580	113.5	23.44
0.652	119.0	21.37
0.725	123.0	20.00
0.797	127.0	18.96
0.870	129.5	17.93
0.942	132.0	16.89
1.014	134.5	16.41

* Saturation profile available

TABLE D-12

OIL PRODUCTION AND PRESSURE HISTORY

RUN NUMBER 21

$\tau_j = qt/\phi AL$	Np (cc)	ΔP (kPa)
0.109	23.0*	108.25
0.217	48.0*	85.50
0.326	76.0*	65.50
0.397	94.0	53.10 (B.T.)
0.435	100.0	48.27
0.543	112.0	37.23
0.652	118.5	32.41
0.761	124.5	29.65
0.870	129.5	26.89
0.978	134.0	25.17
1.087	137.5	23.44

* Saturation profile available

TABLE D-13

OIL PRODUCTION AND PRESSURE HISTORY

RUN NUMBER 9

$\tau_i = qt/\phi AL$	Np (cc)	ΔP (kPa)
0.014	1.0	4.14
0.070	15.0	11.38
0.140	32.0*	13.45
0.210	49.0*	15.51
0.245	58.0	16.55
0.320	76.5	18.75
0.356	85.75*	20.00
0.420	102.0	21.86
0.456	110.0*	23.10
0.525	127.5*	25.86
0.600	145.0	27.58
0.630	153.5	29.10
0.644	154.5	30.34 (B.T.)

* Saturation profile available

TABLE D-14

OIL PRODUCTION AND PRESSURE HISTORY

RUN NUMBER 23

$\tau_i = qt/\phi AL$	Np (cc)	ΔP (kPa)
0.036	6.5	8.96
0.080	16.5	10.34
0.109	23.5	10.69
0.146	31.5*	10.89
0.189	41.0	12.07
0.218	48.5*	12.41
0.255	57.5	14.13
0.290	65.5*	15.17
0.328	75.5	17.24
0.364	83.5*	18.62
0.400	92.5	20.69
0.437	109.5*	22.06
0.473	119.0	23.79
0.509	128.0*	25.86
0.546	136.5	27.58
0.582	145.5*	31.37 (B.T.)

* Saturation profile available

TABLE D-15

OIL PRODUCTION AND PRESSURE HISTORY

RUN NUMBER 24

$\tau_i = qt/\phi AL$	Np (cc)	ΔP (kPa)
0.036	6.5	5.17
0.072	16.0*	5.38
0.109	24.5	5.52
0.145	32.5*	5.52
0.181	42.0	5.64
0.217	51.0*	5.79
0.254	58.5	6.90
0.290	67.0*	7.03
0.308	72.0	7.24
0.326	76.0	8.27
0.362	84.5*	8.62
0.399	93.0	9.65
0.435	101.0*	10.34
0.471	110.5	11.03
0.507	119.5*	11.72
0.543	128.0	12.76
0.587	136.5	16.55 (B.T.)

* Saturation profile available

APPENDIX E

EULERIAN SOLUTION PROCEDURE FOR IMMISCIBLE DISPLACEMENT EQUATION

E.1 EULERIAN SOLUTION PROCEDURE FOR THE IMMISCIBLE DISPLACEMENT EQUATION

Consider Eq.(II-7), and differente both sides with respect to ξ to have

$$\frac{\partial f_w}{\partial \xi} = \frac{dG(S^*)}{dS^*}\frac{\partial S^*}{\partial \xi} - \frac{\partial}{\partial \xi}\left\{N_c C(S^*)\frac{\partial S^*}{\partial \xi}\right\} \qquad \text{(E-1)}$$

From Eq.(E-1), substitute the value of $\partial f_w/\partial \xi$ in Eq.(II-6), to get

$$\frac{\partial S^*}{\partial \tau^*} = \frac{\partial}{\partial \xi}\left\{N_c C(S^*)\frac{\partial S^*}{\partial \xi}\right\} - \frac{dG(S^*)}{dS^*}\frac{\partial S^*}{\partial \xi} \qquad \text{(E-2)}$$

One way of handling the second order derivative in Eq.(E-2), with the non-linearity, is to use the differencing scheme proposed by Blair and Weinaug[8] [1969, p.418],

$$\frac{\partial}{\partial \xi}\left\{N_c C(S^*)\frac{\partial S^*}{\partial \xi}\right\} = \frac{1}{\Delta \xi}\left[W\left\{\frac{S^*_{n+1} - S^*_n}{\Delta \xi}\right\} - Z\left\{\frac{S^*_n - S^*_{n-1}}{\Delta \xi}\right\}\right] \qquad \text{(E-3)}$$

where

$$W = \frac{N_c}{2}\left\{C(S^*_n) + C(S^*_{n+1})\right\} \qquad \text{(E-4)}$$

and

$$Z = \frac{N_c}{2}\left\{C(S^*_{n-1}) + C(S^*_n)\right\} \qquad \text{(E-5)}$$

Also

$\Delta \xi$ = step size for the space variable

n = counter for the spatial nodes.

Substituting for $\frac{\partial}{\partial \xi}\left\{N_c C(S^*)\frac{\partial S^*}{\partial \xi}\right\}$ from Eq.(E-3) into Eq.(E-2) one obtains,

$$\frac{\partial S^*}{\partial \tau^*} = \frac{dG(S^*)}{dS^*}\frac{\partial S^*}{\partial \xi} + \frac{1}{\Delta \xi}\left[W\left\{\frac{S^*_{n+1} - S^*_n}{\Delta \xi}\right\} - Z\left\{\frac{S^*_n - S^*_{n-1}}{\Delta \xi}\right\}\right] \qquad \text{(E-6)}$$

Considering i as the counter for points in time and discretizing the remaining derivatives in Eq.(E-6) to have

$$\frac{S^{*i} - S^{*i-1}_n}{\Delta\tau^*} = -\frac{dG(S^{*i})}{dS^*}\frac{1}{2\Delta\xi}\left\{S^{*i}_{n+1} - S^{*i}_{n-1}\right\} + \frac{W}{(\Delta\xi)^2}\left\{S^{*i}_{n+1} - S^{*i}_n\right\} - \frac{Z}{(\Delta\xi)^2}\left\{S^{*i}_n - S^{*i}_{n-1}\right\} \quad \text{(E-7)}$$

Simplifying Eq.(E-7) to obtain,

$$-(A+E)S^{*i}_{n-1} + (1+B+E)S^{*i}_n + (A-B)S^{*i}_{n+1} = S^{*i-1}_n \quad \text{(E-8)}$$

where

$$A = \frac{dG(S^{*i}_n)}{dS^*} \cdot \frac{\Delta\tau^*}{2\Delta\xi} \quad \text{(E-9)}$$

$$B = W\frac{\Delta\tau^*}{(\Delta\xi)^2} \quad \text{(E-10)}$$

and

$$E = Z\frac{\Delta\tau^*}{(\Delta\xi)^2} \quad \text{(E-11)}$$

Note that Eq.(E-8) is fully implicit in the time derivative. Saturations at (i-1)th time step are known and are to be evaluated for the i-th time step.

E.1.1 Initial and Boundary Conditions

The conditions used in the numerical procedure were,

$$S^*(\xi, 0^+) = F(\xi) \qquad 0 \le \xi \le 1 \quad \text{(E-12)}$$

$$S^*(1, \tau^*) = 0 \qquad 0 < \tau^* < \tau^*_{bt} \quad \text{(E-13)}$$

and to get the numerical procedure started the inlet boundary condition for the first time step is

$$S^*(0, \Delta\tau^*) = SI \qquad \text{(E-14)}$$

where SI is assigned an arbitrary value between zero and one. The Eq.(E-8) is solved with Eqs.(E-12) to (E-14) for the first time step and material balance is checked by numerically integrating for the area under the first profile. The area must be equal to $\Delta\tau^*$, the magnitude of the time step, if the choice of SI is correct for that particular data set.

$F(\xi)$ is also arbitrary, and in this numerical procedure a convenient choice was,

$$\left.\begin{aligned} F(\xi) &= -\frac{SI}{\Delta\xi}\,\xi + SI \qquad \xi \leq \Delta\xi \\ \text{or} \\ F(\xi) &= 0 \qquad\qquad\qquad\quad \xi > \Delta\xi \end{aligned}\right\} \qquad \text{(E-15)}$$

It is evident that $F(\xi)$ is different for every choice of SI. In actuality, this function is only used in the first iterate and then the current nodal values are used till convergence is achieved.

Once the profile after the first time step is obtained, the saturation at the inlet will build-up for the subsequent time steps. To enable the saturation to build-up Eq.(E-16) was used. Once again differentiating both sides of Eq.(II-7) with respect to ξ and substituting the resulting $\partial f_w/\partial\xi$ in Eq.(II-6) to obtain,

$$\frac{\partial S^*}{\partial \tau^*} = N_c \left\{ \frac{\partial C(S^*)}{\partial \xi} \frac{\partial S^*}{\partial \xi} + \frac{\partial^2 S^*}{\partial \xi^2} C(S^*) \right\} - \frac{\partial G(S^*)}{\partial \xi} \qquad \text{(E-16)}$$

The finite difference analog of Eq.(E-16) for node 1 can be written as,

$$S_1^{*i+1} = \frac{N_c \Delta\tau^*}{(\Delta\xi)^2} \left\{ C(S_2^{*i}) - C(S_1^{*i}) \right\} (S_2^{*i} - S_1^{*i})$$

$$+ \frac{N_c \Delta\tau^*}{(\Delta\xi)^2} \left\{ S_3^{*i} - 2S_2^{*i} + S_1^{*i} \right\}$$

$$- \left\{ \frac{G(S_2^{*i}) - G(S_1^{*i})}{\Delta\xi} \right\} + S_1^{*i} \qquad \text{(E-17)}$$

Once the inlet end saturation attains a value of unity the third boundary condition becomes,

$$S^*(0, \tau^*) = 1$$

Eq.(E-8) was written for every node and the resulting coefficient matrix was tri-diagonal, facilititating solution by Thomas's procedure. For every time step S_n^{*i}, $C(S_n^{*i})$ and $dG(S_n^{*i})/dS^*$ were iterated upon till convergence was achieved. The time step size, $\Delta\tau^*$, was taken as 0.005 while the spatial axis was divided into one hundred parts to give a step size, $\Delta\xi$, of 0.01.

B30238